Experimental and numerical studies on the water balance of the Upper Mega Aquifer system, Arabian Peninsula

Dissertation

zur Erlangung des akademischen Grades
Doctor rerum naturalium (Dr. rer. nat.)

Stephan Schulz (Dipl. Geoökol.)

geboren in Berlin

Tag der Einreichung: 23. Februar 2017

Tag der mündlichen Prüfung: 24. März 2017

Vom Fachbereich Material- und Geowissenschaften der Technischen Universität Darmstadt

Darmstadt 2017 – D17

Referent: Prof. Dr. Christoph Schüth
Korreferent: Prof. Dr. Ralf Merz
1. Prüfer: Prof. Dr. Randolf Rausch
2. Prüfer: Prof. Dr. Ingo Sass
3. Prüfer: Prof. Dr. Wolfgang Ensinger

HELMHOLTZ ZENTRUM FÜR UMWELTFORSCHUNG UFZ

IAG Institut für Angewandte Geowissenschaften

TECHNISCHE UNIVERSITÄT DARMSTADT

Stephan Schulz

Dissertation
Thema: "Experimental and numerical studies on the water balance of the Upper Mega Aquifer system, Arabian Peninsula"

Eingereicht am 23. Februar 2017

Referent: Prof. Dr. Christoph Schüth
Korreferent: Prof. Dr. Ralf Merz
1. Prüfer: Prof. Dr. Randolf Rausch
2. Prüfer: Prof. Dr. Ingo Sass
3. Prüfer: Prof. Dr. Wolfgang Ensinger

Prof. Dr. Christoph Schüth
Fachgebiet Hydrogeologie
Institut für Angewandte Geowissenschaften
Technische Universität Darmstadt (D17)
Schnittspahnstraße 9
64287 Darmstadt

Eidesstattliche Erklärung (Declaration of authorship)

Ich erkläre hiermit, die vorliegende Dissertation ohne Hilfe Dritter und nur mit den angegebenen Quellen und Hilfsmitteln angefertigt zu haben. Alle Stellen, die aus Quellen übernommen wurden, sind als solche kenntlich gemacht worden. Diese Arbeit hat in dieser oder ähnlicher Form noch keiner Prüfungsbehörde vorgelegen. Die schriftliche Fassung stimmt mit der elektronischen Fassung überein.

Darmstadt, den 21. Februar 2017

Stephan Schulz

Short CV

Since 02/2016 **Research Assistant at Technische Universität Darmstadt**

Institute of Applied Geosciences, Hydrogeology Group

Research fields:

- Hydrology and Hydrogeology of arid regions
- Numerical groundwater flow modelling
- Conceptual hydrological modelling
- Groundwater recharge

11/2011 to 01/2016 **PhD Student at Helmholtz Centre for Environmental Research**

Department: Catchment Hydrology

PhD-thesis title: "Experimental and numerical studies on the water balance of the Upper Mega Aquifer system, Arabian Peninsula"

10/2005 to 10/2011 **Student at Technische Universität Freiberg**

Studies: Geoecology

Diploma-thesis title: "Groundwater recharge estimation using the hydrological model J2000g in the Zarqa River Catchment, NW-Jordan"

Foreword

This thesis is a cumulative dissertation, which comprises three publications in ISI listed journals. The initial idea of the present research work was the development of a three dimensional, large-scale numerical groundwater model of the Upper Mega Aquifer system on the Arabian Peninsula. I recognised early that the study area bears practically unlimited research potential and that some of the upcoming ideas could also help to improve the intended groundwater model. Form the large pool of ideas, two of the conducted studies yielded quite extensive research projects. Both of these studies broach the issue of water balance components. The first one addresses the process of groundwater recharge in a karst area. The second one deals with the groundwater evaporation from salt pans, which are a very common geographic feature on the Arabian Peninsula. The third and final larger work package encompasses the model set-up and its calibration.

The major part of the work was carried out at the Helmholtz Centre for Environmental Research - UFZ in Halle. Following my time with the UFZ, the thesis was finished at the TU Darmstadt. Furthermore, I undertook seven research trips to Saudi Arabia resulting in altogether approximately six months of field work. This thesis was basically conducted within the framework of the IWAS project funded by the German Federal Ministry of Education and Research (BMBF). Additionally, GIZ IS (Gesellschaft für Internationale Zusammenarbeit – International Services) and Dornier Consulting provided substantial support as our project partner.

Now, just one day ahead of the submission of this thesis, I would like to say some words of thanks. First and foremost, I would like to thank my research buddy Nils Michelsen for sharing all the passion and curiosity for new ideas throughout the last years. I really enjoyed our trips through the deserts of Saudi Arabia, but also the late-night discussions in the office.

I would like to express my gratitude to my mentors Prof. Ralf Merz, Prof. Olaf Kolditz, Prof. Randolf Rausch and Prof. Christoph Schüth for the continuous support and, most importantly, to have enormous trust in me, which allowed me to work as freely as I could do.

During my time at the UFZ, I also had the chance to work with a few students, who supported me during different projects. Big thanks go to Marcel Horovitz for the great support during our salt pan study, to Simon Franchini for the exhausting recharge studies in the sand dunes, to Jan Mahler for the studies on the drilling cores with the micro CT and to Jakob Sohrt for the studies on the TRMM data sets.

Moreover, I would like to mention my colleagues and friends at UFZ, at TU Darmstadt and in Saudi Arabia. I would like to thank all of you for all types of support and also for being good colleagues and friends.

Of course, very special thanks go to my family, friends and Sarah!

Abstract

Besides a few perennial rivers, like the Euphrates, surface water resources are scarce and often not reliable in its temporal availability on the Arabian Peninsula. Consequently, the region relies on its mainly fossil groundwater reserves, which are predominantly stored in the sedimentary formations of the Arabian Platform. One of its major groundwater reservoirs is the Upper Mega Aquifer (UMA) system. The present thesis comprises three major studies on this aquifer system. The first one deals with a specific type of groundwater recharge: the accumulation of surface water and its discharge into karst features like open shafts and sinkholes. In order to quantify the amount of recharge, a combined approach of time-lapse camera monitoring and water balance modelling was applied. Finally, an average groundwater recharge rate of about 5 mm a^{-1} could be estimated for the As Sulb plateau, which constitutes an outcrop area of the Umm Er Radhuma karst aquifer. Moreover, this study discusses the non-linearity of recharge processes in arid environments. The second study deals with the groundwater evaporation from salt pans. During this study, different methods are used to provide a comprehensive picture of this process. These methods include satellite image analysis for the mapping of salt pan areas, isotopic investigations in order to distinguish between groundwater and seawater dominated salt pans, and a column experiment for the quantification of evaporation rates. A combination of these methods suggests a total annual groundwater loss of 1.3 km^3 for the UMA system caused by the evaporation from salt pans. The third study encompasses the set-up and the calibration of a numerical groundwater flow model. In the course of this study, the phenomenon of fossil groundwater gradients is discussed and a novel calibration scheme is introduced. The final part of this thesis applies the model and three different development scenarios for groundwater abstraction are simulated and discussed.

Table of contents

List of figures

List of tables

Abbreviations

a	Year
a.s.l.	Above sea level
ASR	Aquifer storage recovery
b.g.l.	Below ground level
BP	Before present
b.s.l.	Below sea level
°C	Degree centigrade
d	Day
g	Gram
GRACE	Gravity Recovery and Climate Experiment
^{3}H	Tritium
ITCZ	Intertropical Convergence Zone
Fig.	Figure
K	Hydraulic conductivity
ka	One thousand years
kg	Kilogram
km	Kilometer
l	Liter
m	Meter
MAR	Managed aquifer recharge
mg	Milligram
MPa	Mega Pascal
S	Storativity
S_s	Specific storage
S_y	Specific yield
SGD	Submarine groundwater discharge
Tab.	Table
TDS	Total dissolved solids
TU	Tritium Units
UAE	United Arab Emirates
UMA	Upper Mega Aquifer

1 Introduction

1.1 Background and study aim

The Arabian Peninsula is characterized by semi-arid to hyper-arid climatic conditions, which limits the availability of surface water resources in most of its parts (Scanlon et al., 2006). Consequently, more than 80% of the freshwater consumption on the Arabian Peninsula (not considering Iraq) is covered by groundwater withdrawal (FAO, 2016). However, due to its dry climate, these groundwater resources receive only little replenishment. The main aquifer systems on the Arabian Peninsula are even considered as non-renewable, which means that its renewal period is more than 500 years (Margat et al., 2006; Margat and van der Gun, 2013).

Although the definition of water scarcity is surprisingly difficult, the vast majority of studies agree to classify the whole Arabian Peninsula as water scarce (Rijsberman, 2004). Howard and Bartram (2003) defined a lower threshold of 100 l d^{-1} (37 m^3a^{-1}) per capita as the minimum freshwater requirement for all domestic health and hygiene needs. In order to run a modern society, i.e. the water demand of industry and agriculture has to be considered additionally, a minimum of 500 m^3 of freshwater per year and capita is needed (Falkenmark, 1986). However, regions characterized by a freshwater supply of less than 1000 m^3a^{-1} per capita are still considered as water scarce (Falkenmark et al., 1989). The application of these threshold values leads to the conclusion that all countries on the Arabian Peninsula (besides Iraq) have less renewable freshwater resources than needed in order to run a modern society (Fig. 1-1).

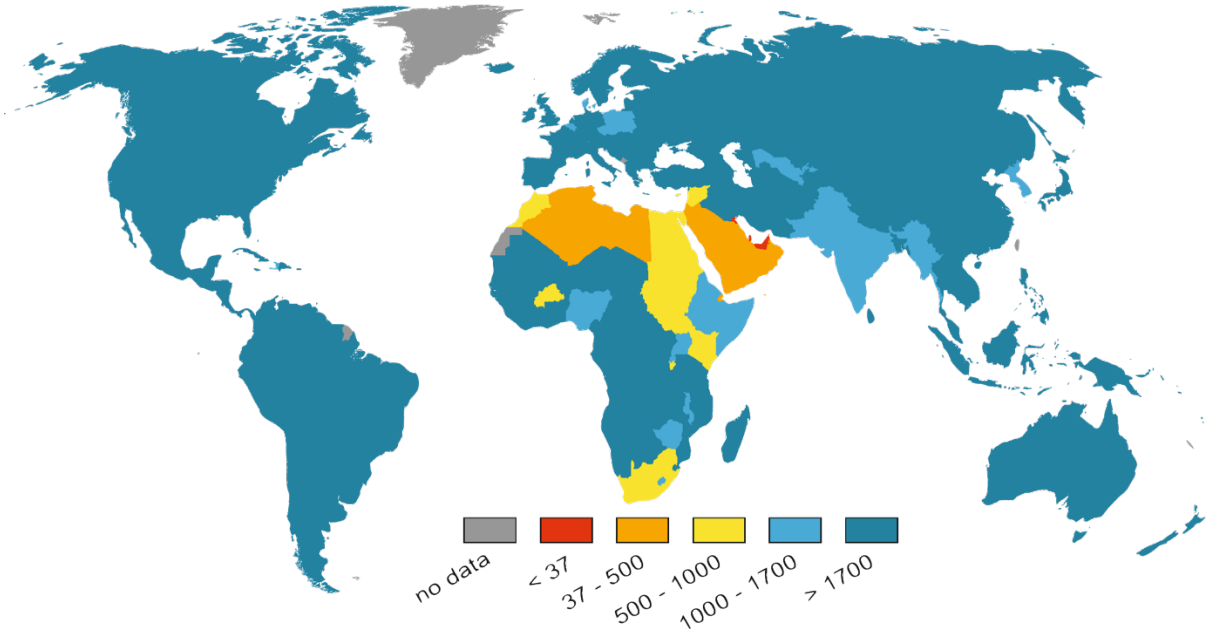

Fig. 1-1: Renewable freshwater resources per capita [m^3a^{-1}] at country-scale for 2015 (FAO, 2016)

Despite their limited renewable freshwater resources, the water demand of the countries on the Arabian Peninsula has dramatically increased over the last decades (Al-Rashed and Sherif, 2000; van der Gun, 2012). This development is caused by various drivers. One of these drivers is the rapid economic and industrial growth after the exploration of the world's largest crude oil reserves. Another one is the ongoing population growth accompanied with rising living standards and increasing per capita water consumption (World Bank, 2005). However, the major factor is the development in the irrigation agriculture. In order to reduce the strong reliance on food imports, especially Saudi Arabia strongly expanded its agricultural productivity (WaterWatch, 2006). Today the agricultural sector is by far the largest water consumer on the Arabian Peninsula (FAO, 2009; World Bank, 2005). The consequence of this increased freshwater demand is a massive overexploitation compared to the availability of renewable freshwater resources (Fig. 1-2).

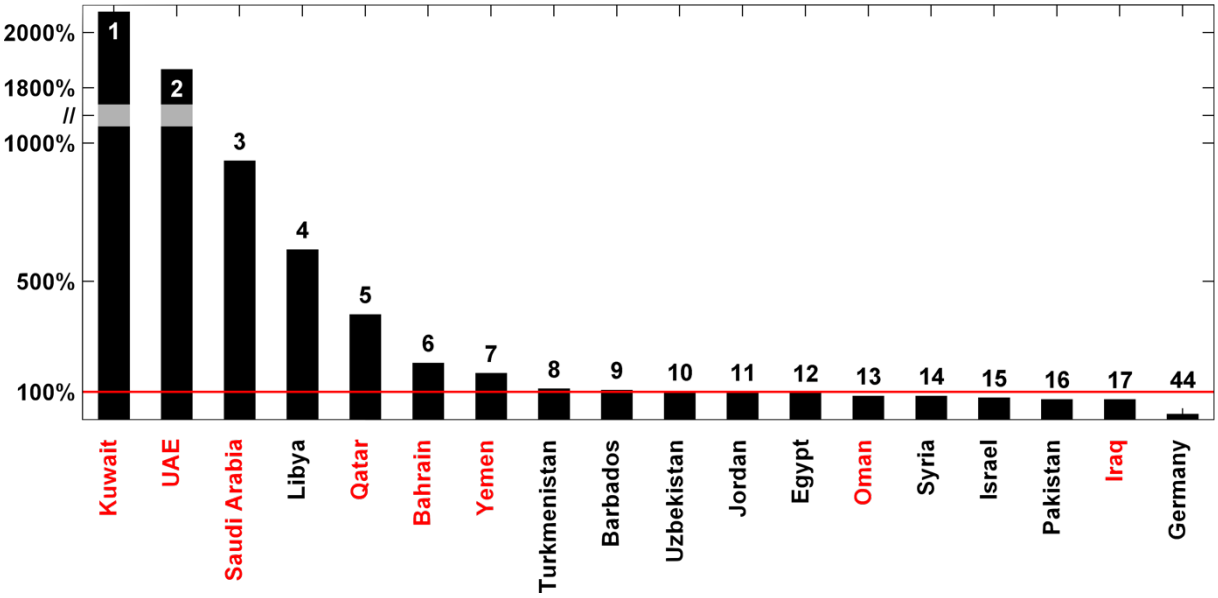

Fig. 1-2: Percentage of freshwater consumption related to the availability of renewable freshwater resources for 2015 (UNDP, 2015)

The outlined water resources situation on the Arabian Peninsula looks very alarming. However, for a complete evaluation of the water resources two main factors are missing.

The first one is the high level of economic development of most of the states of the Arabian Peninsula. Their economic power gives access to non-conventional water resources like seawater desalination and reuse of treated wastewater. These techniques are very promising and have growing potential. Nevertheless, they cannot cover the total water consumption as (i) high transportation costs makes seawater desalination only economically feasible for coastal areas (Zhou and Tol, 2005), (ii) seawater desalination is too expensive for large-scale irrigation agriculture and (iii) treated waste water is only

available in relatively small quantities (World Bank, 2005). Besides these technical solutions, virtual water import via agricultural and industrial products helps to save water. Mekonnen and Hoekstra (2011) calculated for the period between 1996 to 2005 a net virtual water import of about $18 \cdot 10^9$ m^3a^{-1} for Saudi Arabia, which is in the same order of magnitude as its total agricultural water demand (WaterWatch, 2006).

The second major factor, which has to be considered in the evaluation of the water resources of the Arabian Peninsula, is the presence of large fossil groundwater reserves. These fossil resources were filled during wetter periods in the past and are predominantly stored in large sedimentary aquifer systems on the Arabian Platform. Principally, two major aquifer systems can be distinguished: (i) the Lower Mega Aquifer system with the principal aquifers Khuff, Jilh, Minjur, Saq/Disi and Wajid, and (ii) the Upper Mega Aquifer system with the principal aquifers Biyadh, Wasia, Umm Er Radhuma and Dammam (GIZ/DCo, 2013, 2011; GTZ/DCo, 2006; UN-ESCWA and BGR, 2013). These aquifer systems are the backbone of the freshwater water supply for large parts of the Arabian Peninsula. Today, these aquifer systems receive only very limited recharge and they have to be considered as finite. Consequently, wise management schemes must be applied to find a good balance between satisfying today's demand and preserving enough freshwater resources for future generations (Foster and Loucks, 2006; Tsur et al., 1989).

Study aim

The present thesis focuses on one of the major aquifer systems on the Arabian Peninsula: The Upper Mega Aquifer (UMA) system. Generally, two main objectives are pursued. First, this study tries to contribute to the understanding of the UMA system for a better future management. Second, it tries to take part in the scientific discussion about hydro(geo)logical processes in arid environments. To achieve these quite challenging goals, experimental and numerical studies on the water balance of the UMA system were conducted. The three major milestones of this thesis are:

- Analysing groundwater recharge processes (Schulz et al., 2016)
- Estimating the groundwater loss by evaporation from salt pans (Schulz et al., 2015)
- Setting-up and calibrating a numerical groundwater flow model (Schulz et al., 2017)

1.2 Study area

The UMA system comprises a major part Arabian Platform (Fig. 1-3 and Fig. 1-4). In the West and in the South, it is bounded by the outcrops of its geological formations. In the Northwest, it is limited by

a subsurface watershed defined by an important structural high (Hail Arch) close to the Saudi Arabian-Jordan border. In the Northeast, it is limited by the Euphrates and Shatt Al-Arab. In the East, the UMA system is bounded by a virtual line through the deepest areas of the Persian Gulf, also known as the Arabian Gulf. And in the Southeast, it is limited by a major fault at the foot of the Oman Mountains. The bottom of the aquifer system is the Hith aquiclude, which effectively separates the UMA system from underlying aquifers. The top is formed by the Neogene aquifer representing the uppermost unit of the UMA system.

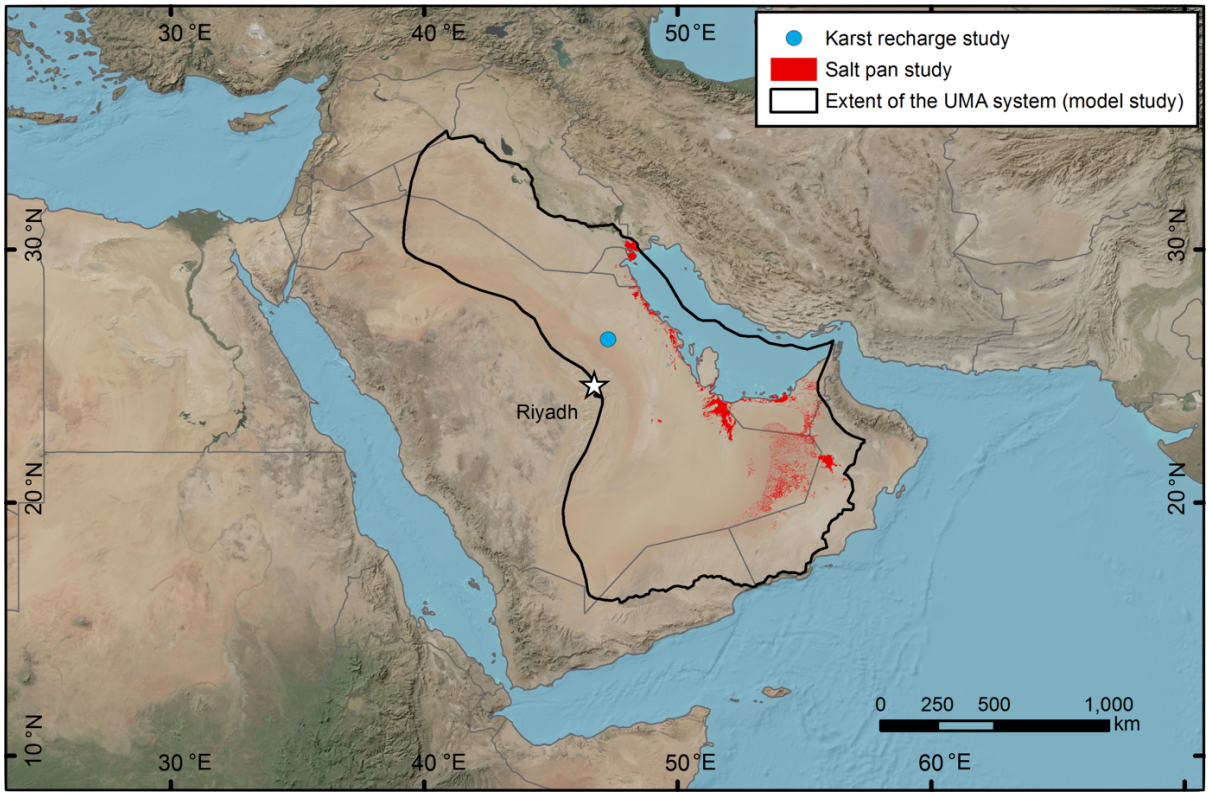

Fig. 1-3: Overview of the study area and location of the major studies cumulated within this thesis (Schulz et al., 2017, 2016, 2015)

Geology

The Arabian Peninsula is separated in two major geologic entities: the Arabian Shield in the West and the Arabian Platform (also called Arabian Shelf) in the East. The Arabian Shield consists of Precambrian rocks and was a part of the African Shield before the Red Sea rifting started in the Cretaceous period. Earlier, the crystalline rocks of the Arabian Shield tilted slightly towards northeast until the Tethys Ocean has transgressed inland to the present limit of the sedimentary beds during the Early Ordovician period. In the following geological ages a successive rising and sinking of the Shield took place, which resulted in a deposition of marine and terrestrial sediments. This process finally formed the sedimentary succession of the Arabian Platform (Powers et al., 1966; Shahin, 2007).

The Upper Mega Aquifer is a part from the Arabian Platform and comprises the sedimentary succession from Lower Cretaceous to the Neogene (Fig. 1-4). The elevation of this succession ranges from about 500 m a.s.l. in its outcrops in the West to about 4000 m b.s.l. in the East. During the deposition of the geological formations, a few tectonic events and sea level fluctuations led to unconformities within the individual sediment strata (GIZ/DCo, 2011).

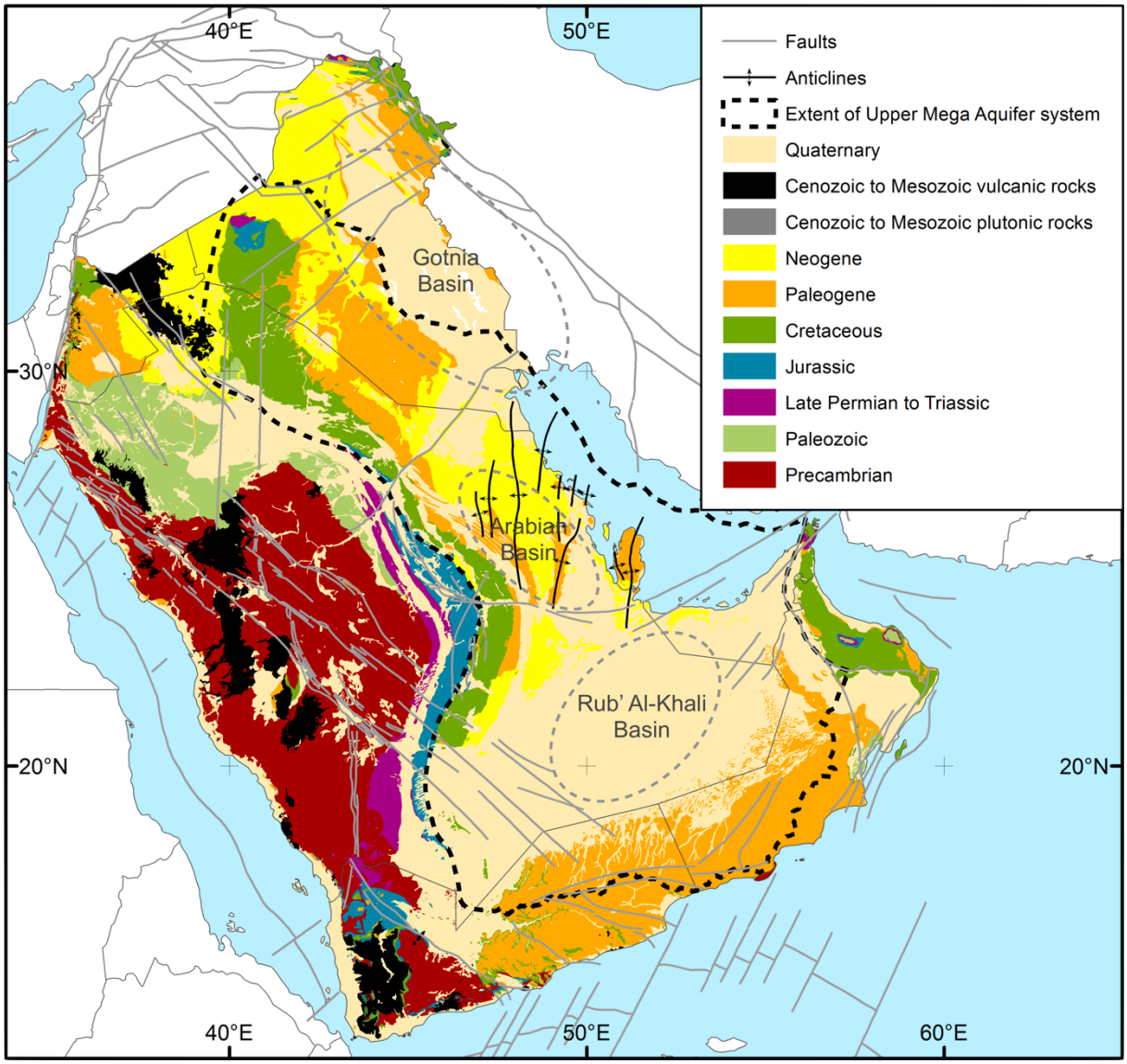

Fig. 1-4: Geological map of the Arabian Peninsula modified after USGS and ARAMCO (1963) and Baniasad et al. (2016)

Climate

The climate of the whole Arabian Peninsula is characterized by high temperatures and low precipitation rates (Fig. 1-5) and therefore, classified as a hot-arid desert climate (Kottek et al., 2006). Mean annual temperatures range from about 20°C in the northern part of the study area to more than

25°C in the Rub' Al Khali desert (Pauw, 2002). Significant differences in temperature are observable between day and night and summer and winter (Fig. 1-5 B). Consequently, summer temperatures of more than 50°C are not uncommon in the Rub' Al Khali desert (Shahin, 2007). Caused by the high temperatures, the potential evaporation ranges on a high level from 2500 mm a^{-1} in coastal areas to 4500 mm a^{-1} in central part of the Rub' Al-Khali desert (Al-Rashed and Sherif, 2000). These differences in potential evaporation are mainly caused by differences in relative humidity (Fig. 1-5 B).

The average annual precipitation in the study area is less than 100 mm on average (Fig. 1-5 A; Pauw, 2002). Generally, no rainfall occurs in the extreme hot and arid summer period from early June to late October. Cyclones, which occurring in the summer month (May and June), and the Indian Monsoon (June to September) originating from the South and strongly influencing the southern part of the Arabian Peninsula (Müller, 2012). However, they are usually not reaching the study area (BRGM, 1977). Rainfall in the study area occurs only in the winter month and is linked with the passage of humid air masses from the Northwest originating the Atlantic and Mediterranean (BRGM, 1977). The interannual variation ranges from almost no precipitation to more than 200 mm per year (BRGM, 1977). Besides the absolute annual amount of rainfall, also its spatiotemporal patterns are important. Convective rainfall leads to extreme spottiness of spatial and temporal precipitation distribution (Wheater, 2010). The erratic nature of the temporal distribution is further discussed in chapter 2 and a novel index, the PDI (precipitation distribution index), is introduced (Schulz et al., 2016).

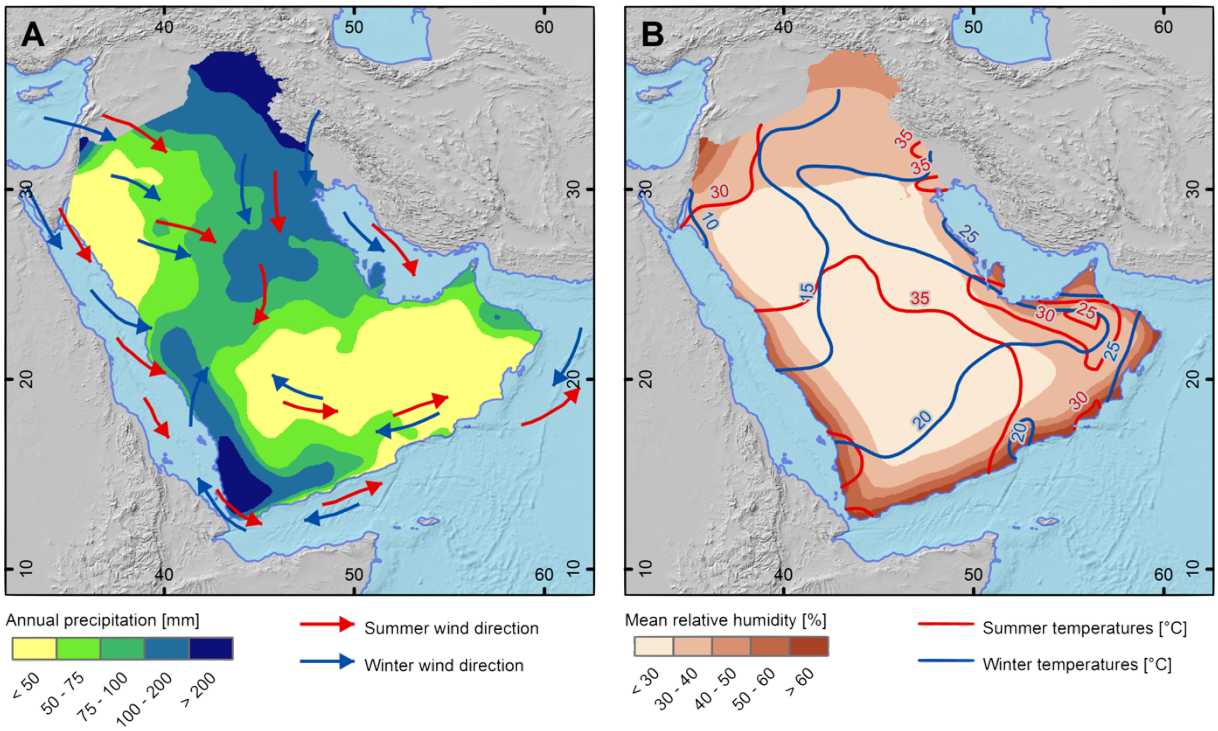

Fig. 1-5: (A) annual precipitation amounts (Kummerow et al., 1998) and prevailing wind directions (Alsharhan et al., 2001); (B) temperature and mean annual relative humidity from reanalysis data sets (Dee et al., 2011)

The climate on the Arabian Peninsula was not constant over time. Various studies report that the Arabian Peninsula has experienced a couple pluvial periods during the Late Pleistocene to Early Holocene (Edgell, 2006; Groucutt and Petraglia, 2012; Sarnthein, 1978). These pluvial periods have an tremendous importance for hydrogeology of the UMA system as it is very likely that the groundwater reserves were filled during these times (Bakiewicz et al., 1982; GIZ/DCo, 2011; Schulz et al., 2017). The last wet period started in the Early Holocene approximately 10 ka BP and gradually recede from about 8 ka BP to 3 ka BP to the present day precipitation rate (Fleitmann et al., 2003). This pluvial was induced by an increased solar radiation (Holocene climatic optimum), which resulted in intensified monsoon and Westerly precipitation (Davis, 1987; Parker et al., 2006). Furthermore, it caused a shift of the Intertropical Convergence Zone (ITCZ) northwards, so that monsoon precipitation reached the southern parts of the study area (Fleitmann et al., 2007).

Although most paleoclimate researchers agree on the wet period in the Early Holocene, only a small number of studies provide quantitative estimates of precipitation rates: (i) 200 ± 50 mm a^{-1} for the Liwa Crescent during the last pluvial period (Wood and Imes, 1995); 150 ± 25 mm a^{-1} for Tayma about 8.5 ka BP (Engel et al., 2012); and minimum 250 mm a^{-1} about 9.3 ka BP and 8.5 to 5.5 ka BP, and 250 mm to 500 mm about 9 ka BP for the Wahiba Sand Sea (Radies et al., 2005). Moreover, Larsen (1983) analysed the remains of mammal fauna and concluded a savanna landscape, which is further supported by a rock art site about 100 km west of Riyadh showing animals like antelopes, ostriches, and buffalos (Annex A 13). These observations fit into the picture drawn by the previously given precipitation rates.

At two different points in time a quantitative information about the spatial distribution of precipitation rates is given. First, present-day precipitation rates are given by the Tropical Rainfall Measurement Mission (Fig. 1-6 B; Kummerow et al., 1998). Second, a global simulation from the Paleoclimate Modeling Intercomparison Project (PMIP2) provides an estimation of annual precipitation amounts for 6 ka BP (Braconnot et al., 2007). Studies conducted by Liu et al. (2007) could show that this simulation provides quite reasonable estimates for north-eastern Africa, which gives some reason for accepting it for the Arabian Peninsula, as well. Based on the combination of both spatial data sets with the relative precipitation change in time (Fig. 1-6 A), provided by Fleitmann et al. (2003), a spatiotemporal precipitation model was set up (Fig. 1-6 C to E). The principal concept of this model is to stretch the relative precipitation curve for each point in time by the ratio of the paleo precipitation model (6 ka BP) and the present-day precipitation.

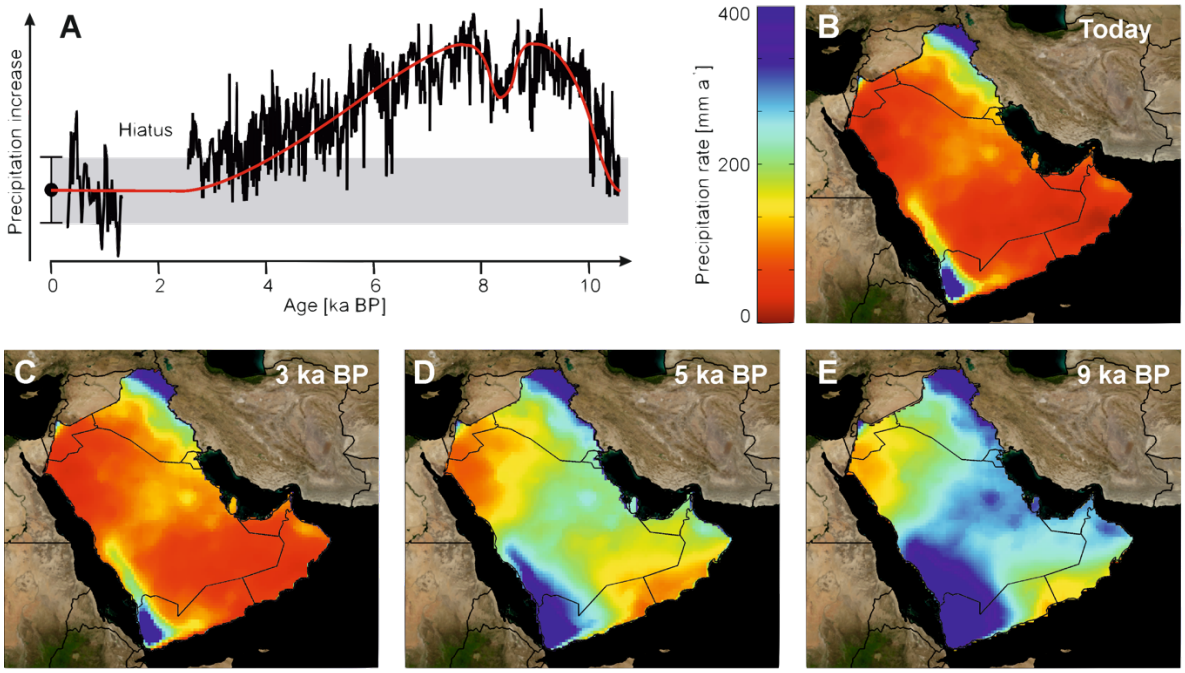

Fig. 1-6: (A) relative change of the precipitation rate during the last 10 ka according to Fleitmann et al. (2003) and Alley et al. (1997); (B) present precipitation rate (Kummerow et al., 1998); (C to E) paleo-precipitation model based on Fleitmann et al. (2003), Kummerow et al. (1998) and Braconnot et al. (2007)

1.3 Hydrogeological setting

The UMA system comprises various geological formations from the Lower Cretaceous to the Neogene. These different geological formations are merged to hydrostratigraphic units following the classification of GIZ/DCo (2014, 2011) and GTZ/DCo (2006). Ten units, consisting of siliciclastic sedimentary rocks, carbonates and evaporates, plus the underlying, sealing Hith anhydrite resulted (Fig. 1-7). In most of its parts, the UMA system is covered by Quaternary surface deposits (e.g. terrace sands, sandy limestone, and salt pan deposits), which are not considered as a part of the aquifer system. The hydrostratigraphic units are the physical framework of the UMA system. Generally, they dip slightly eastwards towards the Persian (Arabian) Gulf. The thickness and the hydraulic properties vary within these units depending on different factors like depositional environment, erosion and tectonics. In the following, these units are described (from the bottom to the top) based on an extensive study by Alsharhan and Nairn (1997).

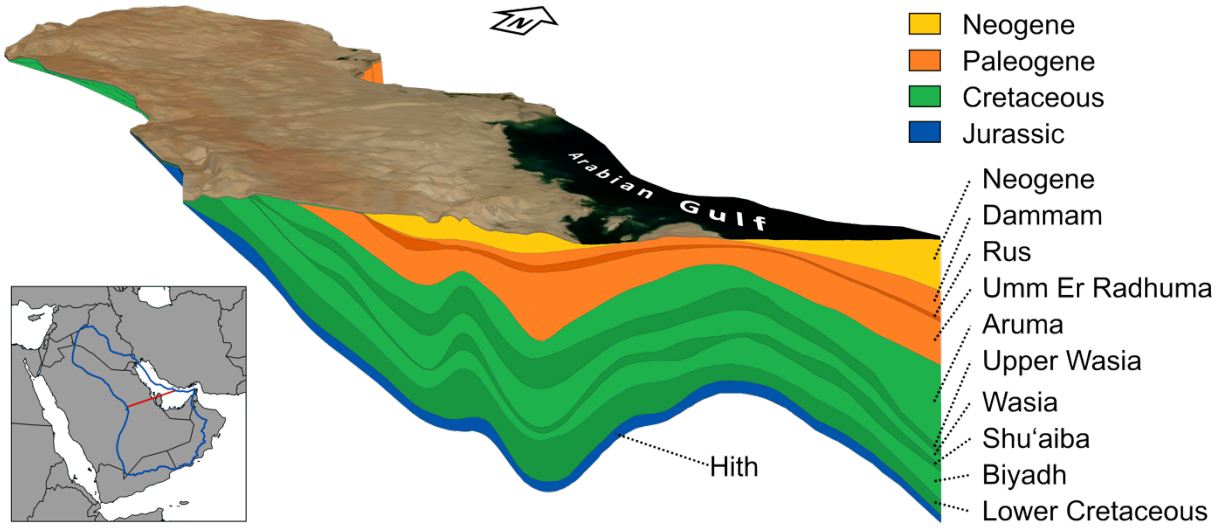

Fig. 1-7: Cross section (length of 705 km) of the UMA system showing its hydrostratigraphic units (vertical exaggeration of 100)

Hydrostratigraphic units

Hith Aquiclude (Late Jurassic, Tithonian): The Hith Anhydrite is the last and most widespread anhydrite unit of the Late Jurassic. It forms an effective seal and separates the UMA system from underlying aquifers in most of its parts. The presence of major oil and gas deposits in the underlying Arab formation and high hydraulic head difference between the UMA system and the underlying aquifers in its eastern parts indicates a good effectiveness of the Hith Aquiclude. It is thickest in the Arabian Basin and thins northward into the Gotnia Basin. In western Abu Dhabi, the Hith formation has a thickness of about 100 m. In Kuwait, its thickness varies from less than 100 m at Dhabi to more than 300 m in the Rugei fields. Saudi Arabia, Bahrain and Qatar it has an average thickness of 140 m, 100 m and 150 m, respectively. In Iraq, the Anhydrite seal is represented by the Gotnia formation, which is about 200 m thick in the type area.

Lower Cretaceous Secondary Aquifer (Early Cretaceous): In Saudi Arabia, the Lower Cretaceous Aquifer comprises the formations Sulaiy, Yamama, and Buwaib. These formations and their local equivalents (e.g. Rayda and Ratawi) mainly consist of interbedded fine grained limestone, mudstone and wackestone, except for the upper part of the Ratawi formation in Kuwait/Iraq (shale and sandstone). The Lower Cretaceous Aquifer prevails over the entire UMA System except for the outermost northwestern part. The Lower Cretaceous Aquifer has an average thickness of 300 m, 400 m, 800 m and up to 900 m in Saudi Arabia, Qatar, Oman, and Kuwait and Iraq, respectively.

Biyadh Principal Aquifer (Early Cretaceous): The lithofacies of the Biyadh formation and its equivalents (e.g. Zubair and Kharaib) follow a gradual change from alluvial sandstones (outcrop areas in the West) to argillaceous mudstones (eastern oil fields of Saudi Arabia) and finally limestones (Qatar,

UAE and Oman). Its thickness varies from 400 m in the outcrop area to more than 600 m in the Ghawar Field, 400 m in Kuwait/Iraq and about 100 m in Oman, Qatar and UAE.

Shu'aiba Aquitard (Early Cretaceous): The Shu'aiba Aquitard consists predominantly of porous/fractured limestone or dolomite with an average thickness of about 100 m. In the basins (e.g. Rub' Al-Khali Basin), the formation is denser and consists of mudstone or wackestone. In the West, the formation is absent and Wasia and Biyadh form one aquifer complex. Generally, vertical leakage through the Shu'aiba Aquitard is very likely.

Wasia Principal Aquifer (Mid Cretaceous): Generally, the Wasia comprises a group of geological formations from the Albian to Turonian time. However, the Wasia Aquifer (Lower Wasia) only consists of the Nahr Umr formation and its equivalents (Khafji, Safaniya and Burgan) from the first half of Albian. The Wasia Aquifer shows some analogies to the Biyadh Aquifer, especially in its outcrops. It is composed of siliciclastic sediments with decreasing thickness and decreasing grain size towards the Southeast. In central Saudi Arabia and Yemen, the Wasia Aquifer consists of 200 to 400 m thick sandstone with a high porosity interbedded with shale and siltstone. The formation reaches its maximum thickness (600 m) in the Rub' Al-Khali Basin. In Kuwait and Iraq, 350 m of well-sorted sands prevail. Towards the Southeast, a succession of limestone and mudstone replaces the sandstone. Thus, in Bahrain, Oman and UAE, it consists predominantly of 150 to 200 m thick argillaceous rocks, shale and marl.

Upper Wasia – Lower Aruma Aquitard/Aquiclude (Mid Cretaceous): Actually, this unit comprises two units (Lower Aruma Aquiclude and Upper Wasia Aquitard), which are merged to a single one. The Lower Aruma Aquiclude consists of about 30 m thick shale and lime mudstone. It is present in the eastern part of the study area and wedges out towards the West. The Upper Wasia Aquitard consists of several formations from the second half of Albian to Turonian. It comprises the members Maudddud, Wara, Ahmadi, Rumaila, and Mishrif. These members are very different. However, they are unified as single members are not large enough to be separated. The basal Mauddud formation consists of limestone interbedded with shale. In most of its parts, it is followed by sandstone (Wara), which is overlaid by shale and limestone. In the Southeast (Oman and UAE) the whole unit consists of limestone. The Upper Wasia Aquitard thins towards the western outcrops and has an average thickness of about 250 m, 350 m and 450 m in Saudi Arabia and Kuwait, in UAE and Qatar, and in Oman, respectively.

The combination of Lower Aruma Aquiclude and Upper Wasia Aquitard forms an effective aquiclude, which separates the Wasia Aquifer from the Aruma Aquifer. This assumption is supported by potentiometric head differences of up to 200 m between both aquifers (GIZ/DCo, 2011). Nevertheless, it is very likely that at some places leakage will occur.

Aruma Secondary Aquifer (Late Cretaceous): The Aruma Aquifer consists of karstified limestone. In the lower part the limestone is interbedded with shale and in the upper part the microporous limestone shows sandy layers. It has an average thickness of about 650 m, 700 m, 750 m and 600 m in Saudi Arabia, in UAE, in Iraq, and in Oman and Kuwait, respectively.

Umm Er Radhuma Principal Aquifer (Paleogene): The Umm Er Radhuma Aquifer consists of karstified limestone. In Saudi Arabia, it is described as a partially dolomitized, microporous (arenitic) limestone with a thickness of about 250 m in the West (outcrop area). In western Iraq, it has a thickness of only 50 to 120 m. Towards the southeastern part of Iraq, the formation becomes thicker and reaches up to 500 m and even up to 650 m in Kuwait. In Qatar, the thickness varies between 270 and 370 m. In the UAE, the lower part of the Umm Er Radhuma Aquifer consists of anhydritic and argillaceous limestone. The upper part consists of limestone interbedded with sandy layers. The total average thickness in the UEA is 370 m. In Oman, the limestone is interbedded with bands of shale and has a thickness of 400 to 650 m.

Rus Aquitard (Paleogene): The Rus Aquitard basically consists of microporous limestone. However, parts of it include layers of gypsum, anhydrite and shale. Those layers have a great influence on the vertical hydraulic conductivity and appear primarily in structural depressions. In the eastern part of Saudi Arabia, the Rus Aquitard consists mainly of limestone with bands of gypsiferous shale and has an average thickness of about 50 m. In Kuwait, the thickness increases to 80 m in the central area, 150 m in the North and even 200 m in the offshore part. In these areas, the limestone alternates with massive, hard, dense anhydrite. In the Southwest of Iraq, the Rus Aquitard has a thickness of up to 100 m and consists predominantly of anhydrite with some limestone, shale and marl. In UAE, dolomitic, argillaceous limestone is followed by massive anhydrites. The total thickness is 100 m in the central part, but thins to the Northeast. In Oman and Yemen, the Rus Aquitard has a thickness of about 130 m, consisting of gypsum and anhydrite with associated dolomite. Depending on the absence of gypsum or anhydrite and the presence of tectonic structures, several hydraulic windows in the Rus Aquitard exist. These hydraulic windows allow cross formation flow between the underlying Umm Er Radhuma Aquifer and the overlying Dammam Aquifer.

Dammam Principal Aquifer (Paleogene): The Dammam Aquifer consists of porous limestone interbedded with marl and shale and is karstified in its upper part. In its outcrops, it has a thickness of only about 30 m, which increases towards East to about 250 m in Iraq, 120 m in southwest Kuwait (offshore 300 m) and 230 m in UAE. The equivalent of Dammam in Yemen is the Habhiya formation (shale alternating with dolomitic limestone) with a thickness of about 250 m. In Oman, Andhur and Qara are the equivalents of Dammam. Together, they have a thickness of about 250 m and consist of porous limestone alternating with shale and marl.

Neogene Secondary Aquifer (Neogene): In Saudi Arabia, mainly three geological units forming the Neogene Aquifer complex. The lowest unit is the Hadrukh, consisting of sandy limestone and calcareous sandstone. It is followed by the Dam, consisting of marl and microporous limestone. And finally, the Hufuf, consisting of marl and sandy limestone. In the UAE, the formations and its local equivalents (Gachsaran, Mishan and Hufuf) are interbedded with massive anhydrite and gypsum layers. The thickness of the Neogene Aquifer increases towards East up to about 650 m in Kuwait and 900 m in the UAE. In Qatar, the Neogene Aquifer is not present.

Complementing maps of aquifer thicknesses are presented in Annex A 1 to A 6.

Aquifer properties

During its formation, the previously described hydrostratigraphic units experienced different depositional environments over space and time. Ziegler (2001) analysed these different depositional environments and mapped the lithofacies distribution for these units. Based on this, nine different hydrofacies types for the UMA system are defined. Hydrofacies types (or zones) are spatial entities showing similar or at least comparable hydrogeological characteristics (hydraulic conductivity and storativity). The concept of these zones is introduced as only a limited number of experimental data, e.g. from pumping test, is available to reliably describe the aquifer properties over the entire study area. The spatial distribution of the hydrofacies zones for the hydrostratigraphic units is presented in Annex A 16.

Parameterization of the hydrofacies zones bases on the description of geological facies and 223 pumping test analyses (Al Abdulkarim, 1982; BRGM, 1976; GDC, 1980a; GIZ/DCo, 2014, 2011; SOGREAH, 1968). All 223 pumping tests were analysed for hydraulic conductivity (K). However, they are very unevenly distributed between the different hydrofacies zones (Tab. 1-1). Thus, only for four zones the hydraulic conductivity could be directly derived from pumping test (Fig. 1-8). Unfortunately, only a minor part of pumping test was conducted with an additional monitoring well. Hence, the geometry of the depression cone could not be analysed in most of the cases, which is a requirement for the determination of the storativity (S). In total, only 33 pumping tests are available for the estimation of S. However, specific storage (S_s) and specific yield (S_y) can only be estimated from pumping tests under confined and unconfined conditions, respectively. As the major part of the UMA system is confined, S_s could be derived from 29 and S_y only from four pumping tests.

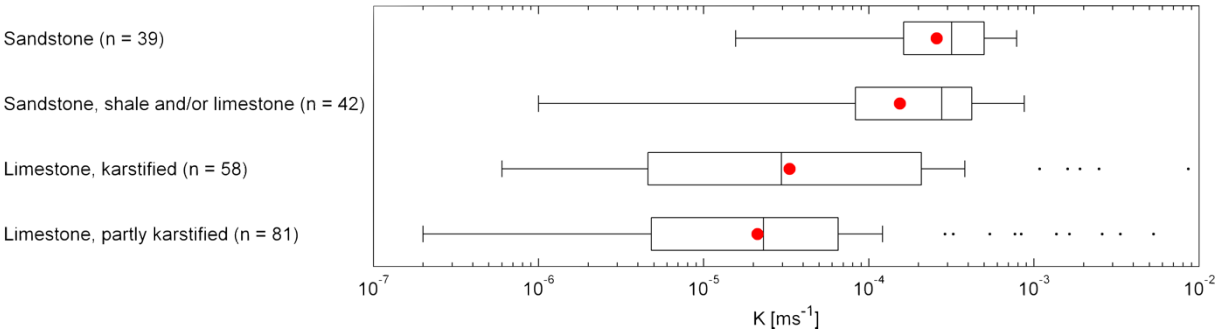

Fig. 1-8: Box plots (maximum whisker length equals 1.5 times the interquartile range) showing the hydraulic conductivities of four hydrofacies zones derived from various pumping tests; the red dot indicates the geometric mean

The major part of aquifer parameters could not directly be derived from pumping tests. Those values were extracted from extensive studies conducted by GIZ/DCo (2014, 2011). They estimated "missing" values based on facies analysis, laboratory tests of drilling cores and experience based knowledge. A summary of aquifer parameters in given in Tab. 1-1.

Calibrated values of horizontal and vertical hydraulic conductivity and specific storage are provided and thoroughly discussed in chapter 4 (Schulz et al., 2017).

Tab. 1-1: Hydraulic properties of all hydrofacies; number in brackets give the number of available pumping tests; * based on pumping test data (geometric mean); all other values based on GIZ/DCo (2014, 2011)

Hydrofacies	K [ms^{-1}]	S_y []	S_s [m^{-1}]
Sandstone	$2.6 \cdot 10^{-4}$ (39) *	0.1 (3)	$2 \cdot 10^{-3}$ (7)
Limestone (karstified)	$3.3 \cdot 10^{-5}$ (58) *	0.026	$4.8 \cdot 10^{-3}$ (0)
Sandstone, shale and/or limestone	$1.5 \cdot 10^{-4}$ (42) *	0.1 (1)	$2.6 \cdot 10^{-4}$ (18) *
Limestone (partly karstified)	$2.1 \cdot 10^{-5}$ (81) *	0.018	$4.2 \cdot 10^{-4}$ (2)
Limestone and dolomite	$3.9 \cdot 10^{-5}$	0.02	$5.6 \cdot 10^{-4}$
Transition zone	$2.5 \cdot 10^{-7}$	0.02	$4 \cdot 10^{-6}$
Limestone (low permeable)	$3.2 \cdot 10^{-9}$	0.025	$3.2 \cdot 10^{-8}$
Shale or limestone and shale	$3.2 \cdot 10^{-10}$ (3)	0.022	$3.2 \cdot 10^{-9}$ (2)
Evaporites	$3.2 \cdot 10^{-11}$	0.016	$3.2 \cdot 10^{-11}$

Potentiometric heads

Groundwater flow direction and volumetric flux depends on the previously described aquifer geometry and its properties, but also on the groundwater head gradients. It is important to note that the

potentiometric head not only depends on the representative water column (static water level in a monitoring well), but also on the density of the water (Post et al., 2007). Therefore, parameters, which have an influence on the groundwater density (temperature and salinity), were mapped during several well survey campaigns (GIZ/DCo, 2014, 2011; GTZ/DCo, 2006). Moreover, the hydrostatic fluid pressure has to be considered as the UMA system (especially the aquifers Wasia and Biyadh) reaches depths of several hundreds of meters. Thus, measured groundwater level data is standardized in order to make them comparable to each other. For standardization, equivalent freshwater heads are used, which were calculated with a set of polynomial equations proposed by Sun et al. (2008). This method is an empirical approach, valid for a temperature range from 0 to 374 °C, a pressure range from 0.1 to 100 MPa and an absolute salinity range from 0 to 40 g/kg. Resulted equivalent freshwater heads for the aquifers of the UMA system are presented in Annex A 1 to A 6.

Natural groundwater flow

The general groundwater flow occurs from the western and southern aquifer outcrop (recharge) areas to the discharge areas in the East. The natural discharge areas of the UMA system are the Persian Gulf and the Euphrates and Shatt Al-Arab, but also the salt pans located mainly at the Gulf coast and in the Rub' Al-Khali desert (chapter 3; Schulz et al., 2015). For the description of the natural flow patterns, it has to be distinguished between the upper and lower part of the UMA system.

The upper part (Paleogene to Neogene) is composed of the Aruma, the Umm Er Radhuma, the Dammam and the Neogene aquifer. These aquifers show an average potentiometric head gradient of about 0.1% with a head range from 350 m a.s.l. in their outcrop areas down to sea level near the Persian Gulf and in the eastern part of the Rub' Al-Khali desert (Annex A 1 to A 4). Their main discharge areas are the groundwater evaporating salt pans, which is further discussed in chapter 4 (Schulz et al., 2017).

The lower part (Cretaceous) is composed of the Wasia and the Biyadh aquifer, which are separated from the overlying aquifers by the shales of the Upper Wasia-Lower Aruma aquitard. As a consequence, the Wasia and the Biyadh aquifer still show potentiometric heads of more than 200 m a.s.l. in the Gulf area, which results in an average head gradient of only about 0.03% (Annex A 5 and A 6). Due to the large hydraulic head gradients between the upper and lower part of the UMA system of more than 200 m under the Gulf and due to the fact that the groundwater flow eastward is inhibited by the Zagros thrust belt, the groundwater of the Wasia/Biyadh aquifer leaks through the shales into the overlying aquifers and subsequently into the Gulf. Hence, the Persian Gulf constitutes the main discharge area of the lower part of the UMA system, which is further discussed in chapter 4 (Schulz et al., 2017).

1.4 Groundwater balance components

Water balance components, also called sinks and source terms, are the driving forces of groundwater systems. In order to understand and manage a groundwater system, a reliable quantification of these terms is of high importance. Not least for this reason, the estimation of selected water balance components is one of the focal points of the present thesis (chapter 2 to 4; Schulz et al., 2017, 2016, 2015).

Due to extensive groundwater withdrawal for irrigation agriculture, industry and domestic supply during the last decades, the natural groundwater balance was considerably changed. Therefore, it has to be distinguished between a pre-industrial (natural) state (Fig. 1-9 A), which lasted approximately until 1950, and a present state (Fig. 1-9 B).

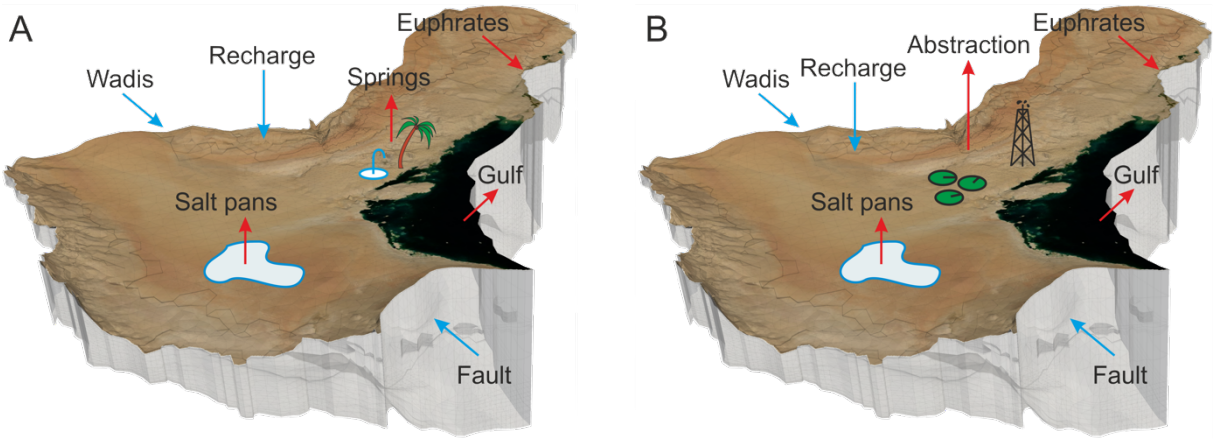

Fig. 1-9: Schematic sketch of sink (red arrows) and source (blue arrows) terms of the UMA system for (A) the natural, pre-industrial state until 1950 and (B) the present state; vertical exaggeration of 100

Groundwater recharge

Groundwater recharge processes for the UMA system are very diverse and yet not completely understood. This is not a particular problem of the UMA system – it is rather a general problem of arid environments. Some difficulties, especially the non-linear nature of recharge processes in dry regions, are discussed by Gee and Hillel (1988) and Schulz et al. (2016, 2013). Another critical, however, solution oriented, overview is given by Kinzelbach et al. (2002).

Groundwater recharge of the UMA system predominantly occurs its western part, because of unconfined conditions and outcropping aquifers. Generally, three different types of natural recharge processes can be distinguished.

The first type is direct groundwater recharge, i.e. rainwater directly percolates through the unsaturated zone to the groundwater (Fig. 1-10 A). This type of recharge might be relevant for the large areas of sand deserts, like the Ad Dahna sand dunes covering the unconfined outcrops of the Umm Er Radhuma aquifer (GDC, 1980b). The occurrence of recent groundwater recharge in these areas was demonstrated by e.g. isotope studies of Dincer et al. (1974).

Second, groundwater recharge can take place indirectly via accumulation of surface water runoff and its subsequent percolation through the beds of the water courses (Fig. 1-10 C). Favourable areas for this type of recharge are the drainage networks of the paleo-river courses (Fig. 1-11), which are often characterized by gravel deposits (GDC, 1980b).

The third type is another type of indirect recharge. During this process, surface water runoff accumulates in channels and discharges through cracks and fissures or karst features like shafts and sinkholes directly into the aquifer (Fig. 1-10 B). This is a very promising type of recharge as already single rainfall events can lead to groundwater recharge (Hartmann et al., 2014). For the case of the As Sulb plateau (part of the Umm Er Radhuma outcrop), this type of recharge was thoroughly investigated during this study (chapter 2; Schulz et al., 2016).

Besides natural groundwater recharge, water authorities aim to artificially replenish the groundwater resources. Those techniques are commonly termed managed aquifer recharge (MAR) or aquifer storage recovery (ASR). For the UMA system, two different types managed aquifer recharge techniques exist: (i) infiltration wells fed by treated sewage effluents (Maliva et al., 2011) or desalinated seawater (Almulla et al., 2005) and (ii) recharge dams mainly fed by accumulated rainwater (Fig. 1-10 D; Al-Turbak and Al-Muttair, 1989). Interesting to note is the phenomenon of unintended artificial groundwater recharge discovered by Michelsen et al. (2016). They observed a rise of the groundwater table caused by the nearby disposal of waste water.

In Annex A 7 an overview of groundwater recharge studies on the Arabian Peninsula is provided. Moreover, Annex A 14 gives a map showing the spatial distribution of groundwater recharge for the UMA systems based on studies by Döll and Fiedler (2008), GDC (1980c), GIZ/DCo (2013) and Thalen (1979).

Fig. 1-10: Different types of groundwater recharge: (A) ongoing studies of direct groundwater recharge in sand dunes; (B) indirect recharge via discharge into karst shafts of the As Sulb plateau; (C) indirect recharge through the beds of Wadi Nissah; (D) ponding water in the recharge dam Al Alb

Other sources

Additional inflow into the Upper Mega Aquifer system originates from the underlying aquifer system via Wadis incising the outcrops of both aquifer systems. In this process, the Quaternary Wadi sediments serve as a hydraulic connection. The total inflow from this source is about $110 \cdot 10^6$ m^3a^{-1} (GIZ/DCo, 2011).

Moreover, an inflow of $44 \cdot 10^6$ m^3a^{-1} into the Neogene aquifer (originating from recharge in the Oman Mountains) via a major fault bounding the UMA system in the Southeast is assumed (GIZ/DCo, 2014).

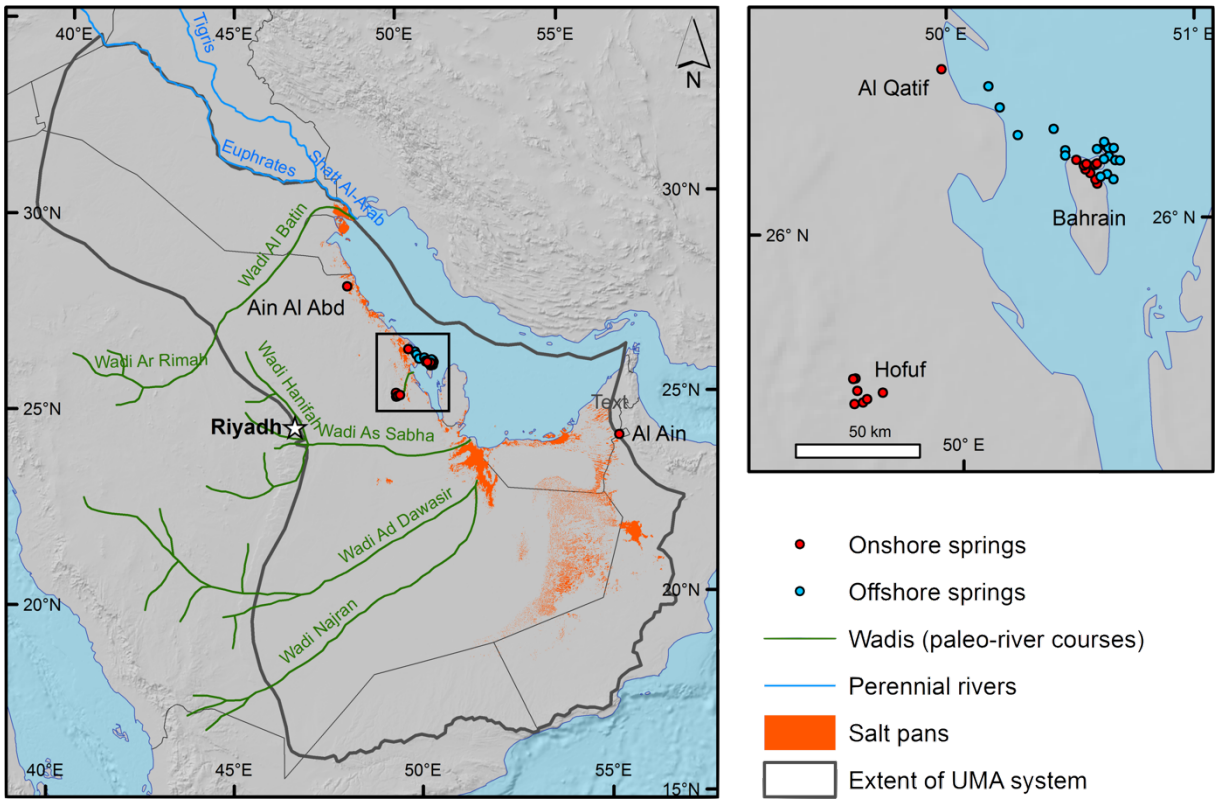

Fig. 1-11: Overview map showing the location of major springs (Al Tokhais and Rausch, 2008; GDC, 1980b), paleo-river courses (Beineke, 2006; Rausch et al., 2013) and the spatial distribution of salt pans (Schulz et al., 2015)

Springs

Springs on the Arabian Peninsula had played an important role in historic times. They formed the basis for settlements and served as water and food sources along the caravan routes of the Arabian Bedouins (Bazuhair and Hussein, 1990). Particularly noteworthy is the Dilmun culture, which developed more than 5000 years ago on the island of Bahrain in the Persian Gulf. This early civilization was known for its trading activities and its wealthy state of life. The fundamental requirement for the development of that culture was the availability of freshwater, which was provided by numerous onshore and offshore karst springs in the northern part of the island and off its coast (Fig. 1-12 B). The tremendous importance of these springs even explains the etymology of the word “Bahrain”, which literally means “two seas”. This refers to the belief of the existence of two oceans: a salty ocean (Persian Gulf) and an underlying freshwater ocean (groundwater system) feeding the springs (Rausch et al., 2014). Another important example is Al-Hasa (Hofuf) in the Eastern Province of Saudi Arabia, where 159 springs with a total discharge in the early 1950s of 316 10^6 m^3a^{-1} formed one of the largest oases of the world (Fig. 1-12 C; Al Tokhais and Rausch, 2008; MoAW, 1984).

Fig. 1-12: (A) submarine karst spring Ghumisa off the coast of Saudi Arabia (GDC, 1980b); (B) discharge measurement of a submarine spring off the coast of Bahrain (GDC, 1980d); (C) Ayn Al-Harrah (Hofuf) in the mid 1930s (MoAW, 1984); Ayn Al Abd in 2010 (photographed by Nils Michelsen)

The major part of springs draining the UMA system are located in the Eastern Province of Saudi Arabia and on the island Bahrain. They were mainly found in and in the vicinity of the cities Al Qatif, Hofuf (Fig. 1-12 C), and Manamah. Besides, numerous offshore springs were located off the north coast of Bahrain and Saudi Arabia near Dammam and Al Qatif (Fig. 1-12 A and B). Al Tokhais and Rausch (2008) estimated a total discharge of all major springs for the beginning of the last century of about $0.5 \cdot 10^9$ m^3 a^{-1}. Due to a falling groundwater level, caused by intensive groundwater abstraction, these springs experienced a strong decrease in its discharge until almost all dried up during the last decades (Al Tokhais and Rausch, 2008).

The discharge of onshore and offshore springs in Bahrain was investigated during several studies over the last decades (Al-Mansour and Al-Aradi, 1986; Al-Noaimi, 2004; BAPCO, 1953; GDC, 1980d; Heim, 1924; Italconsult, 1971; Shahin, 2007). The resulting temporal development is summarized in Fig. 1-13. Starting with $88.7 \cdot 10^6$ m^3, the total discharge of Bahrain's springs has steadily decreased to only $1.2 \cdot 10^6$ m^3 in the year 2000.

The same trend is observable for the springs of Al Hasa and Al Qatif in Saudi Arabia. MoAW (1984) reported about a total spring discharge rate in Al Hasa of about $316 \cdot 10^6$ m^3a^{-1} for the years 1951/52. This value dropped to $227 \cdot 10^6$ m^3 in 1971 (GDC, 1980a) and to $148 \cdot 10^6$ m^3 in 1989 (Bazuhair and

Hussein, 1990). Interesting to note are extensive studies conducted by divers mapping the shape of the karst caves of the Al Hasa springs (BRGM, 1977). The springs in Al Qatif were investigated by Italconsult (1969) in the period from February 1967 to May 1968. They found 32 active springs with a total discharge rate of $13 \cdot 10^6$ m^3a^{-1} (Job, 1978). Eleven years later in 1989 a discharge rate of only $1.7 \cdot 10^6$ m^3a^{-1} could be observed (Bazuhair and Hussein, 1990). For the three main offshore springs in Saudi Arabia (Ghumisa, Halat Al-Khali, Ayn Mizahim) already in 1978 a total discharge of only $0.26 \cdot 10^6$ m^3 was observed (GDC, 1980b).

Today, active springs can be found only at three locations within the extent of the UMA system. First, the spring Ayn Al Abd, which is located in the northeastern part of Saudi Arabia. During investigations in 2008, a discharge rate of $2.5 \cdot 10^6$ m^3a^{-1} could be measured (GTZ/DCo, 2011). Second, springs in the Euphrates depression in Iraq. Here, two different and not dated values are available: $19 \cdot 10^6$ m^3a^{-1} (Wagner, 2011) and $40 \cdot 10^6$ m^3a^{-1} (UN-ESCWA and BGR, 2013). And third, the thermal spring Bu Sukhanah south of the city Al Ain in the UAE. For this spring, a discharge of $0.96 \cdot 10^6$ m^3 and $2.5 \cdot 10^6$ m^3 could be observed in 1984 and 1991, respectively. Actually, Bu Sukhanah is not draining the UMA system. It belongs to the Western Gravel Aquifer, which is recharged in the Oman Mountains and overlays the UMA system (Rizk and Alsharhan, 2003; Shahin, 2007; UN-ESCWA and BGR, 2013).

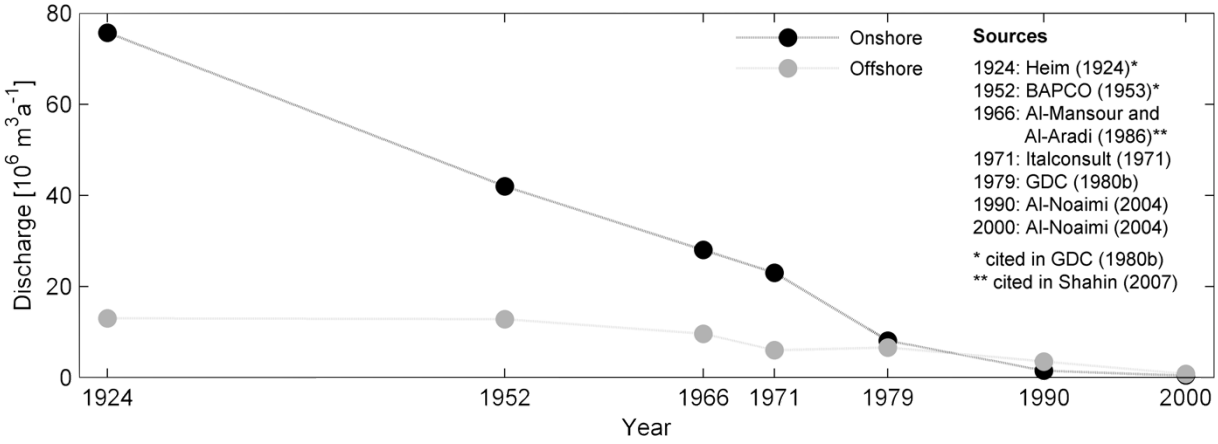

Fig. 1-13: Temporal development of total onshore and offshore spring discharge in Bahrain

Salt pans

Salt pans within the study area are predominantly located at the Persian Gulf coast and in the Rub' Al Khali desert. They are characterized by a shallow water table, which leads to a capillary rise of water to the surface from where it evaporates. Many of these salt pans are fed by groundwater, making them one of the major outflow components of the UMA system. The total area covered by groundwater fed salt pans in the study area is 33,000 km^2. With an annual net groundwater evaporation of about 39

mm, salt pans are responsible for a groundwater loss of about $1.3 \cdot 10^9$ m^3a^{-1} for the UMA system (Schulz et al., 2015).

The study of salt pans and the evaporation from salt pans is a fundamental part of this thesis. A detailed description of this study is presented in chapter 3 (Schulz et al., 2015).

Discharge into the Euphrates and the Shatt Al-Arab

Tigris, Euphrates, Shatt al-Arab and its tributaries form the Mesopotamian plain (Krásný et al., 2006). The old Arabic term of this area is Wadi Ar-Rafedein, which means valley of the two rivers (Shahin, 2007). This area has a tremendous historic importance as it is widely accepted as one of the birthplaces of human civilization handed down through e.g. the tablets of the Epic of Gilgamesh.

Actually, the Euphrates and the Shatt Al-Arab are not directly draining the UMA system. The main part of groundwater discharge occurs indirectly from the Umm Er Radhuma and Dammam karst aquifers (i) via springs (locally forming salt lakes like Sawa and Samawa) and (ii) via upwelling through the alluvial plains, forming swamp-like areas on the river banks (Krásný et al., 2006). Today, the Euphrates and the Shatt Al-Arab are the only rivers draining the UMA system. However, it is important to note that during more pluvial times in the past (described previously in section 1.2) the groundwater level was higher than today, which probably resulted in a few more draining rivers (Fig. 1-11).

A direct quantification of the total amount of groundwater discharging from the UMA system into the Euphrates and Shatt Al-Arab is practically impossible and not much is reported yet. Due to this lack of knowledge the discharge was indirectly estimated in a water balance analysis of a numerical groundwater flow model presented in chapter 4 (Schulz et al., 2017).

Discharge into the Persian Gulf

Besides discrete submarine groundwater discharge (SGD) via springs, the major part of SGD from the UMA system is diffuse leakage from the confined underlying aquifers through the sea floor of the Persian Gulf. Zektser (2007) reported a diffuse discharge rate of $1.0 \cdot 10^9$ m^3a^{-1} for the UMA system, which corresponds in a good approximation to the estimation of $1.2 \cdot 10^9$ m^3a^{-1} derived from the previously mentioned water balance analysis presented in chapter 4 (Schulz et al., 2017).

Groundwater abstraction

Today, man-made groundwater abstraction, especially for irrigation agriculture, is the largest sink of the UMA system. The temporal development of groundwater abstraction from 1950 to 2010 and three different scenarios for its development are presented in chapter 5.

1.5 Numerical groundwater flow model

A major objective of the present thesis is the set-up of a three-dimensional numerical groundwater flow model of the UMA system. The previous sections describe the conceptual base for this model and in chapter 4 (Schulz et al., 2017) the calibration and its challenges are thoroughly presented. Finally, in chapter 5, the model is applied to simulate three different development scenarios for the future groundwater management of the UMA system until the year 2050. All simulations are performed with the numerical open-source modelling package OpenGeoSys (Kolditz et al., 2012).

1.6 References

Al-Mansour, K., Al-Aradi, A., 1986. Country report on water resources and their utilizations in the state of Bahrain. Kuwait.

Al-Noaimi, M.A., 2004. Development of water resources in Bahrain: A combined approach of supply - demand analysis. University of Plymouth.

Al-Rashed, M.F., Sherif, M.M., 2000. Water Resources in the GCC Countries: An Overview. Water Resour. Manag. 14, 59–75. doi:10.1023/A:1008127027743

Al-Turbak, A.S., Al-Muttair, F.F., 1989. Evaluation of dams as a recharge method. Int. J. Water Resour. Dev. 5, 119–124. doi:10.1080/07900628908722423

Al Abdulkarim, A.S., 1982. A Quantitative Study of Wasia Aquifer in Eastern Province of Saudi Arabia. University of Wyoming.

Al Tokhais, A.S., Rausch, R., 2008. The Hydrogeology of Al Hassa Springs, in: The 3rd International Conference on Water Resources and Arid Environments. Riyadh.

Alley, R.B., Mayewski, P.A., Sowers, T., Stuiver, M., Taylor, K.C., Clark, P.U., 1997. Holocene climatic instability: A prominent, widespread event 8200 yr ago. Geology 25, 483. doi:10.1130/0091-7613(1997)025<0483:HCIAPW>2.3.CO;2

Almulla, A., Hamad, A., Gadalla, M., 2005. Aquifer storage and recovery (ASR): A strategic cost-effective facility to balance water production and demand for Sharjah. Desalination 174, 193–204. doi:10.1016/j.desal.2004.08.042

Alsharhan, A.S., Nairn, A.E.M., 1997. Sedimentary Basins and Petroleum Geology of the Middle East. Elsevier, Amsterdam.

Alsharhan, A.S., Rizk, Z.A., Nairn, A.E.M., Bakhit, D.W., Alhajari, S.A., 2001. Hydrogeology of an Arid Region: The Arabian Gulf and Adjoining Areas. Elsevier, Amsterdam.

Bakiewicz, W., Milne, D.M., Noori, M., 1982. Hydrogeology of the Umm Er Radhuma aquifer, Saudi Arabia, with reference to fossil gradients. Q. J. Eng. Geol. Hydrogeol. 15, 105–126. doi:10.1144/GSL.QJEG.1982.015.02.03

Baniasad, A., Rabbani, A., Sachse, V.F., Littke, R., Moallemi, S.A., Soleimany, B., 2016. 2D basin modeling study of the Binak Trough, northwestern Persian Gulf, Iran. Mar. Pet. Geol. 77, 882–897. doi:10.1016/j.marpetgeo.2016.07.025

BAPCO, 1953. Submarine springs, general data.

Bazuhair, A.S., Hussein, M.T., 1990. Springs in Saudi Arabia. J. King Abdulaziz Univ. , Earth Sci. 3, 251–257.

Beineke, J., 2006. Spät-quartäre Paläogeographie der Arabischen Halbinsel. Universität Paderborn.

Braconnot, P., Otto-Bliesner, B., Harrison, S., Joussaume, S., Peterchmitt, J.-Y., Abe-Ouchi, A., Crucifix, M., Driesschaert, E., Fichefet, T., Hewitt, C.D., Kageyama, M., Kitoh, A., Laîné, A., Loutre, M.-F., Marti, O.,

Merkel, U., Ramstein, G., Valdes, P., Weber, S.L., Yu, Y., Zhao, Y., 2007. Results of PMIP2 coupled simulations of the Mid-Holocene and Last Glacial Maximum – Part 1: experiments and large-scale features. Clim. Past 3, 261–277. doi:10.5194/cp-3-261-2007

BRGM, 1977. Al Hassa development project groundwater resources study and management programme - The Al Hassa springs study. Riyadh.

BRGM, 1976. Hydrogeological investigations of the Al Wasia aquifer in the Eastern Province of Saudi Arabia. Riyadh.

Davis, A.D., 1987. Determination of mean transmissivity values in the modelling of groundwater flow, in: Solving Problems with Groundwater Models. National Water Well Association, Dublin, OH, pp. 1162–1173.

Dee, D.P., Uppala, S.M., Simmons, A.J., Berrisford, P., Poli, P., Kobayashi, S., Andrae, U., Balmaseda, M.A., Balsamo, G., Bauer, P., Bechtold, P., Beljaars, A.C.M., van de Berg, L., Bidlot, J., Bormann, N., Delsol, C., Dragani, R., Fuentes, M., Geer, A.J., Haimberger, L., Healy, S.B., Hersbach, H., Hólm, E. V., Isaksen, L., Kållberg, P., Köhler, M., Matricardi, M., McNally, A.P., Monge-Sanz, B.M., Morcrette, J.-J., Park, B.-K., Peubey, C., de Rosnay, P., Tavolato, C., Thépaut, J.-N., Vitart, F., 2011. The ERA-Interim reanalysis: configuration and performance of the data assimilation system. Q. J. R. Meteorol. Soc. 137, 553–597. doi:10.1002/qj.828

Dincer, T., Al-Mugrin, A., Zimmermann, U., 1974. Study of the infiltration and recharge through the sand dunes in arid zones with special reference to the stable isotopes and thermonuclear tritium. J. Hydrol. 23, 79–109. doi:10.1016/0022-1694(74)90025-0

Döll, P., Fiedler, K., 2008. Global-scale modeling of groundwater recharge. Hydrol. Earth Syst. Sci. 12, 863–885. doi:10.5194/hess-12-863-2008

Edgell, H.S., 2006. Arabian Deserts: Nature, Origin and Evolution. Springer Netherlands, Dordrecht. doi:10.1007/1-4020-3970-0

Engel, M., Brückner, H., Pint, A., Wellbrock, K., Ginau, A., Voss, P., Grottker, M., Klasen, N., Frenzel, P., 2012. The early Holocene humid period in NW Saudi Arabia – Sediments, microfossils and palaeo-hydrological modelling. Quat. Int. 266, 131–141. doi:10.1016/j.quaint.2011.04.028

Falkenmark, M., 1986. Fresh Water: Time for a Modified Approach. Ambio 15, 192–200.

Falkenmark, M., Lundqvist, J., Widstrand, C., 1989. Macro-scale water scarcity requires micro-scale approaches. Aspects of vulnerability in semi-arid development. Nat. Resour. Forum 13, 258–67.

FAO, 2016. AQUASTAT Main Database [WWW Document]. URL www.fao.org/nr/aquastat/ (accessed 3.21.16).

FAO, 2009. Irrigation in the Middle East region in figures - AQUASTAT Survey - 2008, FAO Water Reports. Food and Agriculture Organization of the United Nations (FAO), Rome.

Fleitmann, D., Burns, S.J., Mangini, A., Mudelsee, M., Kramers, J., Villa, I., Neff, U., Al-Subbary, A.A., Buettner, A., Hippler, D., Matter, A., 2007. Holocene ITCZ and Indian monsoon dynamics recorded in stalagmites from Oman and Yemen (Socotra). Quat. Sci. Rev. 26, 170–188. doi:10.1016/j.quascirev.2006.04.012

Fleitmann, D., Burns, S.J., Mudelsee, M., Neff, U., Kramers, J., Mangini, A., Matter, A., 2003. Holocene forcing of the Indian monsoon recorded in a stalagmite from southern Oman. Science 300, 1737–9. doi:10.1126/science.1083130

Foster, S., Loucks, D.P., 2006. Non-renewable groundwater resources - A guidebook on socially-sustainable management for water-policy makers. UNESCO, Paris.

GDC, 1980a. Umm Er Radhuma Study - Volume 3: Groundwater Resources. Cambridge.

GDC, 1980b. Umm Er Radhuma Study - Volume 3: Hydrology. Cambridge.

GDC, 1980c. Bahrain Study - Volume 3: Hydrology. Cambridge.

GDC, 1980d. Umm Er Radhuma Study - Volume 3: Bahrain Springs. Cambridge.

Gee, G.W., Hillel, D., 1988. Groundwater recharge in arid regions: Review and critique of estimation methods. Hydrol. Process. 2, 255–266. doi:10.1002/hyp.3360020306

GIZ/DCo, 2014. Detailed Groundwater Resources Studies in the Rub' Al Khali Desert. Riyadh.

GIZ/DCo, 2013. Detailed Groundwater Resources Studies of Khuff Jilh Minjur Dhruma and overlying Aquifers. Riyadh.

GIZ/DCo, 2011. Detailed Water Resources Studies of Wasia-Biyadh and Aruma Aquifers. Riyadh.

Groucutt, H.S., Petraglia, M.D., 2012. The prehistory of the Arabian peninsula: Deserts, dispersals, and demography. Evol. Anthropol. Issues, News, Rev. 21, 113–125. doi:10.1002/evan.21308

GTZ/DCo, 2011. Hydrochemical Study of Ayn Al Abd (Wasia-Biyadh-Aruma Water Resources Studies). Riyadh.

GTZ/DCo, 2006. Investigations of Updating Groundwater Mathematical Model(s) for the Umm Er Radhuma and Overlying Aquifers. Riyadh.

Hartmann, A., Mudarra, M., Andreo, B., Marín, A., Wagener, T., Lange, J., 2014. Modeling spatiotemporal impacts of hydroclimatic extremes on groundwater recharge at a Mediterranean karst aquifer. Water Resour. Res. 50, 6507–6521. doi:10.1002/2014WR015685

Heim, A., 1924. Report on spring flows.

Howard, G., Bartram, J., 2003. Domestic Water Quantity, Service Level and Health. Geneva.

Italconsult, 1971. Water and agricultural studies in Bahrain.

Italconsult, 1969. Water and agricultural development surveys for areas II and III. Rome.

Job, C., 1978. Hydrochemical investigations in the areas of Al Qatif and Al Hasa with some remarks on water samples from Wadi Al Miyah and Wadi As Sah'ba near Haradh, in: Al-Sayari, S.S., Zötl, J.G. (Eds.), Quaternary Period in Saudi Arabia. Springer, Wien/New York, pp. 93–135.

Kinzelbach, W., Aeschbach, W., Alberich, C., Goni, I.B., Beyerle, U., Brunner, P., Chiang, W.-H., Rueedi, J., Zoellmann, K., 2002. A Survey of Methods for Groundwater Recharge in Arid and Semi-arid regions. Nairobi, Kenya.

Kolditz, O., Bauer, S., Bilke, L., Böttcher, N., Delfs, J.O., Fischer, T., Görke, U.J., Kalbacher, T., Kosakowski, G., McDermott, C.I., Park, C.H., Radu, F., Rink, K., Shao, H., Shao, H.B., Sun, F., Sun, Y.Y., Singh, A.K., Taron, J., Walther, M., Wang, W., Watanabe, N., Wu, Y., Xie, M., Xu, W., Zehner, B., 2012. OpenGeoSys: an open-source initiative for numerical simulation of thermo-hydro-mechanical/chemical (THM/C) processes in porous media. Environ. Earth Sci. 67, 589–599. doi:10.1007/s12665-012-1546-x

Kottek, M., Grieser, J., Beck, C., Rudolf, B., Rubel, F., 2006. World Map of the Köppen-Geiger climate classification updated. Meteorol. Zeitschrift 15, 259–263. doi:10.1127/0941-2948/2006/0130

Krásný, J., Alsam, S., Jassim, S.Z., 2006. Hydrogeology, in: Jassim, S.Z., Goff, J.C. (Eds.), Geology of Iraq. Dolin, Prague, pp. 251–287.

Kummerow, C., Barnes, W., Kozu, T., Shiue, J., Simpson, J., 1998. The Tropical Rainfall Measuring Mission (TRMM) Sensor Package. J. Atmos. Ocean. Technol. 15, 809–817. doi:10.1175/1520-0426(1998)015<0809:TTRMMT>2.0.CO;2

Larsen, C.E., 1983. Life and Land Use on the Bahrain Islands. The University of Chicago Press, Chicago.

Liu, Z., Wang, Y., Gallimore, R., Gasse, F., Johnson, T., DeMenocal, P., Adkins, J., Notaro, M., Prentice, I.C., Kutzbach, J., Jacob, R., Behling, P., Wang, L., Ong, E., 2007. Simulating the transient evolution and abrupt change of Northern Africa atmosphere–ocean–terrestrial ecosystem in the Holocene. Quat. Sci. Rev. 26, 1818–1837. doi:10.1016/j.quascirev.2007.03.002

Maliva, R.G., Missimer, T.M., Winslow, F.P., Herrmann, R., 2011. Aquifer Storage and Recovery of Treated Sewage Effluent in the Middle East. Arab. J. Sci. Eng. 36, 63–74. doi:10.1007/s13369-010-0011-y

Margat, J., Foster, S., Droubi, A., 2006. Concept and importance of non-renewable resources, in: Foster, S., Loucks, D.P. (Eds.), Non-Renewable Groundwater Resources - A Guidebook on Socially-Sustainable Management for Water-Policy Amakers. UNESCO, Paris, p. 97.

Margat, J., van der Gun, J., 2013. Groundwater around the World: A Geographic Synopsis. CRC Press/Taylor & Francis Group.

Mekonnen, M.M., Hoekstra, A.Y., 2011. National water footprint accounts: the green, blue and grey water footprint of production and consumption. Delft.

Michelsen, N., Dirks, H., Schulz, S., Kempe, S., Al-Saud, M., Schüth, C., 2016. YouTube as a crowd-generated water level archive. Sci. Total Environ. 568, 189–195. doi:10.1016/j.scitotenv.2016.05.211

MoAW, 1984. Water Atlas of Saudi Arabia. Ministry of Agriculture and Water, Riyadh.

Müller, T., 2012. Recharge and residence times in an arid area aquifer. Technische Universität Dresden.

Parker, A.G., Goudie, A.S., Stokes, S., White, K., Hodson, M.J., Manning, M., Kennet, D., 2006. A Record of Holocene Climate Change from Lake Geochemical Analyses in Southeastern Arabia. Quat. Res. 66, 465–476. doi:10.1016/j.yqres.2006.07.001

Pauw, E. De, 2002. An Agroecological Exploration of the Arabian Peninsula. ICARDA - International Center for Agricultural Research in the Dry Areas, Dubai.

Post, V., Kooi, H., Simmons, C., 2007. Using Hydraulic Head Measurements in Variable-Density Ground Water Flow Analyses. Ground Water 45, 664–671. doi:10.1111/j.1745-6584.2007.00339.x

Powers, R.W., Ramirez, C.D., Redmond, C.D., Elberg, E.L., 1966. Geology of the Arabian Peninsula: Sedimentary Geology of Saudi Arabia. U.S. Geological Survey, Washington.

Radies, D., Hasiotis, S.T., Preusser, F., Neubert, E., Matter, A., 2005. Paleoclimatic significance of Early Holocene faunal assemblages in wet interdune deposits of the Wahiba Sand Sea, Sultanate of Oman. J. Arid Environ. 62, 109–125. doi:10.1016/j.jaridenv.2004.09.021

Rausch, R., Dirks, H., Al-Ajmi, H., 2013. Zur Hydrogeologie des „Oberen Mega-Aquifer-Systems“ auf der Arabischen Halbinsel, in: Simon, T. (Ed.), Jh. Ges. Naturkde. Württemberg, Sonderband. pp. 119–146.

Rausch, R., Dirks, H., Kallioras, A., Schüth, C., 2014. The Riddle of the Springs of Dilmun-Does the Gilgamesh Epic Tell the Truth? Groundwater 52, 640–644. doi:10.1111/gwat.12214

Rijsberman, F.R., 2004. Water Scarcity: Fact or Fiction?, in: 4th International Crop Science Congress. Brisbane.

Rizk, Z.S., Alsharhan, A.S., 2003. Water resources in the United Arab Emirates. pp. 245–264. doi:10.1016/S0167-5648(03)80022-9

Sarnthein, M., 1978. Sand deserts during glacial maximum and climatic optimum. Nature. doi:10.1038/272043a0

Scanlon, B.R., Keese, K.E., Flint, A.L., Flint, L.E., Gaye, C.B., Edmunds, W.M., Simmers, I., 2006. Global synthesis of groundwater recharge in semiarid and arid regions. Hydrol. Process. 20, 3335–3370. doi:10.1002/hyp.6335

Schulz, S., de Rooij, G.H., Michelsen, N., Rausch, R., Siebert, C., Schüth, C., Al-Saud, M., Merz, R., 2016. Estimating groundwater recharge for an arid karst system using a combined approach of time-lapse camera monitoring and water balance modelling. Hydrol. Process. 30, 771–782. doi:10.1002/hyp.10647

Schulz, S., Horovitz, M., Rausch, R., Michelsen, N., Mallast, U., Köhne, M., Siebert, C., Schüth, C., Al-Saud, M., Merz, R., 2015. Groundwater evaporation from salt pans: Examples from the eastern Arabian Peninsula. J. Hydrol. 531, 792–801. doi:10.1016/j.jhydrol.2015.10.048

Schulz, S., Siebert, C., Rödiger, T., Al-Raggad, M.M., Merz, R., 2013. Application of the water balance model J2000 to estimate groundwater recharge in a semi-arid environment: a case study in the Zarqa River catchment, NW-Jordan. Environ. Earth Sci. 69, 605–615. doi:10.1007/s12665-013-2342-y

Schulz, S., Walther, M., Michelsen, N., Rausch, R., Dirks, H., Al-Saud, M., Merz, R., Kolditz, O., Schüth, C., 2017. Improving large-scale groundwater models by considering fossil gradients. Adv. Water Resour. accepted.

Shahin, M., 2007. Water Resources and Hydrometeorology of the Arab Region, Water Science and Technology Library. Springer Netherlands, Dordrecht. doi:10.1007/1-4020-5414-9

SOGREAH, 1968. Water and Agricultural Development Studies in Area V. Riyadh.

Sun, H., Feistel, R., Koch, M., Markoe, A., 2008. New equations for density, entropy, heat capacity, and potential temperature of a saline thermal fluid. Deep Sea Res. Part I Oceanogr. Res. Pap. 55, 1304–1310. doi:10.1016/j.dsr.2008.05.011

Thalen, D.. C.P., 1979. Ecology and Utilization of Desert Shrub Rangelands in Iraq. Springer Netherlands, Dordrecht. doi:10.1007/978-94-009-9622-9

Tsur, Y., Park, H., Issar, A., 1989. Fossil groundwater resources as a basis for arid zone development? Int. J. Water Resour. Dev. 5, 191–201. doi:10.1080/07900628908722433

UN-ESCWA, BGR, 2013. Inventory of Shared Water Resources in Western Asia. United Nations Publication, Beirut.

UNDP, 2015. Human Development Report. New York.

USGS, ARAMCO, 1963. Geologic map of the Arabian Peninsula - U.S. Geological Survey Misc. Inv. Map I-270 A, scale 1:2,000,000.

van der Gun, J., 2012. Groundwater and Global Change: Trends, Opportunities and Challenges. United Nations Educational, Scientific and Cultural Organization, Paris.

Wagner, W., 2011. Groundwater in the Arab Middle East. Springer Berlin Heidelberg, Berlin, Heidelberg. doi:10.1007/978-3-642-19351-4

WaterWatch, 2006. Historic Groundwater Abstractions at National Scale in the Kingdom of Saudi Arabia - An independent remote sensing investigation. Wageningen.

Wheater, H.S., 2010. Hydrological processes, groundwater recharge and surface-water/groundwater interactions in arid and semi-arid areas, in: Wheater, H.S., Mathias, S.A., Lin, X. (Eds.), Groundwater Modelling in Arid and Semi-Arid Areas. Cambridge University Press, Cambridge, p. 156.

Wood, W.W., Imes, J.L., 1995. How wet is wet? Precipitation constraints on late quaternary climate in the southern Arabian Peninsula. J. Hydrol. 164, 263–268. doi:10.1016/0022-1694(94)02551-L

World Bank, 2005. A Water Sector Assessment Report on the Countries of the Cooperation Council of the Arab States of the Gulf.

Zektser, I.S., Dzhamalov, R.G., Everett, L.G., 2007. Submarine Groundwater. CRC Press/Taylor & Francis Group, Boca Raton.

Zhou, Y., Tol, R.S.J., 2005. Evaluating the costs of desalination and water transport. Water Resour. Res. 41, n/a-n/a. doi:10.1029/2004WR003749

Ziegler, M.A., 2001. Late Permian to Holocene Paleofacies Evolution of the Arabian Plate and its Hydrocarbon Occurrences. GeoArabia 6, 445–504.

2 Estimating groundwater recharge for an arid karst system using a combined approach of time-lapse camera monitoring and water balance modelling

Stephan Schulz[a], Gerrit H. de Rooij[a], Nils Michelsen[b], Randolf Rausch[b,c], Christian Siebert[a], Christoph Schüth[b], Mohammed Al-Saud[d], Ralf Merz[a]

[a] Helmholtz Centre for Environmental Research – UFZ, 06120 Halle, Germany

[b] Technische Universität Darmstadt, 64287 Darmstadt, Germany

[c] GIZ International Services, 11461 Riyadh, Saudi Arabia

[d] Ministry of Water and Electricity, Riyadh, Saudi Arabia

2.1 Abstract

Groundwater is the principal water resource in semi-arid and arid environments. Therefore, quantitative estimates of its replenishment rate are important for managing groundwater systems. In dry regions, karst outcrops often show enhanced recharge rates compared with other surface and sub-surface conditions. Areas with exposed karst features like sinkholes or open shafts allow point recharge, even from single rainfall events. Using the example of the As Sulb plateau in Saudi Arabia, this study introduces a cost-effective and robust method for recharge monitoring and modelling in karst outcrops. The measurement of discharge of a representative small catchment ($4.0 \cdot 10^4 m^2$) into a sinkhole, and hence the direct recharge into the aquifer, was carried out with a time-lapse camera. During the monitoring period of two rainy seasons (autumn 2012 to spring 2014), four recharge events were recorded. Afterwards, recharge data as well as proxy data about the drying of the sediment cover are used to set up a conceptual water balance model. The model was run for 17 years (1971 to 1986 and 2012 to 2014). Simulation results show highly variable seasonal recharge–precipitation ratios between 0 and 0.27. In addition to the amount of seasonal precipitation, this ratio is influenced by the interannual distribution of rainfall events. Overall, an average annual groundwater recharge for the doline (sinkhole) catchment on As Sulb plateau of 5.1mm has estimated for the simulation period.

2.2 Introduction

Semi-arid and arid regions represent about 30% of the global terrestrial environment. In these areas, groundwater is the primary water resource because surface water resources are scarce and often unreliable (Scanlon et al., 2006). Consequentially, the replenishment rate of the groundwater resources is a key component of the hydrological cycle and of great importance for water management.

Generally, groundwater recharge highly depends on climatic conditions, and also on surface and sub-surface conditions (de Vries and Simmers, 2002). Especially in semi-arid to arid regions, karst aquifers are often exposed and have no or only a thin soil cover. In those areas, karst features like open shafts, corrosionally extended joints, and sinkholes (which are termed dolines later, after Waltham et al. (2005)) are conduits for point recharge (Ford and Williams, 2007; Goldscheider and Drew, 2007). Rainfall accumulates in channels that funnel the water to these features, through which it discharges directly into the aquifer. In such settings, even single rainfall events can lead to recharge (Hartmann et al., 2014; Somaratne, 2014). Enhanced recharge in semi-arid and arid karst areas is a worldwide phenomenon and can be found for instance in Portugal (de Vries and Simmers, 2002), Europe and Mediterranean (Hartmann et al., 2015), Brazil (Fernandes et al., 2011), Australia (Somaratne, 2014), Syria (Lamoreaux et al., 1989), Lebanon (Rizk and Margane, 2011), and Saudi Arabia (Hötzl, 1995).

An important example of the decline of water resources in arid areas is the Arabian Peninsula. Because of virtual absence of surface water bodies, countries there heavily rely on groundwater resources. The main part of the groundwater is a fossil resource that originates from humid periods during the Holocene and Pleistocene (Hötzl, 1995; Lloyd and Farag, 1978). During the last several decades, the Gulf Cooperation Council countries experienced a rapid population and economic growth. Consequently, water demand increased dramatically, and current withdrawal exceeds replenishment (Al-Rashed and Sherif, 2000). Nevertheless, this recharge is still a key component of the hydrological balance and has to be considered in water management assessments. Quantifying this recharge is particularly difficult given the erratic and sparse nature of recharge events, the limited availability of data regarding the hydrogeological makeup of the region, local meteorology, and the hostile conditions to which measurement equipment is exposed.

Methods to estimate recharge into karst aquifers are often indirect, for instance, by analysing discharge from springs that show a response to recharge events in their vicinity (Allocca et al., 2014; Andreo et al., 2008; Geyer et al., 2008; Jukić and Denić-Jukić, 2004; Schmidt, 2014). When such springs are absent, the chloride mass balance (CMB) approach can be deployed (Scanlon et al., 2006). Jones and Banner (2003) compared oxygen isotopic composition ($\delta\ ^{18}O$) of rainwater and groundwater to estimate the amount and timing of recharge. Others analysed the enrichment of $\delta\ ^{18}O$ in pore water of the unsaturated zone (Allison et al., 1985; Leaney and Herczeg, 1995). It is important to note that stable isotope methods as well as CMB are only valid for diffuse recharge with a reasonably steady influx of water (Wood, 1999). This is usually not the case in arid areas. Moreover, such methods can only be used to estimate recharge for past events – they have no predictive capability and cannot be used in scenario studies (Scanlon et al., 2006).

Besides indirect estimates, groundwater recharge can be measured directly by monitoring dripping water rates in karst caves (McDonald and Drysdale, 2007; Sheffer et al., 2011). This approach obviously

requires an accessible cave system. A less restrictive direct method is monitoring the inflow into exposed karst features like dolines or open shafts. This approach assumes point recharge as the dominant process. Concentrated discharge into the karst system can be measured with different methods, e.g. streamgages (Rosenberry and LaBaugh, 2008), flow meters (Hauwert, 2009; Tobin and Schwartz, 2012), or tipping buckets (Friederich and Smart, 1982). These discharge monitoring systems are prone to clogging and are not always sufficiently robust for harsh arid environment field conditions, which may include extreme temperature fluctuations, sand storms, and significant sediment loads. Additionally, in arid regions, monitoring sites are often located in remote areas, making frequent maintenance difficult.

The direct method of estimating groundwater recharge has potential, but older studies exposed the limitations of the technology available then: The harsh conditions proved to be particularly challenging for equipment with moving parts. One objective of this study is therefore to develop a robust and cost-efficient monitoring strategy for direct measurement of point recharge. We explored the use of a time-lapse camera, observing a v-notch weir. This method is robust and cost-efficient and only requires minimal maintenance. Furthermore, the camera provides information on the drying of the sediment cover. The second objective is to develop a conceptual water balance model for groundwater recharge estimation that is as simple as possible, given the limited capability to collect data in arid areas and the general lack of long time series of data. Generally, this study aims to provide useful methods for other researchers in the field of dry land hydrology and aims to contribute to the important discussion about hydrological processes in arid to semi-arid environments.

2.3 Materials and methods

Study area

The significance of recent groundwater recharge becomes particularly apparent for the karstified Umm Er Radhuma limestone aquifer, one of the major groundwater resources of the Arabian Peninsula. Here, groundwater recharge during the past millennia in the outcrops (e.g. As Sulb Plateau) drove the discharge of former artesian springs in Bahrain, Al Hassa and Al Qatif (Hötzl, 1995; Rausch et al., 2014; Fig. 2-1 A). These springs supported settlements for several thousands of years, until water abstraction from wells since the 1930s caused the water table to decline until finally, the springs went dry in the 1990s (Rausch et al., 2014). Al Tokhais and Rausch (2008) assumed that limiting water abstraction to meet only domestic demand might be able to reactivate the springs in about 20 years. It must be noted though that this estimate relies heavily on recharge data of which the accuracy is difficult to assess.

The As Sulb Plateau is part of the As Summan Plateau, which is located in the northeast of Saudi Arabia (Fig. 2-1 A). It has an area of about 1400 km^2 where the karstified Umm Er Radhuma limestone aquifer

is directly exposed (Hötzl, 1995). The As Sulb Plateau is an endorheic karst area, where small catchments are drained by karst features like dolines, open shafts, and caves (Fig. 2-1 B and C). These catchments have a cover of well-sorted aeolian sand, usually not thicker than a few tens of centimetres. Sieve analysis and statistical evaluation according to Blott and Pye (2001) give a mean grain size of the sand cover of 0.25mm. Because of the thin sediment cover and the omnipresence of the karst features, point recharge induced by sporadic and highly intense precipitation events is assumed to be the dominant recharge process (Hötzl, 1995). The annual precipitation and potential evapotranspiration rate are approximately 90 and 4500 mm, respectively. Usually, rainfall only occurs in the wet season from November to May and is highly variable in time and space (Hötzl et al., 1993). Because of the hyper-arid conditions, there is almost no vegetation cover.

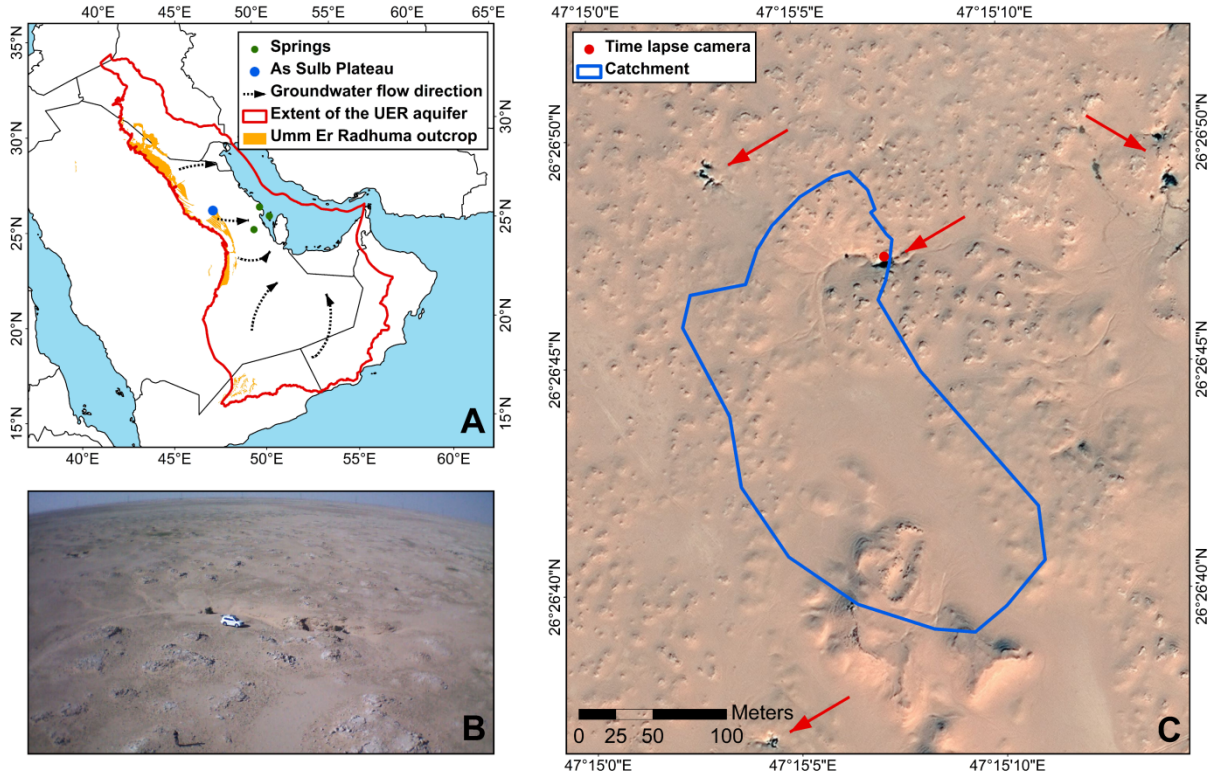

Fig. 2-1: (A) General overview of the study site location; (B) aerial photograph of the investigated catchment (direction of view is north); and (C) extent of the investigated (western) catchment and position of time-lapse camera; red arrows showing the location of karst dolines or open shafts

Previous work

Hötzl et al. (1993) installed a gauging station (float-based stream gauge) at the inflow of a karst shaft for two micro-catchments ($4.0 \cdot 10^4$ m^2 and $9.9 \cdot 10^4$ m^2) on the As Sulb plateau. The work reported here was carried out at the same location. The Hötzl et al. (1993) measuring system ran from 1 March 1987 for 6 weeks and recorded two discharge events per catchment. Both catchments show the same

runoff-precipitation ratio of about 0.01 during two precipitation events of 5 mm in 20 and 25 min, respectively. Independently, they used a simple event-based water balance model in order to estimate recharge over a longer time period. The model accounted for transmission loss in the channel but neglected any water storage. Running the model for a period from 1974 to 1989, Hötzl et al. (1993) estimated an average recharge rate of about 44 mm a^{-1}, which corresponds to a recharge-precipitation ratio of approximately 0.48.

In their study, Hötzl et al. (1993) also report on tritium (^3H) values of rain and groundwater samples collected between 1986 and 1989. For rain water, they found concentrations ranging between approximately 5 and 10 tritium units (TU). These values are consistent with ^3H levels measured in Bahrain precipitation (IAEA/WMO, 2015). Of the 18 analysed groundwater samples, only one had a ^3H concentration above the detection limit, accounting for 1.6 TU. Without knowing the exact mixing ratio between fossil groundwater and a modern recharge component, it was not possible to estimate the mean tritium concentration of the resulting groundwater column. Therefore, it was not possible to derive an exact recharge rate. However, ^3H values of groundwater sampled by Hötzl et al. (1993) and the monitored runoff–precipitation ratio of about 0.01 both indicate that their estimate of 44 mm a^{-1} may be too high.

Meteorological data

Weather data (precipitation, air temperature, relative humidity, solar radiation, and wind speed) have been recorded by Ma'aqla meteorological station, 11 km northeast of the investigated catchment. Continuous time series of daily data are available from 1971 to 1986 and 2012 to present (MoWE, 2014). In 2012, the station was replaced by a new one, providing hourly data. Even though convective rainfall in particular varies strongly on spatial scales smaller than the distance between the weather station and our field site, we adopted this dataset for our site.

The temporal distribution of rainfall is expected to affect the fraction of it that eventually replenishes the aquifer. Heavy and clustered rain showers are likely to generate the most recharge. To quantify this, we introduce a novel precipitation distribution index, which incorporates rainfall amounts, antecedent rainfall, and time between rainfall events for a given time period:

$$PDI = \sum_{k=1}^{n-1} \frac{P_k + P_{k+1}}{\left(S_{k+1} - S_k\right)^2} \tag{2-1}$$

where PDI is the precipitation distribution index (mm day^{-2}), n is the number of rainy days in the time period considered, P_k is the daily sum of rainfall at the kth rainy day (mm), and S_k is the day number of

the kth rainy day since the start of the time period. We calculated the PDI for every year for which reliable records were available, using 1 July as the starting date of a year-long period.

Field site set-up

Numerous karst dolines are spread over the As Sulb plateau. After thoroughly investigating the plateau, we found a doline (26.446 N, 47.252 E; Fig. 2-1 B and C) with a clearly definable catchment and no other draining outlets but the doline. The catchment has a representative sediment cover, and a possibility to fix the camera in a suitable position. This doline has two inflow channels (west and east). We installed a time-lapse camera at the inflow of the western channel, a v-notch weir (90°, maximum notch width of 54 cm), and a scale gauge (2 cm between scale marks) about 1m upstream of the weir. The camera was a trail camera (Bushnell Trophy Cam HD) with an infrared mode, which allows continuous operation day and night. It took pictures in 15-min intervals from 18 November 2012 to 28 September 2014. The data were collected every 6 months.

The camera captured the water level at the gauge as well as the surrounding soil surface. The latter was helpful in determining the time period during which the topsoil remained wet after rainfall. Because of the rarity of discharge events and hence the limited number of images of it, the water level was derived from the photographs by reading the water level at the scale gauge. Afterwards, discharge through the western channel (Q) was calculated based on the water level (h) according to Shen (1981)

$$Q = C\frac{8}{15}\sqrt{2g}\tan\frac{\theta}{2}h^{2.5} \qquad (2\text{-}2)$$

where Q is the discharge ($m^3\ s^{-1}$), C is the coefficient of discharge, g is the gravitational acceleration ($m\ s^{-2}$), θ is the angle included between the sides of the notch (rad), and h is the potentiometric head of the upstream water surface above the vertex of the notch (m). The coefficient of discharge was determined with the Barr–Strickland formula (Shen, 1981) after conversion from feet to metres:

$$C \approx 0.566 + \frac{0.0157}{\sqrt{3.28h}} \qquad (2\text{-}3)$$

with g = 9.81 m s^{-2} and θ = 90°, this expresses Q as a function of h only:

$$Q \approx \left(1.337 + \frac{0.0371}{\sqrt{3.28h}}\right) h^{2.5} \qquad (2\text{-}4)$$

In order to calculate the total amount of discharge per rainfall event, the observed discharges were interpolated (cubic spline) and subsequently estimated by trapezoidal integration of the discharge curve.

From elevation mapping, we estimated the catchment area of the western channel to be $4.0 \cdot 10^4\ m^2$.

2.4 Groundwater recharge model

Water balance

A simple conceptual water balance model was designed to simulate groundwater recharge under our specific conditions. The model operates with daily time steps. Its starting point is the water balance equation for the unsaturated zone:

$$\frac{\mathrm{d}S}{\mathrm{d}t} = P - I - ET - Q - GWR \tag{2-5}$$

where S is the storage in the unsaturated zone (mm), termed soil storage throughout the paper, P is the precipitation rate (mm day^{-1}), I is the interception rate (mm day^{-1}), ET is the evapotranspiration rate (mm day^{-1}), Q is the surface runoff rate leaving the doline catchment (mm day^{-1}), and GWR is the groundwater recharge rate (mm day^{-1}). All variables are time dependent.

The geological settings of the outcrop, with sealed limestone as an impermeable base underneath the sediment cover only permit groundwater recharge through the dolines, which permeate the limestone base (Hötzl et al., 1993). The catchment is only drained by the doline, and no surface runoff is leaving the catchment. Thus, Q is set at zero. Vegetation is very sparse, and consequently, interception is nearly zero, irrespective of the rainfall rate and duration. After rainfall, evaporation is the dominant pathway for transferring water from the unsaturated zone to the atmosphere, except possibly after heavy rains. We therefore approximate actual evapotranspiration by actual evaporation (ET = e_{act}) and assume I to be zero at all times. Because of the small catchment size, we have almost no retention during transmission. These simplifications lead to

$$GWR = \frac{\mathrm{d}SWS}{\mathrm{d}t} + P - e_{act} \tag{2-6}$$

where SWS denotes the soil water storage (mm). The sand cover of the As Sulb plateau has infiltration rates of more than 1 mm min^{-1}, which is usually larger than the precipitation rate (Hötzl et al., 1993). That means that fast interflow or surface runoff in the draining channels, and hence groundwater recharge, only occurs if the soil water storage is full, at which time the storage change dSWS/dt is necessarily zero.

Storage

In our model, we distinguish between two soil water storages (SWS): a top-soil storage (SWS 1) and a main storage (SWS 2). The top-soil storage represents storage in the soil layer directly under the soil surface. This small reservoir reflects the fact that small amounts of rain only moisten the top-soil layer from which it can evaporate readily. SWS 1 is not a physical storage as it is only a part of SWS 2 (Fig. 2-

2). Preliminary calculations indicate that the top-soil storage capacity (SWS 1_{max}) should be rather small to allow the reservoir to fill and empty quickly and not dominate the water dynamics. We therefore set SWS 1_{max} at 6 mm, representing the mean potential evaporation of 1 day during the rainy season (November to May), as established through application of Equations (2-7) to (2-9) for that period. This somewhat arbitrary choice will be scrutinized in a sensitivity analysis.

As soon as the top-soil storage (SWS 1) exceeds its capacity, it completely drains into the main storage (SWS 2). Groundwater recharge occurs if the main storage exceeds its maximum capacity (Fig. 2-2). The capacity of the main storage depends on various catchment properties like channel network, soil texture, and spatial distribution of the soil depth. These properties are difficult to determine. Therefore, the main storage capacity (SWS 2_{max}) will be the fitting parameter of the model. It can be estimated for individual recharge events by calculating the water balance for the period starting after a prolonged dry period so that both SWS 1 and 2 can be assumed zero at that time. According to Equation (2-6), the accumulated difference between rainfall and actual evaporation is collected in storage. By the time groundwater recharge starts for the first time since the start of the calibration period, this collected storage sufficed to fill SWS 2 in excess of its capacity. When groundwater recharge stops, SWS 2 is exactly at its capacity. For the subsequent dry period, this is the starting point, and the water balance between this time and the next groundwater recharge event provides another estimate of the magnitude of SWS 2_{max}.

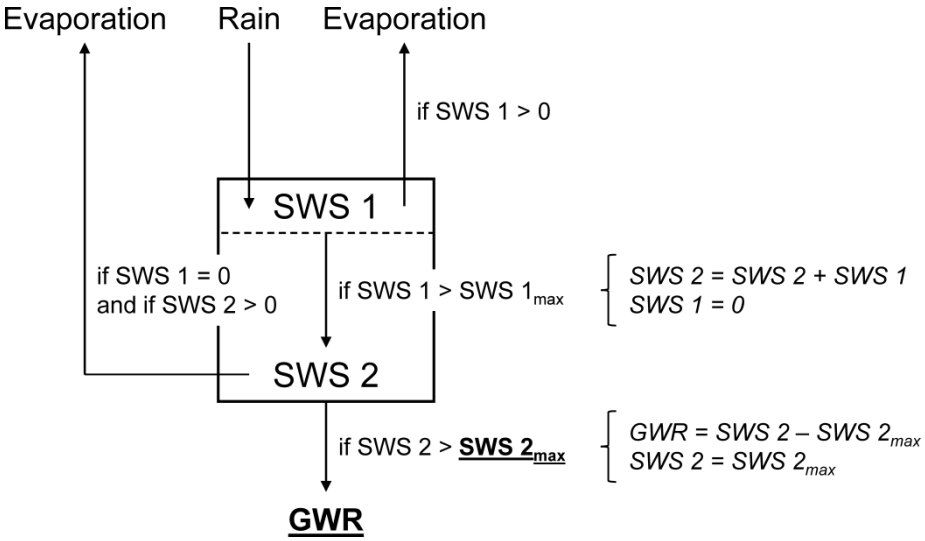

Fig. 2-2: Basic structure of the model with an estimated top-soil storage capacity (SWS 1_{max}) and a main storage capacity (SWS 2_{max}) as the fitting parameter

Evaporation

Evaporation is estimated from the potential evaporation and a reduction function that is related to albedo. This approach dovetails with the use of a camera to monitor water levels because the albedo can be determined from the images that were captured to determine water levels. The method presented later therefore is very well suited for environments that are too harsh or remote for many conventional monitoring sensors.

Potential evaporation is estimated with the simplified Penman (1948) evaporation equation introduced by Valiantzas (2006):

$$e_{pen} \approx 0.047 \times R_S \times \sqrt{T + 9.5} - 2.4 \times \left(\frac{R_S}{R_A}\right)^2 + 0.09 \times (T + 20) \times \left(1 - \frac{RH}{100}\right) \quad (2\text{-}7)$$

with

$$R_A = \begin{cases} 3 \times N \times \sin(0.131 \times N - 0.95 \times lat) & if \quad |lat| \geq 23.5 \times \frac{\pi}{180} \\ 118 \times N^{0.2} \times \sin(0.131 \times N - 0.2 \times lat) & if \quad |lat| < 23.5 \times \frac{\pi}{180} \end{cases} \quad (2\text{-}8)$$

with

$$N = 4 \times lat \times \sin(0.53 \times m - 1.65) + 12 \quad (2\text{-}9)$$

where e_{pen} is the potential evaporation rate (mm day^{-1}), RS is the solar radiation (W m^{-2}), T is the temperature (°C), RA is the incoming solar radiation (MJ m^{-2} day^{-1}), RH is the relative humidity (%), N is the daylight hours (h), lat is the latitude (deg), and m is the rank of the month (1…12).

Actual evaporation [e_{act} (mm day^{-1})] only equals potential evaporation [e_{pot} (mm day^{-1})] (i) as long as water is stored in the top-soil layer (SWS 1) or (ii) through evaporation from SWS 2 for a certain time period after larger rain events (Fig. 2-2). When the soil dries, it can sustain e_{pot} for a limited time only (Idso et al., 1974; Ritchie, 1972). Jackson et al. (1976) and Salvucci (1997) stated that the time at which e_{act} drops below e_{pot} is characterized by an abrupt change of albedo (breakage of liquid connections between water stored in the soil and the surface). We used the photos of the time-lapse camera in order to determine this moment. The first dried soil patches (signalling an abrupt change of albedo) appeared approximately 2 days after significant wetting (Fig. 2-3). Hence, we set the time to drying [during which e_{act} equals e_{pot}; t_d (day)] to 2 days.

Soil hydraulic properties and moisture status are important factors for e_{act}, but difficult to determine over space and time. Salvucci (1997) realized that td is soil dependent and used it as a proxy for other soil characteristics. We adopt his relationship between e_{act}, e_{pot}, and t_d (Salvucci, 1997):

$$e_{act}(t) \cong \begin{cases} e_{pot}(t) & if \quad t < t_d \\ e_{pot}(t) \times \frac{8}{\pi^2} \times \frac{t_d}{t} & if \quad t \geq t_d \end{cases} \tag{2-10}$$

where t is the time after significant wetting (day) (Fig. 2-3).

'Significant wetting' is achieved when the actual evaporation equals potential evaporation again. It is assumed that this amount must be large enough to percolate into deeper soil layers. Thus, the daily sum of rainfall must be large enough that SWS 1 exceeds its capacity and hence drains into SWS 2 (Fig. 2-2) to achieve significant wetting. Note that water from smaller rain events remains in top-soil storage (SWS 1) and evaporates entirely if no additional rain falls.

Obviously, evaporation stops as soon as both SWS 1 and SWS 2 are empty.

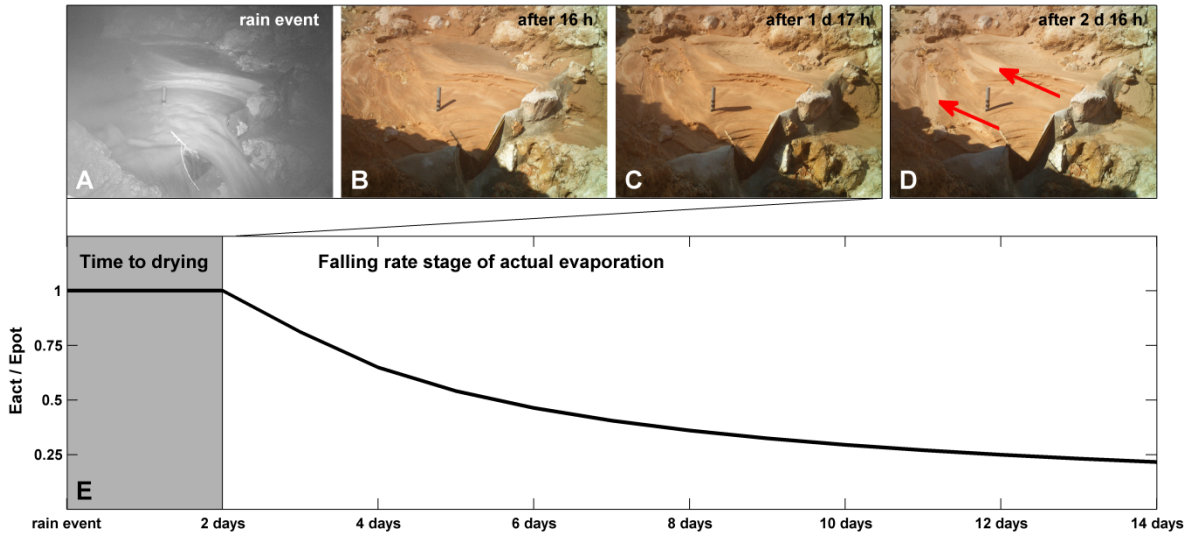

Fig. 2-3: (A) Discharge generated by a large rain event; (B and C) wet soil surface that does not limit evaporation; (D) first dry patches on the soil surface after 2 days (red arrows); and (E) change of actual evaporation–potential evaporation ratio after significant wetting according to the evaporation estimation after Salvucci (1997)

Parameter estimation

The capacity of SWS 2 is the single parameter that requires calibration, and it can be calibrated on groundwater recharge events. The first such event occurred after almost a year into the observation period, which itself started 138 days after the last rainfall. We therefore considered it acceptable to assume that both SWS 1 and 2 were empty at the start of the observation period. For each day at which groundwater recharge started during the observation period, the following mass balance equation applies:

$$SWS2_{\max} = \sum_{i=1}^{G_j} P_i - \sum_{i=1}^{G_j} GWR_i - \sum_{i=1}^{G_j} e_{act,i} \tag{2-11}$$

Here, the individual terms within the sums are all daily accumulated values of the rates for which the symbols stand and therefore have the unit millimetre. The day counter i equals one for the first day of the observation period. G_j denotes the number of days since the start of the observation period that passed when groundwater recharge event j started. Values for P_i were taken from the nearest weather station, and $e_{act,i}$ was calculated with Equation (2-10). The values of SWS 1_{max} and t_d were set to their estimates given earlier.

Sensitivity analysis

The estimate for SWS 1_{max} does not have a strong observational basis (Section on Storage); in order to test the sensitivity of model output on the value of SWS 1_{max}, we selected six values: 0, 1, 2, 6, 10, and 20 mm. We analysed the impact on SWS 2_{max} by re-calibrating its value as described earlier for each imposed value of SWS 1_{max}.

In addition, we simulated groundwater recharge with different parameterizations for the monitoring period (from 18 November 2012 to 28 September 2014) and compared them with observed recharge. We ran 1071 simulations with SWS 1_{max} ranging from 0 to 20 mm and SWS 2_{max} ranging from 0 to 50 mm, both in 1 mm increments. In order to evaluate the goodness of fit of each simulation, we used the bias error:

$$biaserror = \left| \sum_{i=1}^{G_j} obsGWR_i - \sum_{i=1}^{G_j} simGWR_i \right| \quad (2\text{-}12)$$

where G_j denotes the number of days during the monitoring period, $obsGWR_i$ is the observed groundwater recharge, and $simGWR_i$ is the simulated groundwater recharge.

2.5 Results

Observational record of recharge events

The installed equipment, including the v-notch weir, scale gauge, and camera functioned during the entire observation period of nearly 2 years without maintenance, thereby demonstrating its robustness in a desert environment. It recorded four surface runoff events. From the gauge readings, we estimated the total recharge of these events to be (i) 1.2 mm on 19 November 2013, (ii) 2.8 mm on 20 November 2013, (iii) 0.1 mm on 5 January 2014, and (iv) 3.2 mm on 6 January 2014 (Fig. 2-4 E). During the second and fourth events, the weir was overflowing. Nevertheless, the flow rates were estimated with Equation (2-4), and thus, recharge amounts on 20 November 2013 (2.8 mm) and on 6

January 2014 (3.2 mm) have to be seen as a lower limit. The amounts of rainfall during the day of these recharge events, as estimated from the nearest weather station, were 19.9, 5.7, 15.6, and 9.8 mm, respectively. Smaller rainfall events were recorded, which did not generate discharge into the doline (Fig. 2-4). In total, there were 54, 30, and 2 days with more than 0.1, 1, and 10 mm, respectively, of rainfall in the 679-day observation record.

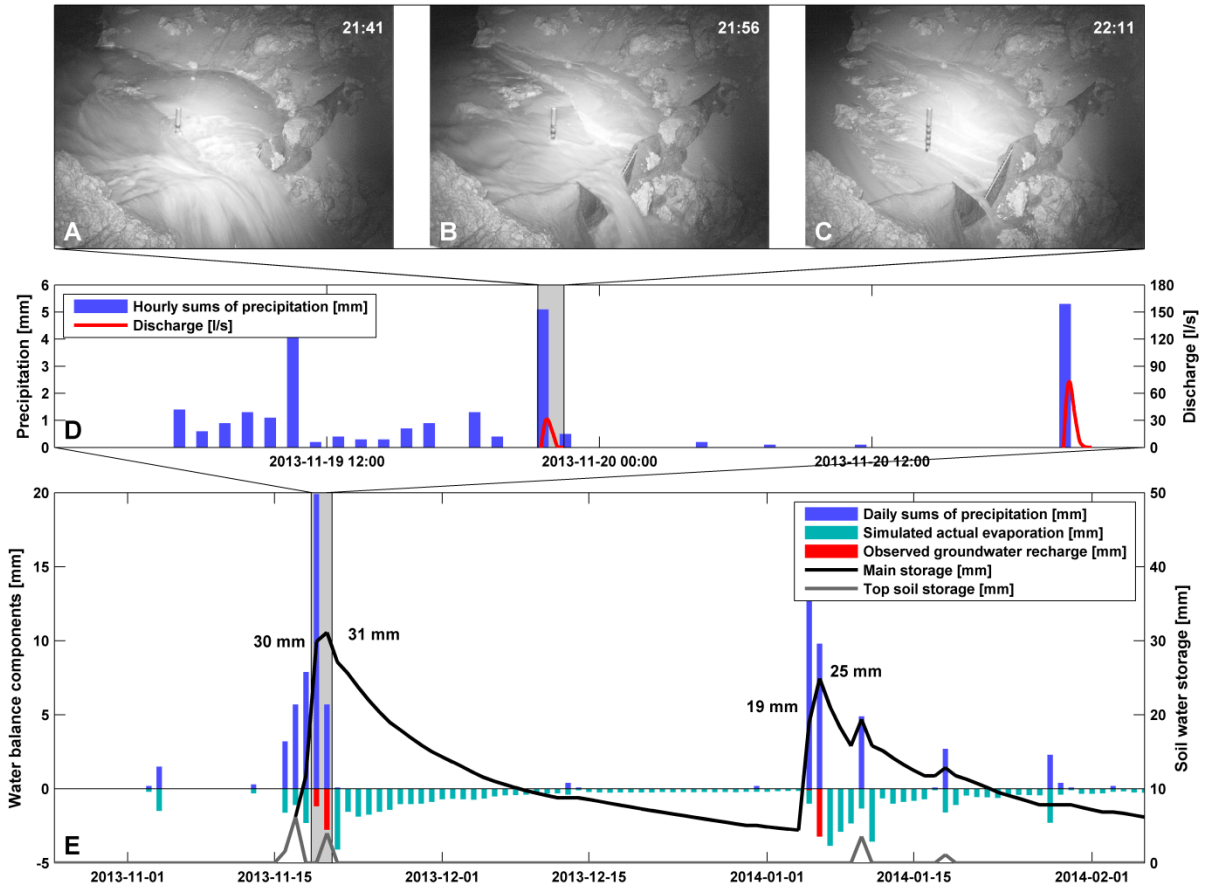

Fig. 2-4: (A–C) photographs of the recharge event on 19 November 2013; (D) hourly sums of precipitation and two recharge events from 19 November 2013 to 20 November 2013; (E) daily sums of water balance components (precipitation, evaporation, and groundwater recharge; left axis) and soil water storage at the end of the day (right axis) with SWS 1_{max} = 6 mm from 25 October 2013 to 6 February 2014, values give SWS 2_{max} for the four recharge events

Parameter estimation

With t_d = 2 days and SWS 1_{max} =6 mm, the estimates of SWS 2_{max} for the four recharge events were 30, 31, 19, and 25 mm, respectively. The variability in these values reflects the uncertainty in the precipitation, runoff, and evaporation data, as well as the approximate nature of the conceptual model itself. For recharge estimates by the model, we used the arithmetic mean of 26 mm for SWS 2_{max}.

Interannual variation of recharge

We ran all simulations with input taken from the 15-year (1971–1986) and 2-year records (2012–2014) of the Ma'aqla meteorological station. The mean annual groundwater recharge over the total simulation period is 5.1 mm (with SWS 1_{max} = 6 mm and SWS 2_{max} = 26 mm) with annual recharge–precipitation ratios varying between 0 and 0.27. Clustered and heavy rain showers lead to larger PDI values, which therefore indicate favourable groundwater recharge conditions. Annual rainfall sums, simulated annual recharge (with SWS 1_{max} = 6 mm and SWS 2_{max} = 19, 26, and 31 mm), and annual PDI values for the two available long-term records were calculated (Fig. 2-5).

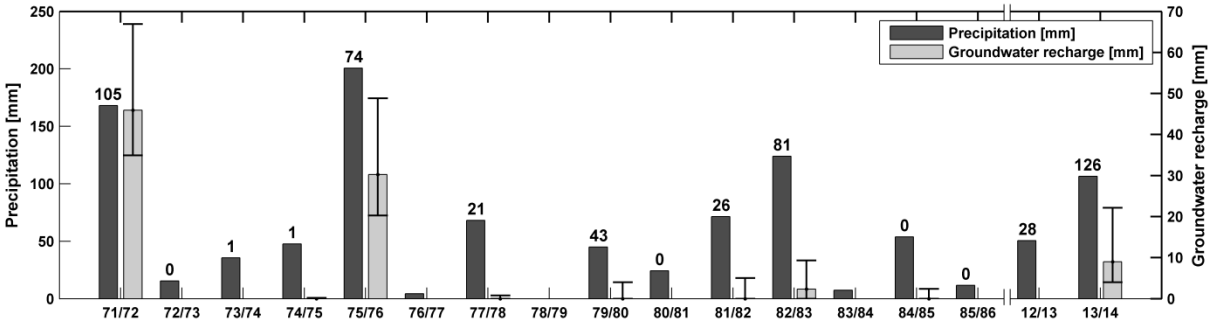

Fig. 2-5: Annual sums of precipitation and simulated groundwater recharge for 6mm of top-soil storage capacity and a main storage capacity of 26mm (grey bars), 19mm (top whisker), and 31mm (lower whisker). The numbers above rainfall sums bars give the precipitation distribution index

Model sensitivity to storage parameters

The calibrated values of SWS 2_{max} for the various values of SWS 1_{max} and the four recharge events used for calibration are given in Tab. 2-1. The capacity of the main soil storage (SWS 1_{max}) is dependent on the capacity of the top-soil storage (SWS 2_{max}; Tab. 2-1).

Tab. 2-1: Calibrated values of the capacity of the main soil storage reservoir [SWS 2 (mm)] for different top-soil storage capacities and observed recharge events; the bottom row gives the mean values and the coefficients of variation (CV)

Recharge event	**Capacity of the top soil storage reservoir (SWS 1 [mm])**					
	0	**1**	**2**	**6**	**10**	**20**
1	30	30	30	**30**	30	30
2	31	31	31	**31**	31	31
3	15	20	20	**19**	19	19
4	20	25	25	**25**	25	25
Mean (CV)	24 (0.32)	27(0.19)	27 (0.19)	**26 (0.21)**	26 (0.21)	26 (0.21)

For recharge events 1 and 2, the magnitude of SWS 2_{max} is about 30 mm for all SWS 1_{max}. For events 3 and 4, SWS 2_{max} is significantly lower and almost constant except for SWS 1_{max} = 0. Using the calculated means of SWS 2_{max} (Tab. 2-1), we calculated mean annual recharge amounts of 7.2, 5.6, 5.5, 5.1, 5.8, and 5.3 mm (average: 5.8 mm). The coefficient of variation (CV) of the top-soil storage capacity (1.17) is considerably higher than the CV of the simulated recharge (0.16), indicating a limited sensitivity to the top-soil storage. Nevertheless, inclusion of a top-soil storage led to substantially lower estimates of groundwater recharge. Even a very small reservoir (1 mm capacity) reduced the mean groundwater recharge rate by 22%. Increasing the reservoir's capacity by an order of magnitude (to 20 mm) had only a marginal effect: The recharge rate only dropped by additional 5 percentage points.

For SWS 1_{max} = 6 mm, we calculated the annual recharge rates for the values of SWS 2_{max} for all four recharge events (bold values in Tab. 1-1): 3.8, 3.5, 9.4, and 5.6 mm a^{-1}, respectively. The CV of mean annual groundwater recharge is 0.49. This is more than double the CV value of the corresponding main storage capacities (bold value in the bottom row of Tab. 2-1; CV = 0.21). This shows clearly the sensitivity of groundwater recharge to the capacity of the main storage reservoir.

These findings (high sensitivity to SWS 2_{max} and limited sensitivity to SWS 1_{max}) are corroborated by the simulations for 1071 combinations of SWS1max and SWS2_{max}. Varying SWS 2_{max} results in high bias errors except for a narrow band of values (Fig. 2-6). This indicates a high sensitivity for the main storage capacity. A broader range of SWS 1_{max} allows good fits of total simulated and observed recharge, in line with the limited sensitivity to SWS1_{max} (Tab. 2-1).

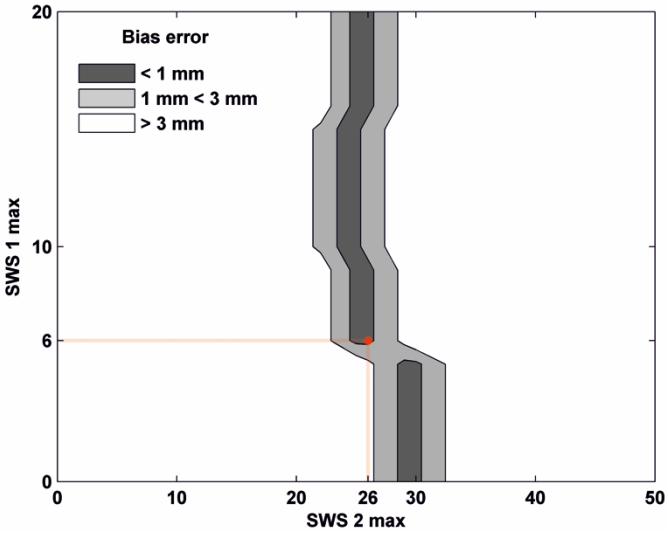

Fig. 2-6: Bias error for different storage parameterizations. The red dot indicates the parameterization used for the final groundwater recharge estimation

2.6 Discussion

Time-lapse recordings of recharge events (Fig. 2-4 A-C) showcase the abrupt and extreme nature of such events, supporting the case for robust, low-maintenance technology. Model results show the evolution of the two storage components in response to rainfall (Fig. 2-4 E). The top-soil storage is mostly empty, but nevertheless effectively filters out small rainfall events, and temporarily halts evaporation from the main reservoir after rainfall. The main effect of the top-soil reservoir is to simulate more realistic actual bare soil evaporation in order to prevent minor rain showers from contributing to the overall storage, thereby nullifying their contribution to groundwater recharge. It appears that this effect can already effectively be achieved by a small reservoir, so the decision whether or not to have such a reservoir in the model has a larger effect on the simulated groundwater recharge than the choice of the reservoir capacity.

The CV of mean annual groundwater recharge generated with different main storage capacities while the top-soil storage capacity is fixed (SWS 1_{max} =6 mm and CV = 0.49) is more than twice as large as the CV of the main storage capacity (Tab. 2-1; CV = 0.21). Clearly, groundwater recharge is sensitive to the capacity of the main storage reservoir, which cannot be independently measured. Observation periods covering several recharge events will be necessary for proper model calibration. In arid environments, this may easily take several years. Even then, various estimates may exhibit considerable variability. This should be taken into consideration when the model is used for scenario studies or to provide estimates of the amount of water that can sustainably be withdrawn from an aquifer.

Finally, the model run with a top-soil storage capacity of 6 mm and a main storage capacity of 26 mm estimated from the four recharge events gave a mean annual recharge rate of 5.1 mm for the investigated doline catchment. This is roughly in line with the estimate of 8 mm a^{-1} for the central part

of the As Summan Plateau (GDC, 1980), but very different from the estimate of 44 mm a^{-1} (48% of rainfall) by Hötzl et al. (1993). The tritium data from Hötzl et al. (1993) suggest that their estimate, which was based on a simpler model without soil storage, was much too high. The model of Hötzl et al. (1993) was strictly event based and ignored any storage in the soil, which is likely to be an oversimplification of model structure. Model results show two instances of the effect of antecedent rainfall (Fig. 2-4 E). In the first (magnified in Fig. 2-4 D), there was 19.9 mm of rainfall on 19 November 2013, which produced 1.2 mm of recharge. The next day, 5.7 mm of rainfall yielded 2.8 mm of recharge. Likewise, the second event features two consecutive rainfall events on an initially almost dry soil, with the second event producing much more groundwater recharge in spite of less rain. This intricate behaviour cannot be reproduced by a model that does not take into account the effect of previous wetting events.

Rainfall records show very large interannual variations (Fig. 2-5). The second wettest year (168 mm) produced the largest amount of recharge (46 mm). The ratio between total recharge and total rainfall ranges from 0 to 0.27, with a weighted average of 0.09. The highest ratios were achieved by the wettest years, making annual groundwater recharge sums even more skewed than the rainfall sums. Because of the extreme temporal variability, care should be taken in extrapolating these values to longer periods (Martínez-Santos and Andreu, 2010; Schulz et al., 2013). Strahler (Strahler, 1960) recommended that 30 years or more is needed to yield meaningful averages.

Dry years contributed little or no recharge according to the model simulations, which is consistent with the observed regime of recharge events, the relatively short observation period notwithstanding. For those years that did produce groundwater recharge, the correlation between the amounts of rainfall and recharge is quite low. For the 2 years with the highest total rainfall, the PDI seems to be a better indicator for groundwater recharge than total rainfall, indicating the importance of clustered and heavy rain storms. For years with intermediate amounts of rainfall, the interplay between total rainfall and PDI is more intricate, and neither can serve as an indicator for groundwater recharge on its own.

The method we developed within this study is transferable to other regions, like other karst outcrops of the Umm Er Radhuma aquifer, the karstified Dammam outcrops in Qatar (Sadiq and Nasir, 2002), or to other karst outcrops where point recharge can be considered as the dominant recharge process. For each location, the model needs to be parameterized. The time to drying can be estimated directly from low-cost time-lapse camera data, while the main storage capacity requires calibration on multiple recharge events. The topsoil storage capacity is less sensitive and can therefore be roughly estimated, e.g. based on potential evaporation. However, a larger number of recharge events would raise the possibility to fit the capacity of both soil water storages.

2.7 Conclusions

In view of the severe limitations in data availability in arid regions and the difficulties associated with field work, cost-effective and very robust technology (v-notch weir, scale gauge, and camera) in combination with a parsimonious conceptual model of the local hydrology is a promising approach to tackle groundwater recharge estimation in arid regions where point recharge is dominant. We also demonstrated that time-lapse cameras – normally used for qualitative observations – can be used to make quantitative field observations when combined with suitable auxiliary equipment and provide input to quantitative models.

Although, in our case, weather data from a meteorological station at some distance (11 km) proved worthwhile, the installation of a weather station on site is recommended. In case of multiple dolines, several weir-gauge-camera configurations can be installed around a single weather station. Given the rarity of recharge events, the field set-up should remain operational for a few years to gather enough data for model calibration and an estimation of the model error.

In summary, the present study introduces different tools, which help to improve our understanding of hydrological processes in arid to semi-arid environments. The cost-effective and robust monitoring in combination with conceptual modelling proved to be an effective tool to analyse the nonlinear behaviour of groundwater recharge processes. Furthermore, we established the novel PDI, which describes the temporal distribution of rainfall events. Besides total amount of annual precipitation, it serves as an additional indicator for favourable recharge conditions.

2.8 Acknowledgements

The authors thank the Ministry of Water and Electricity of Saudi Arabia for providing meteorological datasets. Furthermore, this work was kindly supported by GIZ IS (Gesellschaft für Internationale Zusammenarbeit – International Services) and Dornier Consulting. We acknowledge support from the BMBF funded project IWAS (grant code: 02WM1027).

2.9 References

Al Tokhais, A.S., Rausch, R., 2008. The Hydrogeology of Al Hassa Springs, in: The 3rd International Conference on Water Resources and Arid Environments. Riyadh.

Allison, G., Stone, W., Hughes, M., 1985. Recharge in karst and dune elements of a semi-arid landscape as indicated by natural isotopes and chloride. J. Hydrol. 76, 1–25. doi:10.1016/0022-1694(85)90088-5

Allocca, V., Manna, F., De Vita, P., 2014. Estimating annual groundwater recharge coefficient for karst aquifers of the southern Apennines (Italy). Hydrol. Earth Syst. Sci. 18, 803–817. doi:10.5194/hess-18-803-2014

Al-Rashed, M.F., Sherif, M.M., 2000. Water Resources in the GCC Countries: An Overview. Water Resour. Manag. 14, 59–75. doi:10.1023/A:1008127027743

Andreo, B., Vías, J., Durán, J.J., Jiménez, P., López-Geta, J.A., Carrasco, F., 2008. Methodology for groundwater recharge assessment in carbonate aquifers: application to pilot sites in southern Spain. Hydrogeol. J. 16, 911–925. doi:10.1007/s10040-008-0274-5

Blott, S.J., Pye, K., 2001. Gradistat: A grain size distribution and statistics package for the analysis of unconsolidated sediments. Earth Surf. Process. Landforms 26, 1237–1248. doi:10.1002/esp.261

de Vries, J., Simmers, I., 2002. Groundwater recharge: an overview of processes and challenges. Hydrogeol. J. 10, 5–17. doi:10.1007/s10040-001-0171-7

Fernandes, M.G., Cota, S., Braga, Jr., P.V., Velásquez, L.M., Rodrigues, P., De Paula, R.S., 2011. Hydrodynamic Characterization of a Karst Aquifer in the Brazilian Semi-Arid Region with Time Series Analysis of Hydrology Data, in: World Environmental and Water Resources Congress 2011. American Society of Civil Engineers, Reston, VA, pp. 970–980. doi:10.1061/41173(414)100

Ford, D., Williams, P., 2007. Karst Hydrogeology and Geomorphology. John Wiley & Sons, Inc., Chichester.

Friederich, H., Smart, P.L., 1982. The Classification of autogenic percolation waters in karst aquifers: A study in G.B. Cave, Mendip Hills, England. UBSS Proc. 16, 143–159.

GDC, 1980. Umm Er Radhuma Study - Volume 3: Groundwater Resources. Cambridge.

Geyer, T., Birk, S., Liedl, R., Sauter, M., 2008. Quantification of temporal distribution of recharge in karst systems from spring hydrographs. J. Hydrol. 348, 452–463. doi:10.1016/j.jhydrol.2007.10.015

Goldscheider, N., Drew, D., 2007. Methods in Karst Hydrogeology. Taylor & Francis, London.

Hartmann, A., Gleeson, T., Rosolem, R., Pianosi, F., Wada, Y., Wagener, T., 2015. A large-scale simulation model to assess karstic groundwater recharge over Europe and the Mediterranean. Geosci. Model Dev. 8, 1729–1746. doi:10.5194/gmd-8-1729-2015

Hartmann, A., Mudarra, M., Andreo, B., Marín, A., Wagener, T., Lange, J., 2014. Modeling spatiotemporal impacts of hydroclimatic extremes on groundwater recharge at a Mediterranean karst aquifer. Water Resour. Res. 50, 6507–6521. doi:10.1002/2014WR015685

Hauwert, N.M., 2009. Groundwater flow and recharge within the Barton Springs segment of the Edwards Aquifer, southern Travis and northern Hays Counties, Texas. University of Texas at Austin.

Hötzl, H., 1995. Groundwater recharge in an arid karst area (Saudi Arabia), in: Application of Tracers in Arid Zone Hydrology: Proceedings of the Vienna Symposium. pp. 195–207.

Hötzl, H., Wohnlich, S., Zötl, J.G., Benischke, R., 1993. Verkarstung und Grundwasser im As Summan Plateau (Saudi Arabien). Steirische Beiträge zur Hydrogeol. 44, 5–157.

IAEA/WMO, 2015. Global Network of Isotopes in Precipitation (GNIP) [WWW Document]. URL http://www.iaea.org/water (accessed 3.9.15).

Idso, S.B., Reginato, R.J., Jackson, R.D., Kimball, B.A., Nakayama, F.S., 1974. The Three Stages of Drying of a Field Soil1. Soil Sci. Soc. Am. J. 38, 831. doi:10.2136/sssaj1974.03615995003800050037x

Jackson, R.D., Idso, S.B., Reginato, R.J., 1976. Calculation of evaporation rates during the transition from energy-limiting to soil-limiting phases using albedo data. Water Resour. Res. 12, 23–26. doi:10.1029/WR012i001p00023

Jones, I.C., Banner, J.L., 2003. Estimating recharge thresholds in tropical karst island aquifers: Barbados, Puerto Rico and Guam. J. Hydrol. 278, 131–143. doi:10.1016/S0022-1694(03)00138-0

Jukić, D., Denić-Jukić, V., 2004. A frequency domain approach to groundwater recharge estimation in karst. J. Hydrol. 289, 95–110. doi:10.1016/j.jhydrol.2003.11.005

Lamoreaux, P.E., Hughes, T.H., Memon, B.A., Lineback, N., 1989. Hydrogeologic assessment—Figeh Spring, Damascus, Syria. Environ. Geol. Water Sci. 13, 73–127. doi:10.1007/BF01664696

Leaney, F.W., Herczeg, A.L., 1995. Regional recharge to a karst aquifer estimated from chemical and isotopic composition of diffuse and localised recharge, South Australia. J. Hydrol. 164, 363–387. doi:10.1016/0022-1694(94)02488-W

Lloyd, J.W., Farag, M.H., 1978. Fossil Ground-Water Gradients in Arid Regional Sedimentary Basins. Groundwater 16, 388–392. doi:10.1111/j.1745-6584.1978.tb03251.x

Martínez-Santos, P., Andreu, J.M., 2010. Lumped and distributed approaches to model natural recharge in semiarid karst aquifers. J. Hydrol. 388, 389–398. doi:10.1016/j.jhydrol.2010.05.018

McDonald, J., Drysdale, R., 2007. Hydrology of cave drip waters at varying bedrock depths from a karst system in southeastern Australia. Hydrol. Process. 21, 1737–1748. doi:10.1002/hyp.6356

MoWE, 2014. Weather station data.

Penman, H.L., 1948. Natural Evaporation from Open Water, Bare Soil and Grass. Proc. R. Soc. Lond. A. Math. Phys. Sci. 193, 120–145.

Rausch, R., Dirks, H., Kallioras, A., Schüth, C., 2014. The Riddle of the Springs of Dilmun-Does the Gilgamesh Epic Tell the Truth? Groundwater 52, 640–644. doi:10.1111/gwat.12214

Ritchie, J.T., 1972. Model for predicting evaporation from a row crop with incomplete cover. Water Resour. Res. 8, 1204–1213. doi:10.1029/WR008i005p01204

Rizk, J.A., Margane, A., 2011. Protection of Jeita Spring - Special Report No. 7: Mapping of Surface Karst Features in the Jeita Spring Catchment. Ballouneh.

Rosenberry, D.O., LaBaugh, J.W., 2008. Field Techniques for Estimating Water Fluxes Between Surface Water and Ground Water. U.S. Geological Survey Techniques and Methods, Reston, Virginia.

Sadiq, A.M., Nasir, S.J., 2002. Middle Pleistocene Karst Evolution in the State of Qatar, Arabian Gulf. J. Cave Karst Stud. 64, 132–139.

Salvucci, G.D., 1997. Soil and moisture independent estimation of stage-two evaporation from potential evaporation and albedo or surface temperature. Water Resour. Res. 33, 111–122. doi:10.1029/96WR02858

Scanlon, B.R., Keese, K.E., Flint, A.L., Flint, L.E., Gaye, C.B., Edmunds, W.M., Simmers, I., 2006. Global synthesis of groundwater recharge in semiarid and arid regions. Hydrol. Process. 20, 3335–3370. doi:10.1002/hyp.6335

Schmidt, S., 2014. Hydrogeological characterisation of karst aquifers in semi-arid environments at the catchment scale – Example of the Western Lower Jordan Valley. Georg-August-Universität Göttingen.

Schulz, S., Siebert, C., Rödiger, T., Al-Raggad, M.M., Merz, R., 2013. Application of the water balance model J2000 to estimate groundwater recharge in a semi-arid environment: a case study in the Zarqa River catchment, NW-Jordan. Environ. Earth Sci. 69, 605–615. doi:10.1007/s12665-013-2342-y

Sheffer, N.A., Cohen, M., Morin, E., Grodek, T., Gimburg, A., Magal, E., Gvirtzman, H., Nied, M., Isele, D., Frumkin, A., 2011. Integrated cave drip monitoring for epikarst recharge estimation in a dry Mediterranean area, Sif Cave, Israel. Hydrol. Process. 25, 2837–2845. doi:10.1002/hyp.8046

Shen, J., 1981. Discharge Characteristics of Triangular-notch Thin-plate Weirs. United States Government Printing Office, Washington.

Somaratne, N., 2014. Characteristics of Point Recharge in Karst Aquifers. Water 6, 2782–2807. doi:10.3390/w6092782

Strahler, A.N., 1960. Physical Geography, 2nd ed. John Wiley & Sons, New York.

Tobin, B., Schwartz, B., 2012. Quantifying concentrated and diffuse recharge in two marble karst aquifers: Big Spring and Tufa Spring, Sequoia and Kings Canyon National Parks, California, USA. J. Cave Karst Stud. 74, 186–196. doi:10.4311/2011JCKS0210

Valiantzas, J.D., 2006. Simplified versions for the Penman evaporation equation using routine weather data. J. Hydrol. 331, 690–702. doi:10.1016/j.jhydrol.2006.06.012

Waltham, T., Bell, F.G., Culshaw, M.G., 2005. Sinkholes and Subsidence, Karst and Cavernous Rocks in Engineering and Const. Springer Berlin Heidelberg, Berlin, Heidelberg. doi:10.1007/b138363

Wood, W.W., 1999. Use and Misuse of the Chloride-Mass Balance Method in Estimating Ground Water Recharge. Groundwater 37, 2–3. doi:10.1111/j.1745-6584.1999.tb00949.x

3 Groundwater evaporation from salt pans: Examples from the eastern Arabian Peninsula

Stephan Schulz[a], Marcel Horovitz[a], Randolf Rausch[b,c], Nils Michelsen[b], Ulf Mallast[a], Maximilian Köhne[a], Christian Siebert[a], Christoph Schüth[b], Mohammed Al-Saud[d], Ralf Merz[a]

[a] Helmholtz Centre for Environmental Research – UFZ, 06120 Halle, Germany

[b] Technische Universität Darmstadt, 64287 Darmstadt, Germany

[c] GIZ International Services, 11461 Riyadh, Saudi Arabia

[d] Ministry of Water and Electricity, Riyadh, Saudi Arabia

3.1 Abstract

The major groundwater resources of the Arabian Peninsula are stored in the large sedimentary basins in its eastern part. Evaporation from continental salt pans (playas) is an important process in water resources assessments of its upper principal aquifers – the Upper Mega Aquifer system – as it constitutes a significant sink. However, literature values on evaporation rates vary widely and usually report about coastal salt pans where seawater evaporation is assumed. The present study applies different methods to provide a comprehensive picture of groundwater evaporation from salt pans of the Upper Mega Aquifer system. A remote sensing approach provided the spatial distribution and total salt pan area of about 36,500 km². Hydrochemical and isotopic investigations revealed that from about 10% (3,600 km^2 ± 1,600 km^2) of the mapped salt pan area seawater evaporates. To estimate the groundwater evaporation rate from continental salt pans a laboratory column experiment was set up, implying a mean annual evaporation rate of about 42 mm ± 13 mm. In-situ analysis of water table fluctuations in the field suggested about 3 mm a^{-1} originate from recently infiltrated rainwater leading to an annual net groundwater evaporation of 39 mm ± 13 mm. Relating this number to the mapped salt pan area, from which groundwater evaporates, provides a total annual groundwater loss of 1.3 km^3 ± 0.5 km^3 for the Upper Mega Aquifer system.

3.2 Introduction

Salt pans are ubiquitous in arid to semiarid environments throughout the world and common geographic features on the Arabian Peninsula (Yechieli and Wood, 2002). Some types of salt pans have a shallow water table and capillary rise causes its evaporation from the surface (Jaeger, 1942). Those, which are fed by inflowing groundwater, are important discharge areas for the connected aquifers and hence relevant for quantitative water resources assessments.

Salt pan or salt flat is the generic term for different hydrological systems (Jaeger, 1942). In order to avoid confusion, we need to clarify the definition of two terms, which are inconsistently used throughout the literature: playa and sabkha. Playas are intracontinental basins, where capillary rise causes groundwater discharge due to evaporation. In contrast, sabkhat (plural of sabkha) are marginal marine mudflats (Briere, 2000), where evaporating water originates from tidal flooding (Butler, 1969) and seawater intrusion induced by evaporative pumping (Hsü and Siegenthaler, 1969; Jaeger, 1942). Especially, in older studies the term continental sabkha was commonly used as a synonym for playa, e.g. USGS and ARAMCO (1963) and Kinsman (1969). Note that all types of salt pans (including playas) are usually termed "sabkhat" throughout the Arabian countries.

Prominent examples for groundwater discharging salt pans (playas), besides those on the Arabian Peninsula, are for instance the Bonneville Salt Flats in Utah, USA (Mason and Kipp, 1998), Owens Lake in California, USA (Tyler et al., 1997), salt flat basins in the Chilean Altiplano (Hernández-López et al., 2014), playas in central Mexico (Menking et al., 2000) or playas in central Australia (Jacobson and Jankowski, 1989; Lloyd and Jacobson, 1987). In contrast, coastal salt pans, which predominantly evaporate seawater, are known from Chott el Djerid, Tunisia (Richards and Vita-Finzi, 1982), northwest Libya (Abdel Galil and El-Fergany, 2011), northwest Mexico (Castens-Seidell, 1984), and southern Australia (Bye and Harbison, 1991).

Estimates concerning evaporation rates from salt pans on the Arabian Peninsula vary widely. For the Eastern Province of Saudi Arabia, the Saudi Arabian Ministry of Water and Agriculture estimated an annual evaporation rate of 60 to 100 mm (cited in Al-Saafin, 1996). Al-Saafin (1996) conducted own investigations on water table fluctuations indicating an annual evaporation of 63 mm for the salt pan Al Fasl. Using the example of a salt pan (Al-Khiran) in southern Kuwait, Robinson and Gunatilaka (1991) suggested an annual evaporation rate of groundwater between 20 mm and 40 mm. Similar to the previously mentioned study, Patterson and Kinsman (1981) analysed water table fluctuations and estimated an annual net evaporation of 120 mm and 60 mm from coastal and continental salt pans, respectively. Their calculations are based on total porosities of salt pan sediments and not on specific yield, translating reported estimates to be an upper limit (Patterson and Kinsman, 1981). A few years earlier, Patterson (1972) introduced another method. He derived evaporation rates from the amount of anhydrite present in the capillary fringe. Results indicated an average annual evaporation of 60 mm over the last 4,000 to 5,000 years. Shehata and Lotfi (1993) applied empiric equations about evaporation rates depending on potential evaporation and water level and concluded an annual evaporation from salt pans along the Arabian Gulf coast of about 120 mm. Sanford and Wood (2001) introduce a fourth method. They based their estimations of evaporation rates on in-situ humidity chamber experiments and calculated an evaporation rate of 69 mm a^{-1} for salt pans in Abu Dhabi and 50 mm a^{-1} for the salt pan Matti (located in Abu Dhabi and Saudi Arabia), respectively. Most of the

previously cited studies report about evaporation rates from coastal salt pans, where sea water evaporation is assumed. However, the greater part of salt pans on the eastern Arabian Peninsula is located further inland (predominantly in the Rub' Al-Khali desert; USGS & ARAMCO, 1963).

Total groundwater evaporation from salt pans depends on their spatial distribution and cumulative surface area. However, available data from the geological map (USGS and ARAMCO, 1963) date back more than 50 years and may not represent current salt pan distribution, due to temporal dynamics in relation to dune movements and construction activities (Kumar and Abdullah, 2011; GDC, 1980). Second, due to the large scale of the geological map (1:2,000,000), indicated salt areas have a low spatial resolution of details and do not reveal true extents. This is already obvious by comparing the geological map with high-resolution satellite images.

This study focuses on groundwater evaporation from salt pans located inland. Quantifying and assessing evaporation loss of groundwater from these salt pans is important to close the water balance of the connected aquifer system. In detail, four research questions were addressed: (i) What is the spatial distribution of salt pans on the eastern Arabian Peninsula? (ii) What are contributing water sources to evaporation – spatial salt pan differentiation dominated either by groundwater or by seawater evaporation? (iii) How much water evaporates from previously infiltrated precipitation? And (iv) what are representative evaporation rates from inland salt pans?

In general, this study aims to provide important quantitative information about salt pans of the Upper Mega Aquifer system on the Arabian Peninsula. Moreover, presented methods may serve as a template for other researchers investigating salt pan systems.

3.3 Study area

The whole Arabian Peninsula can be considered as water scarce (Rijsberman, 2004) induced by the given (hyper-) arid climatic conditions. Average annual precipitation is less than 100 mm (Pauw, 2002), while potential evaporation reaches 2,500 mm a^{-1} in coastal areas. In the central parts of the Rub' Al-Khali desert this number may even rise to 4,500 mm a^{-1} (Al-Rashed and Sherif, 2000) mainly caused by significantly lower air humidity in comparison to the coast. Due to the resulting lack of surface water, the region relies on its mainly fossil (non-renewable) groundwater resources. The groundwater is predominantly stored in sedimentary formations of the Arabian Shelf, also called Arabian Platform (Al-Rashed and Sherif, 2000). Its upper principal aquifers are the Wasia-Biyadh sandstone aquifer and the karstified Umm Er Radhuma and Dammam limestone aquifers. Separated by layers with lower hydraulic conductivities these units form the Upper Mega Aquifer system (Kalbus et al., 2011). Due to its regional importance, the study area covers the extent of the Upper Mega Aquifer system with an area of about 1.7 x 10^6 km^2 (Fig. 3-1), containing about 90% of the salt pans on the Arabian Peninsula

(USGS and ARAMCO, 1963). Most of them are located at the Arabian Gulf coast and in the Rub' al Khali desert (Al-Saafin, 1996).

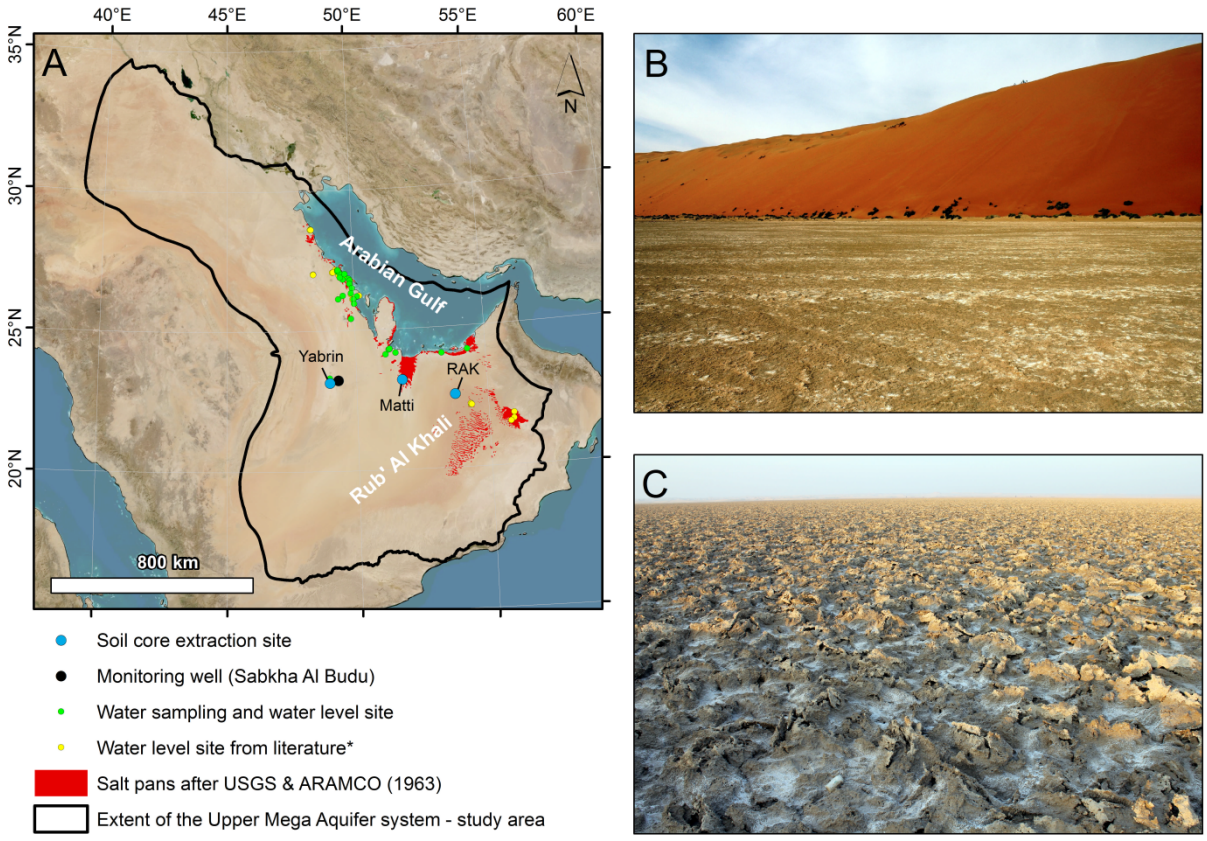

Fig. 3-1: Overview of study area (A) and photographs of an interdune salt pan in the Rub' Al Khali desert (B) and the salt pan Al Budu (C); * water level sites after Al-Saafin (1996), Barth (1998), Heathcote and King (1998), Robinson and Gunatilaka (1991), Smith (1981)

Salt pan properties

The playa (groundwater evaporating salt pan) soil matrix consists predominantly of siliciclastic sediments. The capillary rise of highly saline water and its subsequent evaporation causes evaporites (e.g. gypsum, anhydrite, halite) to be present in the capillary fringe (Kinsman, 1969; Smith, 1982). Depending on soil texture the capillary rise may occur from water levels ranging from several centimetres to 2 m below ground level (Sultan et al., 2008). Although the groundwater table shows seasonal fluctuations, its mean distance to the surface remains constant over longer periods of time (Yechieli and Wood, 2002). This is caused by steady-state equilibrium between aeolian sedimentation and deflation. As soon as the groundwater table falls for a longer time period the surface dries out and is eroded until the top of the capillary fringe is reached. In case of a rising groundwater table the surface becomes wetter and additional aeolian sediments will be trapped (Kinsman, 1969; Yechieli and

Wood, 2002). In contrast to playas, sabkhat (seawater evaporating salt pans) are supratidal surfaces and its matrix mainly consist of carbonate sediments and associated evaporates (Kinsman, 1969).
A literature review about water level of salt pans in the study area as well as measurements during this study is provided in Annex A 8. Water level measurement sites are shown in Fig. 3-1.

3.4 Methods

Spatial distribution of salt pans

Remote sensing data for the whole study area, i.e. 39 Landsat 8 (hereafter referred to as LDCM – Landsat Data Continuity Mission) images recorded between September 18, 2013 and February 25, 2014, were analysed for salt pan distribution. In addition, elevation information was obtained from the Shuttle Radar Topography Mission (SRTM) Version 2.0 dataset (Jarvis et al., 2008). Based on this data analyses, areas with non-salt-pan features were iteratively removed through global thresholds (Fig. 2-2). Non-salt-pan features include:

i. the Arabian Gulf area (elevation ≤ 0 m),
ii. slopes > 3° (only flat depressions characterize salt pan areas (GDC, 1980)),
iii. urban areas (partly superimpose salt pan areas and were therefore excluded using the entropy measure of a 3x3 grey level co-occurrence matrix (Haralick et al., 1973)),
iv. densely vegetated areas (representing irrigation areas that as well partly superimpose salt pan areas requiring an exclusion through the application of normalised difference vegetation index (NDVI) value > 0.15), and
v. dry aeolian sand areas (incorporating mobile sand superimposing salt pan areas (GDC, 1980)) through the application of a modified normalised difference water index (MNDWI) after Xu (2006).

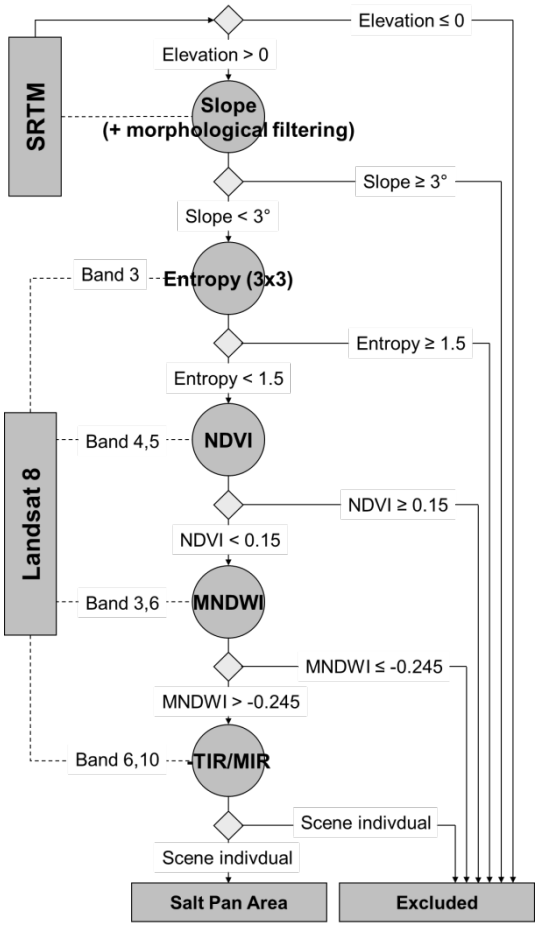

Fig. 3-2: Flowchart picturing the applied decision tree classification to extract salt pan areas (note: rectangles represent data sets, circles show calculated auxiliary products, diamonds stand for decision criteria, dotted lines indicate used data sets and solid lines represent the process chain)

Remaining pixels represent potential salt pans. To further refine these areas, spectral salt pan characteristics in the mid-infrared and thermal-infrared range of the electromagnetic spectrum were used. The main spectral differentiation concerns the wetness/water coverage of salt pan areas and evaporites (halite and gypsum) as well as wet salt pan deposits (sand, silt, clay) at the base and along the fringe of salt pans. The resulting reflectance is considerably lower in the mid-infrared (MIR) spectrum compared to surrounding coarse grained aeolian sand accumulation. At the same time, heat capacity also differs significantly between wet salt pan areas and aeolian sand. In turn, thermal radiation is higher from wet areas (salt pans) than for non-salt-pan areas at the time of recording (10-11 a.m. GMT).

To account for both distinctive spectral features (low reflectance in MIR and higher thermal radiation) that characterise wet areas (salt pans), a ratio between inversed thermal-infrared (LDCM-band 10) and mid-infrared (LDCM-band 6) bands was applied. Resulting ratios representing salt pan areas plot in a range between -1.53 (±0.37) and -4.15 (±0.77). To obtain correct scene-individual thresholds and hence to derive salt pan areas within the previously extracted potential areas, we used salt pan

reference sites obtained through field campaigns and WorldView-2 high resolution satellite images provided by DigitalGlobe.

Origin of salt pan brines

Close to the coastline, water evaporating from salt pans might not originate from groundwater but from seawater. However, seawater and groundwater differ significantly in their hydrochemistry (i.e. Cl-/Br- ratios) and in the isotopic signature of sulphur ($^{34}S/^{32}S$) in sulphate (Patterson and Kinsman, 1977; Robinson and Gunatilaka, 1991).

In order to identify the origin of salt pan brines, water samples were collected from the Arabian Gulf (n = 3), from wells tapping the Umm Er Radhuma aquifer (n = 4), and from auger holes or hand dug pits in salt pans at varying distances from the coastline (n = 26). Sampling sites are shown in Fig. 3-1 and coordinates are given in Annex A 9. Samples for anion analysis were filtered (0.45 µm) and filled in 30 ml HDPE-bottles. Samples for the determination of cations were additionally acidified with concentrated HNO_3. For the analysis of the sulphur isotopic signature of dissolved sulphate unfiltered samples were collected in 500 ml LDPE-bottles. Cations and anions were determined by Ion Chromatography (ICS-2000, Thermo Scientific Dionex) and Inductively Coupled Plasma Optical Emission Spectrometry (Spectro Acros, Spectro Analytical Instruments), respectively. The sulphur isotope ratios $^{34}S/^{32}S$ were measured, after sample preparation (USGS RSIL Lab Code 1951), by Isotope Ratio Mass Spectrometry (delta S, Finnigan MAT). The $^{34}S/^{32}S$ ratios are expressed in per mil (‰) using the conventional delta-notation relative to the Canyon Diablo Troilite (CDT) standard.

Infiltrated precipitation

It has to be considered that rainwater might percolate through the salt pan surface during rain events as described by Sanford and Wood (2001). Consequentially, infiltrated rainwater will evaporate in addition to (or instead of) groundwater after rain events.

In order to estimate the influence of infiltrating rainwater, the annual precipitation rate for the previously mapped salt pan area was first derived from the Tropical Rain Measurement Mission (TRMM) V6 data set (Kummerow et al., 1998) using the area-weighted mean. Second, a 3.5 m deep well was installed in the salt pan Al Budu (23.237° N, 49.299° E) and equipped with a groundwater data logger measuring piezometric water level. The barometric correction of the data was based on air pressure data from the nearest weather station in Haradh (100 km distance). Results of the corrected water level were compared with rain events recorded in Yabrin (35 km distance). Both datasets, air pressure and precipitation, were provided by MoWE (2014). Furthermore, three undisturbed 250 ml

soil samples were extracted from the saturated zone next to the observation well. These soil samples were analysed for their effective porosity (equals approximately specific yield) by subtracting the sample weight at field capacity from the weight of the fully saturated sample.

Evaporation rate

The evaporation rate was determined by a column experiment. For that purpose, three undisturbed soil cores were taken from continental salt pans (Yabrin – 23.152° N, 48.970° E, Matti – 23.199° N, 51.753° E and an interdune salt pan in the Rub' Al Khali desert – 22.605° N, 53.754° E; Fig. 3-1). Extraction sites show differences with respect to soil texture, salt crust, and chemical composition of groundwater (Annex A 9 and A 10) covering the variety of continental salt pans. According to field observations, the soil cores were taken from representative locations. They have a height of approximately 50 cm and a diameter of 16 cm. They were extracted from the top layer (including salt crust) of the salt pans with specially developed sampling equipment. A technical drawing and a picture captured during operation are provided in Annex A 11 and A 12.

The basic idea of this column experiment is to measure the evaporation rate depending on variable boundary conditions such as water level (pressure head at the bottom of the column) as well as temperature and humidity at the top of the column. In order to adjust the water level, a micro porous membrane was installed at the bottom of the soil core and connected to a hanging water column represented by a height-adjustable LDPE-bottle (Fig. 3-3). Inside the bottle, the water level, which represented the pressure head in the soil column, was kept constant. This was realized by continuously pumping water, which had the same chemical composition as the respective salt pan brine, from a storage tank into the height-adjustable bottle. The brines used in the column experiment were reconstructed individually according to water sample analysis of the extraction sites (Annex A 9). Water, which did not flow from the bottle into the soil column, flowed back via an overflow into the storage tank. This setup allows simulating water levels below the bottom of the soil column as for salt pan soils the dominant water transport at 0.5 m b.g.l. occurs in the liquid phase and water vapor transport at this depth is negligible. Due to the fact that the whole system is closed except for the top of the soil column, the long-term (several days) average of the water loss in the tank corresponds to the evaporation loss at the top of the column. The water loss in the storage tank was gravimetrically determined and continuously recorded. Likewise, temperature and humidity as evaporation-drivers were permanently measured at the top of the column and recorded. In order to adjust temperature an infrared-heat-lamp controlled by a thermostat was installed at the top of each column (Fig. 3-3). All data (weight of the storage tank, temperature and humidity) were recorded at 15 minutes intervals. Besides, wind influences the evaporation rate. Wind affects evaporation by removing more humid air

layers above the soil surface. In case of this experiment, air movement was induced by convection driven by the temperature gradient from the heat spot of the infrared-lamp above the top of the column to cooler air of its surroundings. This effectively removed the more humid air layers at the top of the column. Wind speed itself does not significantly affect the diffusion-dominant evaporation stage (Davarzani et al., 2014). Therefore, we neither simulated (e.g. with a fan) nor measured wind speed.

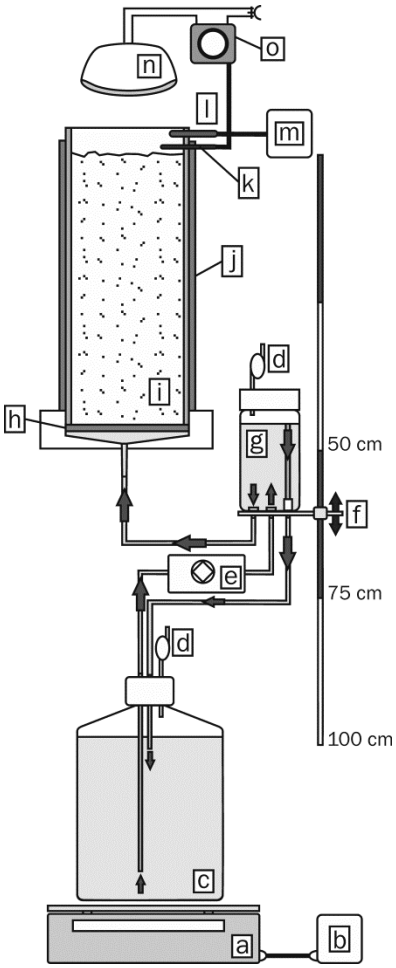

Fig. 3-3: Schematic sketch of the column experiment (a – balance; b – data logger; c – storage tank; d – fermentation lock; e – peristaltic pump; f – water level adjustment; g – level-drain-bottle; h – micro porous membrane; i – undisturbed soil column; j – thermal insulation; k – temperature sensor of thermostat; l – temperature and humidity sensor; m – data logger; n – infrared-heating-lamp; o - thermostat)

3.5 Results

Spatial distribution of salt pans

In general, classified salt pan areas (Fig. 3-4) show a comparable spatial distribution as the existing data set (USGS and ARAMCO, 1963). Significant spatial differences between both sets exist in the northern and eastern part of the study area for which the presented approach yields smaller salt pan areas. On the other hand, the small scale reveals noteworthy differences in mapped salt pan extents.

While the USGS & ARAMCO (1963) data set is rather generalized due to the coarse scale of mapping, the presented approach provides a high level of detail. Even small-scale inter-dune salt pans could be outlined in detail. Another observable trend is the change along the coast. Recently, evaporation-impeding construction activities superimpose previously mapped salt pan areas and provide a significant difference to current coastal salt pans. These changes and the level of detail lead to a total classified salt pan area of about 36,500 km^2 and hence to 33% more than mapped before in the study area.

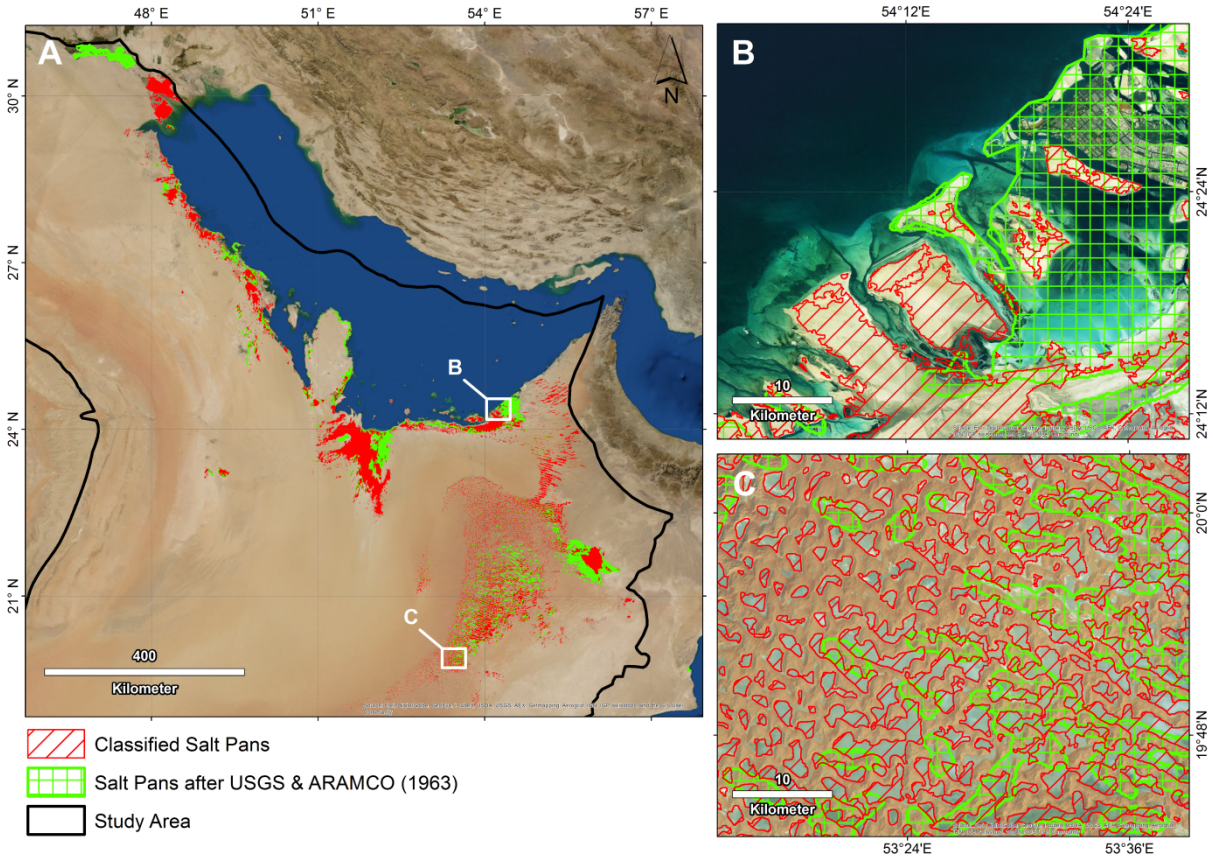

Fig. 3-4: Spatial distribution of salt pan areas in comparison to the only available data set of USGS & ARAMCO (1963) in general (A) and as detailed view on coastal- (B) and inland- (C) salt pans to emphasize the small scale differences

Origin of salt pan brines

Sulfate in modern seawater is characterized by a $\delta^{34}S$ value of 21 ‰ CDT (Clark and Fritz, 1997), which is relatively high compared to many groundwater samples. Hence, $\delta^{34}S$ is a powerful tool for identifying seawater in salt pan environments (Robinson and Gunatilaka, 1991). The obtained values range between 7.4 and 20.8 ‰ CDT (Annex A 9). The highest values accounting for 20.3, 20.5, and 20.8 ‰

CDT were found for the three seawater samples and fall into the range reported for the Arabian Gulf in the literature (20.1 - 20.9 ‰ CDT) (Moser et al., 1978; Robinson and Gunatilaka, 1991). The values plotted against their corresponding distances to the Arabian Gulf are presented in Fig. 3-5. Molar Cl^-/Br^- ratios were also been included as an independent indicator for seawater impact as ratios of less than 1,000 represent seawater while continental groundwater usually shows ratios larger than 5,000. Water samples of mixed origin fall between these threshold values (Patterson and Kinsman, 1977).

It can be seen that the Arabian Gulf samples exhibit a distinct signature with high $\delta^{34}S$ values (see above) and low Cl^-/Br^- ratios (max. Cl^-/Br^-: 1.315). A cluster of salt pan samples can be identified due to elevated $\delta^{34}S$ values (ca. 19 - 20 ‰ CDT), scattering in the range that characterizes seawater-influenced salt pan brines (19 ± 2 ‰ CDT) (Robinson and Gunatilaka, 1991). Furthermore, they stand out due to their coastal location (< 9 km) and their low to moderate Cl^-/Br^- values, mostly falling into the 1,000 – 5,000 class that reflects a mixed origin (Patterson and Kinsman, 1977). This pattern points towards a significant seawater impact. All remaining salt pan water samples as well as the groundwater samples taken from boreholes show less enriched $\delta^{34}S$ signatures that are comparable to values reported by Shampine et al. (1979) for aquifers of the Upper Mega Aquifer system (e.g. Wasia: 15.2 ± 5.04 ‰, Umm Er Radhuma: 13.3 ± 2.28 ‰, Khobar: 13.4 ± 2.70 ‰, Alat: 11.3 ± 2.78 ‰, Neogene: 12.3 ± 1.24 ‰) and springs in the Eastern Province (9.0 - 12.4 ‰) (Moser et al., 1978). Thus, a continental origin seems likely. Within this group, three samples (S 9, S 5, S 12) have comparably low Cl^-/Br^- ratios, suggesting a seawater impact. However, this is not supported by the low $\delta^{34}S$ values.

Fig. 3-5 reveals that sample S 19 is the salt pan with continental water closest to the coastline (3 km, see dashed line). Sample S 4, on the other hand, represents the seawater-influenced sample most distant from the coast (9 km, see second dashed line). The total salt pan area within 3 km and 9 km distance to the coastline is 2,000 km² and 5,100 km², respectively. Assuming a boundary at 6 km from the coastline, the mean value between the closest continental water and furthest seawater influenced salt pan, results in a total sabkha (salt pan influenced by seawater) area of 3,600 km² ± 1,600 km^2 whereby the error estimation derives from the upper (9 km) and lower boundary (3 km), respectively.

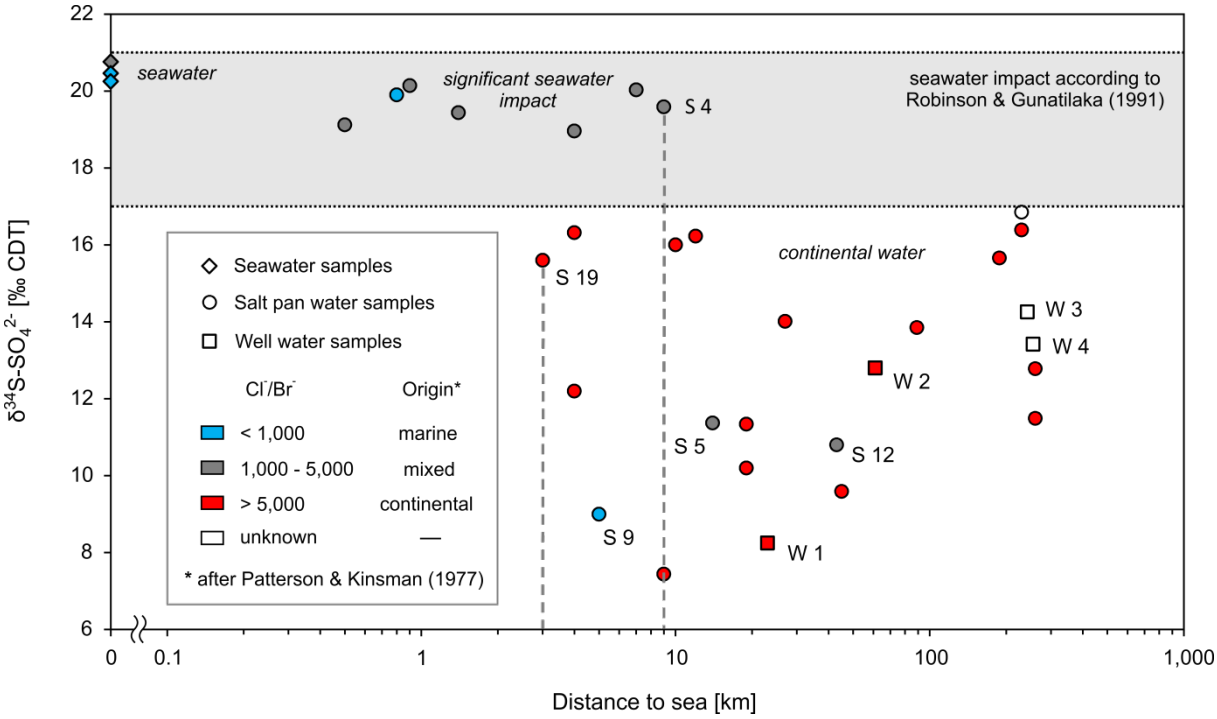

Fig. 3-5: Relationship between $\delta^{34}S$ and distance to the Arabian Gulf. The shaded area depicts the $\delta^{34}S$ range typical for seawater-influenced salt pan brines (Robinson and Gunatilaka, 1991). Note that the Cl^-/Br^- classes and the associated origin interpretation are based on Patterson & Kinsman (1977). Own interpretations based on isotopic and Cl^-/Br^- signatures are presented in italic

Infiltrated precipitation

During the monitoring period of the water table in the salt pan Al Budu from December 2012 to February 2014, four large (min. 10 mm) rain events (14.8, 36.1, 15.2, and 10 mm) with corresponding rise in water level (28, 32, 41, and 15 mm) were observed (Fig. 3-6). Analyzing undisturbed soil samples suggested an effective porosity of about 3% which is in agreement with an estimated effective porosity ranging from 3% to 8% derived from the soil texture analysis (clayey silt; see Annex A 10) after Hölting and Coldewey (2009). In order to determine the amount of infiltrated rainwater to the groundwater table, recorded water level rises were multiplied with the effective porosity of 3%. Comparing the amount of infiltrated water to the amount of the previous rain event lead to the conclusion that 5.7, 2.7, 8.1, and 4.5% (on average approximately 5%) of precipitation infiltrated to the salt pan water table. TRMM data analyses gave an area-weighted mean annual precipitation of 54 mm for the years 2000 to 2010 and the previously mapped salt pan area. This is in line with reported values of 30-100 mm a^{-1} (Al-Saafin, 1996). Assuming that the calculated recharge-precipitation-rate of 5% is transferable to other salt pans in the study area, we suggest that about 3 mm of precipitation per year infiltrate to the salt pan water table (hereafter referred to as groundwater recharge).

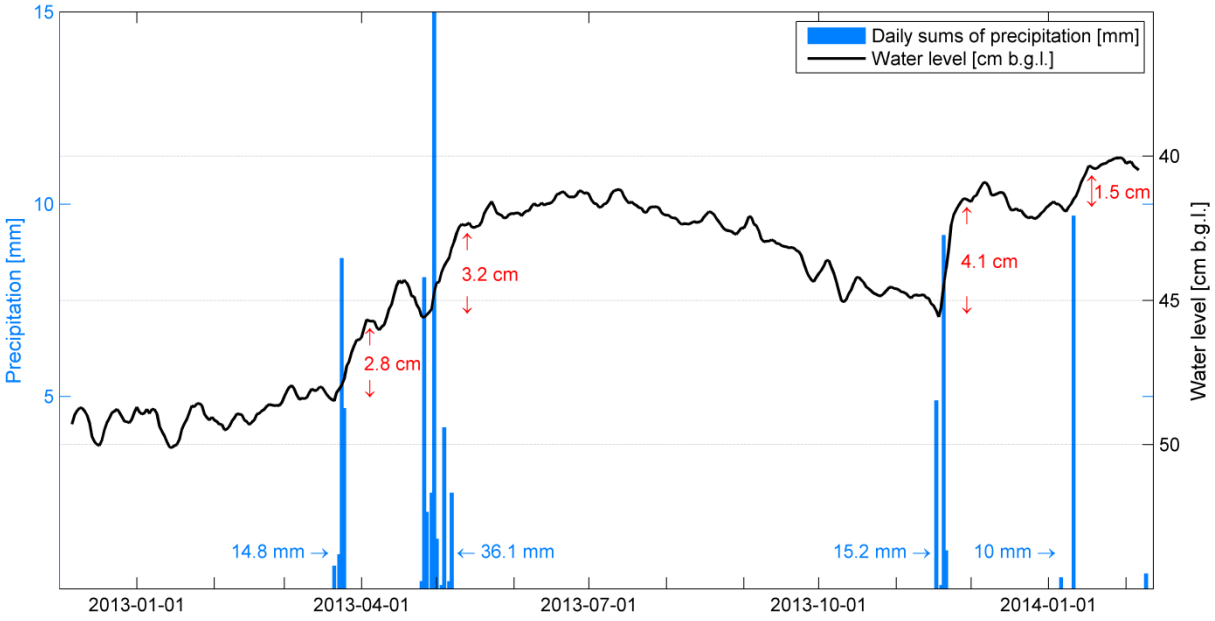

Fig. 3-6: Water table fluctuations (running average of 5 days) in depth below ground level (b.g.l.) and daily sums of precipitation in the salt pan Al Budu from December 2012 to February 2014; red numbers showing the water level rise after rain events (blue numbers)

Evaporation rate from exemplary salt pan soil cores

The column experiment was run with different settings of water level, temperature and humidity (Tab. 1). Each setting was run for one to three weeks until steady state conditions were reached (constant daily water loss in the storage tank over several days).

Tab. 3-1: Results of the column experiment (WL – Water level [m b.g.l.], Temp. – Temperature [°C], H – Humidity [%], E – Evaporation [mm a^{-1}])

WL [m b.g.l.]	Yabrin			Matti			Rub' Al Khali		
	T [°C]	H [%]	E [mm/a]	T [°C]	H [%]	E [mm/a]	T [°C]	H [%]	E [mm/a]
0.5	38.8	23.0	**59.3**	38.8	23.3	**69.2**	38.6	26.6	**98.0**
0.5	32.2	29.9	**47.1**	32.2	30.5	**51.8**	32.1	29.8	**62.6**
0.5	26.7	51.2	**39.0**	26.7	51.9	**39.5**	23.5	44	**50.1**
0.75	36.8	26.5	**48.6**	36.8	26.3	**50.8**	36.8	25.2	**82.8**
0.75	31.9	27.8	**39.8**	30.6	34.3	**36.6**	31.5	29.9	**56.9**
0.75	20.7	32.2	**31.0**	20.5	27.2	**19.2**	20.7	30.9	**38.7**
1	37.3	11.0	**38.1**	37.1	10.5	**31.1**	37.4	10.4	**57.1**
1	31.8	15.9	**29.8**	31.9	18.4	**22.6**	31.9	17.4	**34.5**
1	22.5	38.0	**19.9**	22.9	44.7	**15.6**	22.5	37.1	**20.9**

In total, nine evaporation rates (mean values for several days of constant evaporation) and the corresponding water level, temperature and relative humidity (Tab. 3-1) served to set up a multiple regression model for each column extracted from the salt pan Yabrin, Matti and Rub' Al Khali, respectively (Eq. 3-1 to 3-3). The regression model type used is based on previous studies about evaporation (Valiantzas, 2006) and evaporation depending on water level (Hernández-López et al., 2014; Johnson et al., 2010).

$$E_{Yabrin} = 0.724 \cdot T \cdot \left(1 - \frac{H}{100}\right) \cdot WL^{-1.119} + 15.440 \qquad (R^2 = 0.88) \qquad (3\text{-}1)$$

$$E_{Matti} = 0.869 \cdot T \cdot \left(1 - \frac{H}{100}\right) \cdot WL^{-1.373} + 6.301 \qquad (R^2 = 0.90) \qquad (3\text{-}2)$$

$$E_{Rub'Al\ Khali} = 1.798 \cdot T \cdot \left(1 - \frac{H}{100}\right) \cdot WL^{-0.931} + 1.672 \qquad (R^2 = 0.82) \qquad (3\text{-}3)$$

where E is the evaporation rate [mm a^{-1}]; T is temperature [°C]; H is relative humidity [%]; WL is water level [m b.g.l.]; and R^2 is the coefficient of determination.

To calculate the long term evaporation rates from salt pans, the regression models from the column experiment were applied to long-term monthly averages of temperature and humidity for the period 1979 to 2012, extracted from ECMWF (European Centre for Medium-Range Weather Forecasts) ERA-interim reanalysis datasets (Dee et al., 2011). The area-weighted mean of temperature and humidity were calculated for the previously mapped salt pan area. Water levels were derived from 26 measurements during this study and additional 23 measurements from other studies (Annex A 8; measurement sites are shown in Fig. 3-1). The median and the mean error of in total 49 measurements is 0.75 m b.g.l. and 0.28 m b.g.l., respectively. We chose the median instead of the arithmetic mean as it is more robust to extreme values, which, most likely, do not represent typical salt pan water levels.

Calculated monthly evaporation rates of the three salt pan examples are shown in Fig. 3-7. A clear seasonality in evaporation is visible for all three salt pan locations. In summer temperature is higher and hence evaporation rates are increasing. For the salt pan Yabrin, Matti, and the interdune salt pan in the Rub' Al Khali desert (RAK) the annual mean evaporation rate for a water level of 0.75 m b.g.l. is 35 mm, 32 mm, and 48 mm, respectively.

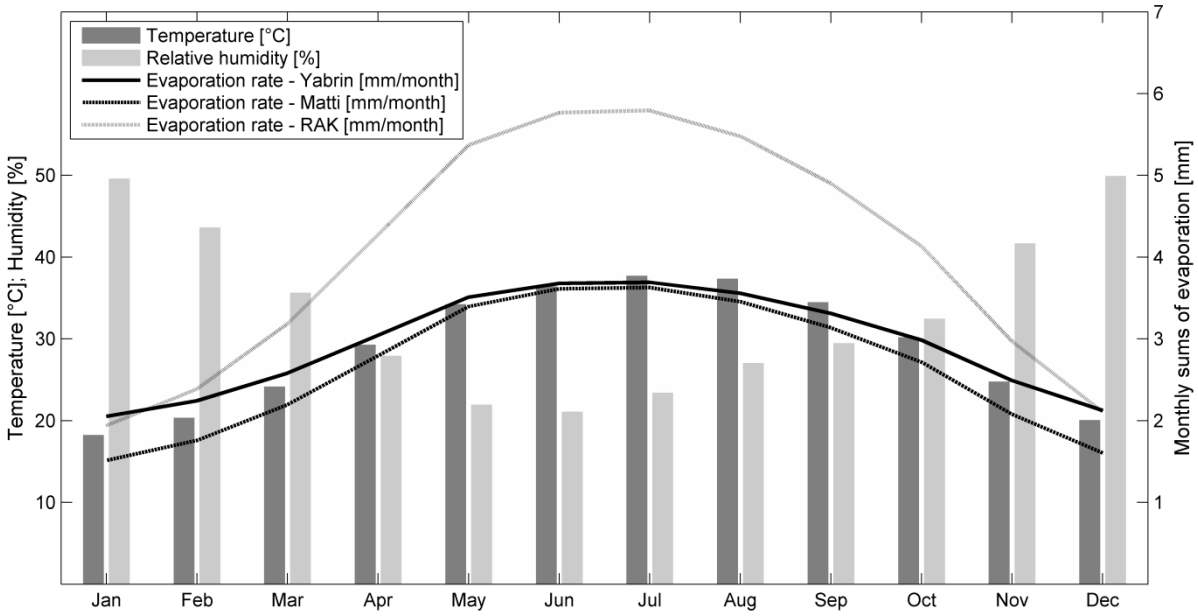

Fig. 3-7: Long-term monthly temperature and relative humidity (ECMWF ERA-interim reanalysis datasets) and corresponding monthly sums of evaporation for the salt pans Matti, Yabrin, and the interdune salt pan in the Rub' Al Khali assuming a water level of 0.75 m b.g.l.

There are several sources of uncertainty in the estimation of evaporation rates. First, the assumed water level of 0.75 m b.g.l. is accompanied by a high degree of uncertainty given the limited number observations and sparse information in literature. Second, the three analyzed soil column experiments provide information about the evaporation at its point of extraction only. Although representative sites were selected based on field observations, the extrapolation of point information into spatial information introduces uncertainty. Due to these reasons, we derived the evaporation estimation for the study area and its error, accounting for the uncertainty in water level and the uncertainty in the regression models. Thus, we calculated in total nine evaporation rates with the three regression models (Eq. 3-1 to 3-3) using the median water level (0.75 m b.g.l.) and the median water level minus its mean error (0.47 m b.g.l.) and plus its mean error (1.03 m b.g.l.), respectively. We suggest the resultant arithmetic mean (42 mm a^{-1}) with a mean error of 13 mm a^{-1} is our best estimate for the evaporation rate from continental salt pans (playas).

3.6 Discussion

Spatial distribution

Mapping salt pans based on remote sensing techniques provided a spatially high-resolution picture of the current salt pan spatial distribution. In general, the spatial distribution is in line with the previous

map provided by USGS and ARAMCO (1963). However, on the smaller scale significant differences appear which was already discussed in section 3.5 and highlighted in Fig. 3-4. Due to their wide-spread distribution and their occurrence in remote areas, which are difficult to access (e.g. Rub' Al Khali desert), extensive validation of salt pan mapping results via ground truthing is practically impossible. Nevertheless, some studies specified the size of single salt pans, which could be used for comparison. Significant differences appear only for the salt pan Yabrin. Edgell (2006) reported an approximately four times bigger size compared to mapping during this study. In this context it is worth noting that in recent years the water level of the underlying aquifers in the area of Yabrin dropped due to pumping activities (Reeler et al., 2009), which might be an explanation for the decreasing salt pan extent. For the interdune salt pans in the Rub' Al Khali desert (Uruq Al Mu'taridah) a quantitative comparison is not possible as Edgell (2006) provided only a lower boundary for the size, which underlines the difficulties and uncertainties of providing reliable information in this remote area. However, in general, the mapped salt pan sizes fit well to estimates from other studies indicating a reasonable classification result (Tab. 3-2).

Tab. 3-2: Comparison of mapped salt pan areas with previous data provided by USGS and ARAMCO (1963) and other literature values

Salt pan	This study	USGS and ARAMCO (1963)	Other literature
Yabrin	55	54	204 (Edgell, 2006)
Al Budu	161	209	149 (Edgell, 2006)
Umm As Samim	1,500	4,300	2,400 (König, 2012)
Uruq Al Mu'taridah	12,000	8,000	min. 5,700 (Edgell, 2006)
Within a belt of 100 km from the coast	17,600	13,900	6000 to 8000 (Kinsman, 1969)
Total study area	35,500	27,500	-

Origin of salt pan brines

Salt pans close to the Arabian Gulf coast can be affected by seawater intrusion or tidal flooding, i.e. evaporating water from these coastal salt pans (sabkhat) does not originate from groundwater. Our hydrochemical and isotopic results show that the influence of seawater can reach up to 9 km distance to the coast. On the other hand, the closest salt pan with continental water was sampled in 3 km distance. Therefore, no clear spatial boundary between seawater dominated and groundwater dominated salt pans can be defined. This is expected as variations in geomorphological, hydrological, and sedimentological features along the coastline should have an impact on seawater intrusion, i.e. (i)

orientation of the coast in relation to the dominant wind direction (e.g. shamal wind system), (ii) general surface gradient, (iii) presence of barriers preventing tidal flooding (e.g. chenier ridges), (iv) presence of tidal channels, (v) groundwater gradient (displacing intruded seawater) (Patterson and Kinsman, 1981; Robinson and Gunatilaka, 1991). Consequentially, we assumed the boundary at the mean (6 km) between the closest continental water and furthest seawater influenced salt pan and based the error estimation (± 3 km) on the upper and lower boundary. It is noteworthy that the value of 6 km equals the corresponding distance found by Robinson & Gunatilaka (1991) for southern Kuwait. It is also roughly in line with the transition zone of 4.4 - 6 km identified by Müller et al. (1990), based on $^{87}Sr/^{86}Sr$ analyses of brines and sediments for salt pans in Abu Dhabi. Furthermore, Kinsman (1969) stated that coastal salt pans in the UAE extend locally up to 8 to 10 km inland, which is also in agreement with results from this study.

Net groundwater evaporation rate

The annual net groundwater evaporation from continental salt pans (playas) is a result of total evaporation (42 mm ± 13 mm) minus groundwater recharge (3 mm). The resulting estimate of 39 mm ± 13 mm is at the lower end of the range derived from the literature of 20 mm a^{-1} (Robinson and Gunatilaka, 1991) to 120 mm a^{-1} (Patterson and Kinsman, 1981; Shehata and Lotfi, 1993). It is important to note that most of the previous studies reported about evaporation rates from salt pans close to the Arabian Gulf, however, this study focuses on evaporation of groundwater and hence on evaporation from salt pans further inland. This is relevant as Patterson and Kinsman (1981) stated higher evaporation rates from coastal salt pans (120 mm a^{-1}) than from those which are located more inland (60 mm a^{-1}). The upper boundary of evaporation rates derived from the literature of 120 mm a^{-1} was reported in two studies. First, in the study of Patterson and Kinsman (1981), who mentioned that this value has to be seen as an upper limit. Second, Shehata and Lotfi (1993), who applied empirical equations which are only valid for freshwater and normal soils (Veihmeyer and Brooks, 1954; White, 1932) as they are not accounting for salt pan properties, counteracting evaporation: (i) high ionic strength of the salt pan brines, (ii) re-condensation of evaporated water during night when the relative humidity is high, and (iii) salt encrusted surfaces and hard, well-cemented gypsum crusts in the upper layers of continental salt pans (Kinsman, 1976; Robinson and Gunatilaka, 1991). These salt crusts and other low permeable layers also provide the reason for the small share of 5% of precipitation to infiltrate into salt pans. This is emphasized by the observation during several field trips that water ponds over salt pans for several days after larger rain events. Considering the previous mentioned points, our comparatively low estimate of annual net groundwater evaporation from continental salt pans (playas) of 39 mm ± 13 mm is reasonable.

3.7 Conclusion

Evaporation of shallow groundwater, also called evaporative pumping, from salt pans is of major importance for water resource assessments as it may cause a significant water loss from the connected aquifers. On the Arabian Peninsula this predominantly concerns the vital Upper Mega Aquifer system (Al-Saafin, 1996; GDC, 1980; Hsü and Schneider, 1973).

The present study uses a combination of different methods in order to provide a comprehensive picture of groundwater evaporation from salt pans of the Upper Mega Aquifer system. Mapping based on remote sensing techniques enhanced the estimation of the current salt pan spatial distribution and extent (36.500 km^2), which is about 33% more than previously mapped by USGS & ARAMCO (1963). Approximately 10% of it (3,600 km^2 ± 1,600 km^2) is influenced by seawater, while from the remaining 90% groundwater evaporates. Relating the spatial coverage of salt pans to the annual net groundwater evaporation of 39 mm ± 13 mm from continental salt pans leads to a total annual groundwater loss of 1.3 km^3 ± 0.5 km^3 for the Upper Mega Aquifer system.

The significance of groundwater evaporation from continental salt pans becomes apparent by comparing it with other water balance components. The main inflow component into the Upper Mega Aquifer system is groundwater recharge with estimations ranging from 1.5 $km^3\ a^{-1}$ (Al-Rashed and Sherif, 2000) to 2.9 $km^3\ a^{-1}$ (GIZ/DCo, 2013a, 2013b). Besides groundwater evaporation from salt pans, natural outflow components are spring discharge, submarine groundwater discharge into the Arabian Gulf, and discharge into the Euphrates (Kalbus et al., 2011). Due to falling groundwater levels, caused by modern groundwater abstraction, almost all springs dried up during the last decades. Al Tokhais and Rausch (2008) estimated a spring discharge for the beginning of the last century of about 0.5 $km^3\ a^{-1}$ (onshore and offshore springs). The main part of submarine groundwater discharge into the Arabian Gulf is represented by diffuse regional runoff of confined groundwater and amounts to about 0.2 $l\ s^{-1}\ km^{-2}$, or about 1.0 $km^3\ a^{-1}$ in total (Zektser et al., 2007). However, estimations of groundwater recharge and discharge into the Arabian Gulf are difficult and have to be evaluated as uncertain (Kalbus et al., 2011). Nevertheless, evaporation from salt pans is one of the main drivers for the groundwater flow of the Upper Mega Aquifer system on the Arabian Peninsula.

Countries on the Arabian Peninsula rely on its mainly non-renewable groundwater resources, what makes a smart resource management necessary. Required management strategies can be derived from simulations with groundwater flow models. While in general the present study aims to contribute to the scientific discussion of groundwater evaporation from continental salt pans, provided results might help to improve the reliability of future large scale groundwater flow models of the Upper Mega Aquifer system.

3.8 Acknowledgements

The authors thank the Ministry of Water & Electricity of Saudi Arabia for providing meteorological datasets. Furthermore, this work was kindly supported by GIZ IS (Gesellschaft für Internationale Zusammenarbeit - International Services) and Dornier Consulting. Stephan Schulz and Ulf Mallast acknowledge support from the BMBF funded project IWAS (grant code: 02WM1027) and SPACES (grant code: 02WSP1306A), respectively. The TRMM 3b42_V6 data used in this study were acquired as part of the Tropical Rainfall Measuring Mission (TRMM). TRMM is an international project jointly sponsored by the Japan National Space Development Agency (NASDA) and the US National Aeronautics and Space Administration (NASA) Office of Earth Sciences.

3.9 References

Abdel Galil, M., El-Fergany, E., 2011. Sedimentological Significance and Brine Chemistry of Recent Coastal Sabkha, Northwest Libya. J. King Abdulaziz Univ. Sci. 22, 135–158. doi:10.4197/Mar.22-2.8

Al Tokhais, A.S., Rausch, R., 2008. The Hydrogeology of Al Hassa Springs, in: The 3rd International Conference on Water Resources and Arid Environments. Riyadh.

Al-Rashed, M.F., Sherif, M.M., 2000. Water Resources in the GCC Countries: An Overview. Water Resour. Manag. 14, 59–75. doi:10.1023/A:1008127027743

Al-Saafin, A.K., 1996. The characterization of Sabkhas in the Eastern Parts of Saudi Arabia and its implications for engineering. University of London.

Barth, H.-J., 1998. Sebkhas als Ausdruck von Landschaftsdegradation im zentralen Küstentiefland der Ostprovinz Saudi-Arabiens. Regensburger geographische Schriften, Regensburg.

Briere, P.R., 2000. Playa, playa lake, sabkha: Proposed definitions for old terms. J. Arid Environ. 45, 1–7. doi:10.1006/jare.2000.0633

Butler, G.P., 1969. Modern Evaporite Deposition and Geochemistry of Coexisting Brines, the Sabkha, Trucial Coast, Arabian Gulf. SEPM J. Sediment. Res. Vol. 39. doi:10.1306/74D71BE5-2B21-11D7-8648000102C1865D

Bye, J.A.T., Harbison, I.P., 1991. Transfer of inland salts to the marine environment at the head of Spencer Gulf, South Australia. Palaeogeogr. Palaeoclimatol. Palaeoecol. doi:10.1016/0031-0182(91)90054-U

Castens-Seidell, B., 1984. The anatomy of a modern marine siliciclastic sabkha in a rift valley setting: Northwest Gulf of California tidal flats, Baja California, Mexico. Johns Hopkins University.

Clark, I., Fritz, P., 1997. Environmental Isotopes in Hydrogeology, 1st ed. Lewis Publishers, New York.

Davarzani, H., Smits, K., Tolene, R.M., Illangasekare, T., 2014. Study of the effect of wind speed on evaporation from soil through integrated modeling of the atmospheric boundary layer and shallow subsurface. Water Resour. Res. 50, 661–680. doi:10.1002/2013WR013952

Dee, D.P., Uppala, S.M., Simmons, A.J., Berrisford, P., Poli, P., Kobayashi, S., Andrae, U., Balmaseda, M.A., Balsamo, G., Bauer, P., Bechtold, P., Beljaars, A.C.M., van de Berg, L., Bidlot, J., Bormann, N., Delsol, C., Dragani, R., Fuentes, M., Geer, A.J., Haimberger, L., Healy, S.B., Hersbach, H., Hólm, E. V., Isaksen, L., Kållberg, P., Köhler, M., Matricardi, M., McNally, A.P., Monge-Sanz, B.M., Morcrette, J.-J., Park, B.-K., Peubey, C., de Rosnay, P., Tavolato, C., Thépaut, J.-N., Vitart, F., 2011. The ERA-Interim reanalysis: configuration and performance of the data assimilation system. Q. J. R. Meteorol. Soc. 137, 553–597. doi:10.1002/qj.828

Edgell, H.S., 2006. Arabian Deserts: Nature, Origin and Evolution. Springer Netherlands, Dordrecht. doi:10.1007/1-4020-3970-0

GDC, 1980. Umm Er Radhuma Study - Volume 3: Groundwater Resources. Cambridge.

GIZ/DCo, 2013a. Detailed Groundwater Resources Studies in the Rub' Al Khali Destert, Final Draft - Volume 11: Hydrology. Riyadh.

GIZ/DCo, 2013b. Detailed Groundwater Resources Studies of Khuff Jilh Minjur Dhruma and overlying Aquifers - Volume 13: Hydrology. Riyadh.

Heathcote, J.A., King, S., 1998. Umm as Samim, Oman: A sabkha with evidence for climatic change, in: Alsharhan, A.S., Glennie, K.W., Whittle, G.L., Kendall, C.G.S.C. (Eds.), Quaternary Deserts and Climatic Change. Balkema, Rotterdam, pp. 141–153.

Hernández-López, M.F., Gironás, J., Braud, I., Suárez, F., Muñoz, J.F., 2014. Assessment of evaporation and water fluxes in a column of dry saline soil subject to different water table levels. Hydrol. Process. 28, 3655–3669. doi:10.1002/hyp.9912

Hölting, B., Coldewey, W.G., 2009. Hydrogeologie, 7th ed. Spektrum, Heidelberg.

Hsü, K.J., Schneider, J., 1973. Progress Report on Dolomitization — Hydrology of Abu Dhabi Sabkhas, Arabian Gulf, in: Purser, B.H. (Ed.), The Persian Gulf. Springer Berlin Heidelberg, Berlin Heidelberg, pp. 409–422. doi:10.1007/978-3-642-65545-6_20

Hsü, K.J., Siegenthaler, C., 1969. PRELIMINARY EXPERIMENTS ON HYDRODYNAMIC MOVEMENT INDUCED BY EVAPORATION AND THEIR BEARING ON THE DOLOMITE PROBLEM. Sedimentology 12, 11–25. doi:10.1111/j.1365-3091.1969.tb00161.x

Jacobson, G., Jankowski, J., 1989. Groundwater-discharge processes at a central Australian playa. J. Hydrol. 105, 275–295. doi:10.1016/0022-1694(89)90109-1

Jaeger, F., 1942. Ein besonderer Seentypus: Die Trockenseen oder Pfannen, in: Geologie Der Meere Und Binnengewässer. Koeltz, Koenigstein, pp. 65–103.

Jarvis, A., Reuter, H.I., Nelson, A., Guevara, E., 2008. Hole-filled SRTM for the globe Version 4 [WWW Document]. available from CGIAR-CSI SRTM 90m Database. URL http://srtm.csi.cgiar.org

Johnson, E., Yáñez, J., Ortiz, C., Muñoz, J., 2010. Evaporation from shallow groundwater in closed basins in the Chilean Altiplano. Hydrol. Sci. J. 55, 624–635. doi:10.1080/02626661003780458

Kalbus, E., Oswald, S., Wang, W., Kolditz, O., Engelhardt, I., Al-Saud, M.I., Rausch, R., 2011. Large-scale Modeling of the Groundwater Resources on the Arabian Platform. Int. J. Water Resour. Arid Environ. 1, 38–47.

Kinsman, D.J.J., 1969. Modes of Formation, Sedimentary Associations, and Diagnostic Features of Shallow-Water and Supratidal Evaporites. Am. Assoc. Pet. Geol. Bull. 53, 830–840.

Kinsman, D.J.J., 1976. Evaporites: Relative humidity control primary mineral facies. J. Sediment. Petrol. 46, 273–279.

König, P., 2012. Plant life in the Umm as Samim, Oman – A case study in a major inland sabkha. J. Arid Environ. 85, 122–127. doi:10.1016/j.jaridenv.2012.06.007

Kummerow, C., Barnes, W., Kozu, T., Shiue, J., Simpson, J., 1998. The Tropical Rainfall Measuring Mission (TRMM) Sensor Package. J. Atmos. Ocean. Technol. 15, 809–817. doi:10.1175/1520-0426(1998)015<0809:TTRMMT>2.0.CO;2

Lloyd, J.W., Jacobson, G., 1987. The hydrogeology of the Amadeus Basin, Central Australia. J. Hydrol. 93, 1–24. doi:10.1016/0022-1694(87)90191-0

Mason, J.L., Kipp, K.L., 1998. Hydrology of the Bonneville Salt Flats, Northwestern Utah, and Simulation of Ground-Water Flow and Solute Transport in the Shallow-Brine Aquifer.

Menking, K.M., Anderson, R.Y., Brunsell, N.A., Allen, B.D., Ellwein, A.L., Loveland, T.A., Hostetler, S.W., 2000. Evaporation from groundwater discharge playas, Estancia Basin, central New Mexico. Glob. Planet. Change 25, 133–147. doi:10.1016/S0921-8181(00)00025-4

Moser, H., Pak, E., Rauert, W., Stichler, W., Zötl, J.G., 1978. Isotopic Composition of Waters of Al Qatif and Al Hasa Areas, in: Al-Sayari, S.S., Zötl, J.G. (Eds.), Quaternary Period in Saudi Arabia, Volume 1 - Sedimentological, Hydrogeological, Hydrochemical, Geomorphological, and Climatological Investigations in Central and Eastern Saudi Arabia. Springer, Wien/New York.

MoWE, 2014. Weather station data.

Müller, D.W., McKenzie, J.A., Mueller, P.A., 1990. Abu Dhabi sabkha, Persian Gulf, revisited: Application of strontium isotopes to test an early dolomitization model. Geology 18, 618–621.

Patterson, R.J., 1972. Hydrology and carbonate diagenesis of a coastal Sabkha in Persian Gulf. Princeton University.

Patterson, R.J., Kinsman, D.J.J., 1977. Marine and Continental Groundwater Sources in a Persian Gulf Coastal Sabkha. Am. Assoc. Pet. Geol. Bull. 4, 381–397.

Patterson, R.J., Kinsman, D.J.J., 1981. Hydrologic Framework of A Sabkha Along Arabian Gulf. Am. Assoc. Pet. Geol. Bull. 65, 1457–1475.

Pauw, E. De, 2002. An Agroecological Exploration of the Arabian Peninsula. ICARDA - International Center for Agricultural Research in the Dry Areas, Dubai.

Reeler, C.N., Shaikh, N.Y., Potts, D.T., 2009. An historical cartographic study of the Yabrīn oasis, Saudi Arabia, in: Proceedings of the Seminar for Arabian Studies. pp. 351–358.

Richards, G.W., Vita-Finzi, C., 1982. Marine deposits 35,000–25,000 years old in the Chott el Djerid, southern Tunisia. Nature 295, 54–55. doi:10.1038/295054a0

Rijsberman, F.R., 2004. Water Scarcity: Fact or Fiction?, in: 4th International Crop Science Congress. Brisbane.

Robinson, B.W., Gunatilaka, A., 1991. Stable isotope studies and the hydrological regime of sabkhas in southern Kuwait, Arabian Gulf. Sediment. Geol. 73, 141–159. doi:10.1016/0037-0738(91)90027-B

Sanford, W.E., Wood, W.W., 2001. Hydrology of the coastal sabkhas of Abu Dhabi, United Arab Emirates. Hydrogeol. J. 9, 358–366. doi:10.1007/s100400100137

Shampine, W.J., Dincer, T., Noory, M., 1979. An evaluation of isotope concentrations in the groundwater of Saudi Arabia. IAEA-SM-228/23 23.

Shehata, W., Lotfi, H., 1993. Preconstruction Solution for groundwater rise in sabkha. Bull. Int. Assossiation Eng. Geol. 47.

Smith, C.L., 1981. Reconnaissance investigation of brine in the eastern Rub Al Khali, Kingdom of Saudi Arabia, Open-File Report USGS. United States Geological Survey, Jiddah, Saudi Arabia.

Smith, C.L., 1982. Reconnaissance investigation of evaporites and brines of the Eastern Province, Kingdom of Saudi Arabia. Open-File Rep. USGS.

Sultan, M., Sturchio, N., Al Sefry, S., Milewski, A., Becker, R., Nasr, I., Sagintayev, Z., 2008. Geochemical, isotopic, and remote sensing constraints on the origin and evolution of the Rub Al Khali aquifer system, Arabian Peninsula. J. Hydrol. 356, 70–83. doi:10.1016/j.jhydrol.2008.04.001

Tyler, S.W., Kranz, S., Parlange, M.B., Albertson, J., Katul, G.G., Cochran, G.F., Lyles, B.A., Holder, G., 1997. Estimation of groundwater evaporation and salt flux from Owens Lake, California, USA. J. Hydrol. 200, 110–135. doi:10.1016/S0022-1694(97)00007-3

USGS, ARAMCO, 1963. Geologic map of the Arabian Peninsula - U.S. Geological Survey Misc. Inv. Map I-270 A, scale 1:2,000,000.

Valiantzas, J.D., 2006. Simplified versions for the Penman evaporation equation using routine weather data. J. Hydrol. 331, 690–702. doi:10.1016/j.jhydrol.2006.06.012

Veihmeyer, F.J., Brooks, F.A., 1954. Measurements of cumulative evaporation from bare soil. Eos, Trans. Am. Geophys. Union 35, 601–607. doi:10.1029/TR035i004p00601

White, W.N., 1932. A method of estimating groundwater supplies based on discharge by plants and evaporation from soil.

Yechieli, Y., Wood, W.W., 2002. Hydrogeologic processes in saline systems: playas, sabkhas, and saline lakes. Earth-Science Rev. 58, 343–365.

Zektser, I.S., Dzhamalov, R.G., Everett, L.G., 2007. Submarine Groundwater. CRC Press/Taylor & Francis Group, Boca Raton.

4 Improving large-scale groundwater models by considering fossil gradients

Stephan Schulz[a,], Marc Walther[b,c], Nils Michelsen[a], Randolf Rausch[a], Heiko Dirks[d], Mohammed Al-Saud[e], Ralf Merz[b], Olaf Kolditz[b,c], Christoph Schüth[a]

[a] Technische Universität Darmstadt, 64287 Darmstadt, Germany

[b] Helmholtz Centre for Environmental Research – UFZ, 06120 Halle, Germany

[c] Technische Universität Dresden, 01069 Dresden, Germany

[d] Dornier Consulting, Riyadh, Saudi Arabia

[e] Ministry of Water & Electricity, Riyadh, Saudi Arabia

4.1 Abstract

Due to limited availability of surface water, many arid to semi-arid countries rely on their groundwater resources. Despite the quasi-absence of present day replenishment, some of these groundwater bodies contain large amounts of water, which was recharged during pluvial periods of the Late Pleistocene to Early Holocene. These mostly fossil, non-renewable resources require different management schemes compared to those which are usually applied in renewable systems. Fossil groundwater is a finite resource and its withdrawal implies mining of aquifer storage reserves. Although they receive almost no recharge, some of them show notable hydraulic gradients and a flow towards their discharge areas, even without pumping. As a result, these systems have more discharge than recharge and hence are not in steady state, which makes their modelling, in particular the calibration, very challenging. In this study, we introduce a new calibration approach, composed of four steps: (i) estimating the fossil discharge component, (ii) determining the origin of fossil discharge, (iii) fitting the hydraulic conductivity with a pseudo steady-state model, and (iv) fitting the storage capacity with a transient model by reconstructing head drawdown induced by pumping activities. Finally, we test the relevance of our approach and evaluated the effect of considering or ignoring fossil gradients on aquifer parameterization for the Upper Mega Aquifer (UMA) on the Arabian Peninsula.

4.2 Introduction

In many arid to semi-arid regions, surface water resources are limited and often variable in their temporal availability (Scanlon et al., 2006; Tsur, 1990). Consequently, they have to rely on other water sources. While desalination of seawater is a valuable option, especially for public water supply, typically groundwater is used to cover the large agricultural water demand (FAO, 2009; Margat and van der Gun, 2013). However, due to the arid climates, these groundwater resources receive only limited recharge. Some of the aquifers even have to be considered as non-renewable, which means

that the period needed for replenishment is very long in relation to normal time scales of water management planning. Margat et al. (2006) defined a renewal period of more than 500 years to categorize non-renewable aquifer systems. Nevertheless, some of them hold large quantities of water, which were infiltrated during wetter periods in the past several thousand or even ten-thousands of years ago. These so-called fossil, non-renewable groundwater resources are finite and some of them are already heavily exploited (Fig. 4-1). Prominent examples are: (i) the Great Man-Made River Project tapping the Nubian Aquifer system and the Murzuk Basin in Libya (Salem, 1992); (ii) the southern part of the High-Plains Aquifer in the USA (McGuire, 2009); and (iii) the sedimentary aquifer systems of the Arabian Peninsula (UN-ESCWA and BGR, 2013). Due to intensive pumping activities, the given examples show a water level decrease of more than one hundred meters in some areas over the last decades. Moreover, they are often vulnerable to quality deterioration caused by upconing water with higher salinity from adjacent saline waters (Foster and Loucks, 2006; Reilly and Goodman, 1987). In view of the current population growth, increasing water consumption per capita, and decreasing drilling and pumping costs, which have been observed during the last decades in most arid and semi-arid countries, the stress on fossil, non-renewable aquifers will become even more serious (Al-Rashed and Sherif, 2000; FAO, 2016; Wada et al., 2010). Yet, little of the economic benefit of groundwater exploitation was reinvested into its management. However, sound management strategies are important in order to find the balance between satisfying todays demand on the one hand and keeping appropriate future reserves and minimising quality deterioration on the other hand.

Numerical groundwater flow models are powerful management tools. They are applied to simulate development schemes, predict responses to climate change, and to quantify available resources. The latter is of great importance for non-renewable aquifers. The management approach for non-renewable resources is fundamentally different from that of renewable resources (Foster and Loucks, 2006). The optimal management goal for renewable aquifers is its sustainable use, which is considered as the ‘safe yield’ concept. Here, the key value is the replenishment rate, i.e. groundwater recharge. In contrast, non-renewable aquifers cannot be used sustainably. In that case, groundwater withdrawal implies mining of the reserves. This means that the aquifer storage capacity is the key value for managing non-renewable aquifers. In case of large and deep groundwater reservoirs, it is very expensive to measure the spatial distribution of aquifer storage capacity since deep boreholes and long term pumping tests are required. Therefore, the storage coefficient is commonly one of the parameters, which is fitted during model calibration. This, in turn, implies that good calibration schemes are particularly important for non-renewable aquifer systems, resulting in reliable aquifer parameter configurations and hence enhancing the prediction accuracy of the models.

Although fossil, non-renewable aquifers receive almost no recharge, some of them show notable groundwater gradients and a flow towards discharge areas. It is assumed that these gradients result

from present day recharge but also from recharge mounds formed during pluvial periods, e.g. in the Late Pleistocene to Early Holocene, and their subsequent long-term head decay (Bourdon, 1977; Lloyd and Farag, 1978; Rousseau-Gueutin et al., 2013). It follows that a groundwater system driven by these so-called fossil gradients has more discharge than recharge, even without pumping. Hence, it is not in steady state, which makes its modelling, in particular the calibration, even more challenging. This phenomenon is usually only observed in large aquifer systems as the time for returning to steady-state increases by the flow length from recharge to discharge areas (Rousseau-Gueutin et al., 2013). Neglecting fossil gradients, i.e. assuming steady-state conditions, can lead to fundamental errors in calculating groundwater resources and managing the development of aquifers (Bourdon, 1977).

Yet, only a few studies address such fossil gradients in groundwater flow modelling, typically using two different approaches. (i) Most studies set up a transient model to meet the present-day groundwater heads, assuming initially filled up aquifers (groundwater level at surface) during the last pluvial period. Flux rates (e.g. recharge) are assumed along the calibration of hydraulic conductivity (K) and storage coefficient (S) of the aquifer. Examples are an analogue model for an idealized basin from Lloyd and Farag (1978); numerical models of the Nubian Aquifer System (Heinl and Brinkmann, 1989; Thorweihe and Heinl, 2002; Wright et al., 1982); and theoretical models for an Andean aquifer in Chile (Houston and Hart, 2004), and the Kalahari and Karoo aquifer in the southern part of Africa (De Vries, 1984). (ii) The other type of model setup relies on recent observations. Here, K and S are varied during calibration to reconstruct depression cones induced by pumping activities. Examples are numerical models from a part of the Arabian Aquifer System (Engelhardt et al., 2013) and the Nubian Aquifer System (Gossel et al., 2004).

However, all these studies face at least one of the following calibration problems. The first problem is that for non-steady state (transient) systems the aquifer properties hydraulic conductivity (K) and storage coefficient (S) have to be calibrated simultaneously. Especially for large aquifer systems with many different hydrogeological units, fitting K and S or even Q (flux rates like groundwater recharge) together might lead to non-unique solutions having a good agreement between simulated and observed heads (Carrera and Neuman, 1986). This phenomenon is called equifinality and is thoroughly discussed by Beven (2006). The second problem is that transient models require precise initial conditions (groundwater head distributions) and flux rates (e.g. groundwater recharge) over the entire model period. Considering the very large time scales, i.e. recharge periods, which might sum up to several thousand years, it is almost impossible to obtain reliable information about initial groundwater head distributions and flux rates.

The aim of this study is to introduce and test a new method to calibrate non-steady state models for large aquifer systems with fossil gradients avoiding the aforementioned calibration problems. The new calibration approach comprises four steps: (i) quantifying the fossil discharge component, (ii)

determining the origin of fossil discharge, (iii) fitting K with a pseudo steady-state model, and (iv) fitting S with a transient model for the last decades by reconstructing head drawdown induced by pumping activities. The applicability of the method is presented for the example of a large-scale 3D numerical groundwater flow model using the numerical open-source modelling package OpenGeoSys (Kolditz et al., 2012).

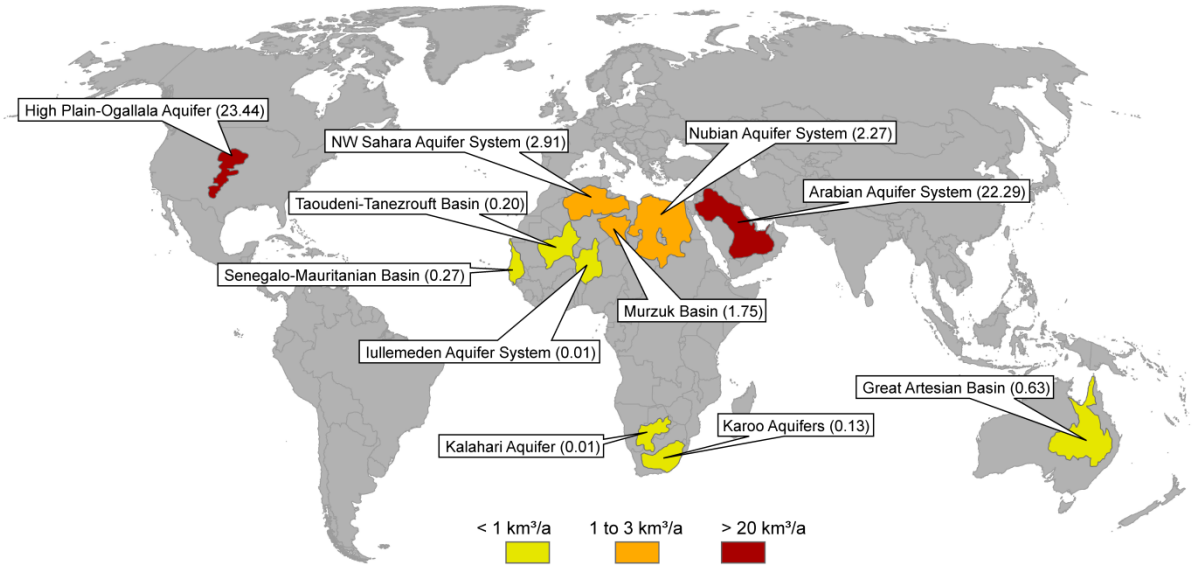

Fig. 4-1: Selected non-renewable, fossil groundwater systems; numbers indicate the annual abstraction rate [$km^3 a^{-1}$] (Margat and van der Gun, 2013); the High Plain-Ogallala Aquifer has to be considered as partly non-renewable as it only receives recharge in its northern part (Gutentag et al., 1984)

4.3 Material and methods

Study area

The study site comprises the Upper Mega Aquifer system of the Arabian Peninsula. The main part of the groundwater resources of the Arabian Peninsula is stored in huge sedimentary basins of the Arabian Platform (Al-Rashed and Sherif, 2000). In its sum, these groundwater reserves are commonly termed Arabian Aquifer System (Fig. 4-1). Its principal sub-systems are the Saq/Disi-Ram Aquifer System, the Wajid Aquifer, the Khuff-Jilh-Minjur Aquifer System, and the so-called Upper Mega Aquifer (UMA) system (GIZ/DCo, 2013; Kalbus et al., 2011; UN-ESCWA and BGR, 2013). The latter is subject of this study. It covers a surface area of about $1.7 \cdot 10^6$ km^2 and comprises a sedimentary succession from the Lower Cretaceous to the Neogene. Its principal aquifers are the Biyadh and Wasia sandstone aquifers and the karstified Umm Er Radhuma and Dammam limestone aquifers, which are interbedded with layers with lower hydraulic conductivities (Fig. 4-2).

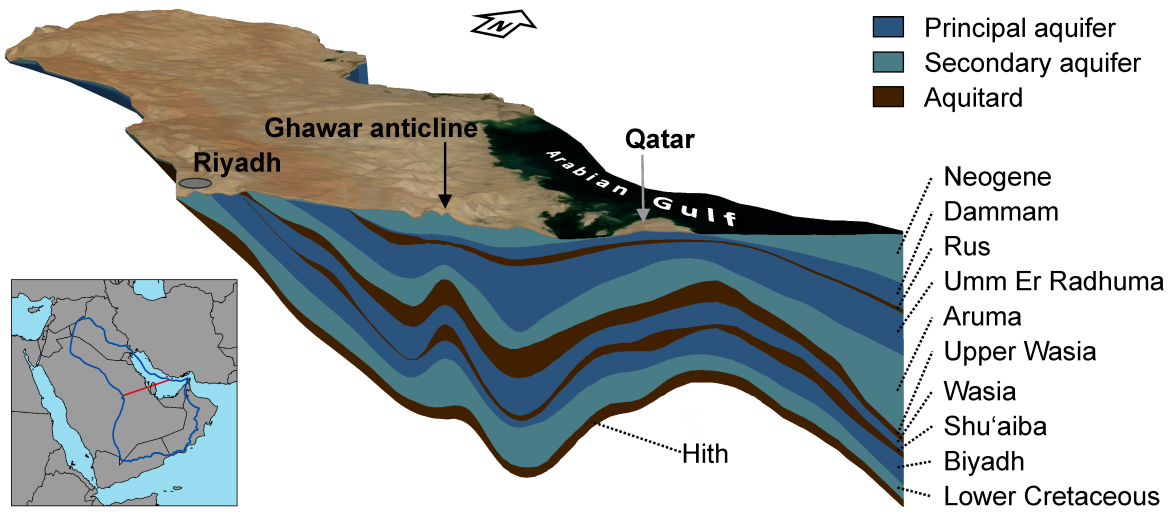

Fig. 4-2: Cross section (red line, 705 km length) and surface extent (blue border) of the Upper Mega Aquifer system (vertical exaggeration of 100)

Past and present day climate

The present-day climate of the Arabian Platform is classified as arid to hyper-arid. It is characterized by average annual temperatures ranging from 20 °C in its northern part to 28 °C in the Rub' Al-Khali desert. Following the temperature gradient, the mean rainfall rate drops from 150 to 40 mm a^{-1} (Pauw, 2002). These climatic conditions lead to very limited groundwater recharge rates from almost no recharge in the sand desert areas (GIZ/DCo, 2014) to about 5 mm a^{-1} in more favourable areas like karst outcrops (Schulz et al., 2016) or 7 mm a^{-1} in wadis (Bendel, 2009). For the whole Upper Mega Aquifer System GIZ/DCo (2014, 2013a) estimated a present day average annual recharge amount of about 2 mm, although the estimation of reliable recharge rates for arid regions is very challenging, due to its non-linear response to infrequent rainfall events (Schulz et al., 2016). However, recharge characteristics and values reported for the Arabian Peninsula are in line with the results of studies conducted in regions with comparable geographic and climatic settings, e.g. central Australia (Cendón et al., 2010; Meredith et al., 2015).

During the Late Pleistocene to Early Holocene, the Arabian Peninsula experienced some pluvial periods (Groucutt and Petraglia, 2012; Sarnthein, 1978). The last wet period occurred at the end of the late glacial maximum starting with a rapid increase in precipitation from 10.3 to 9.6 ka BP and ended with a gradual decrease from 8 to 2.7 ka BP (Fleitmann et al., 2003). Larsen (1983) analysed remains of mammal fauna of paleo-lake sediments indicating a savannah landscape with an arid to semi-arid climate for the wet period. This hypothesis is supported by a rock art site about 100 km west of Riyadh showing animals like antelopes, ostriches, and buffalos, which fit into the picture of a savannah landscape (Annex A 13). In terms of quantities, water balance calculations suggest that the Arabian Peninsula received three to five times more precipitation during the last pluvial period than today

(Engel et al., 2012; Wood and Imes, 1995). As a consequence, groundwater recharge rates were significantly higher than today, however, far less compared to those which are typical for humid areas. Wood and Imes (1995) for instance, estimated a groundwater recharge rate for the Rub' Al-Khali desert of 1.4 mm a^{-1} during the wet periods.

Methods and tools

Our geometric model is a three-dimensional finite element model with about 265,000 elements. To simulate the groundwater flow, we used the open-source, numerical modelling tool OpenGeoSys (Kolditz et al., 2012). The nonlinear parameter estimation during the calibration process was performed with the model-independent parameter estimation software PEST. Basically, PEST varies a defined set of parameters (vertical and horizontal hydraulic conductivity, and the specific storage) to minimize the sum of squared weighted residuals of simulated and observed potentiometric heads. The applied optimization method is the Gauss-Marquardt-Levenberg method (Doherty and Hunt, 2010).

In addition, we used two other criteria to describe and evaluate the fit of simulated and observed heads – the bias and the Kling-Gupta efficiency (KGE).

The bias indicates systematic discrepancies.

$$\text{bias} = \frac{1}{n} \cdot \sum_{i=1}^{n} (h_{sim} - h_{obs}) \tag{4-1}$$

where n is the number of measured groundwater heads, h_{sim} are the simulated heads, and h_{obs} the observed heads.

The KGE accounts for the linear correlation (r, Eq. 4-3), the variability error (α, Eq. 4-4), and the bias error (b, Eq. 4-5) and incorporates them into a single multi-objective criterion. The KGE ranges from -∞ to 1, whereby higher values indicate a better fit (Gupta et al., 2009).

$$\text{KGE} = 1 - \sqrt{(r-1)^2 + (\alpha-1)^2 + (b-1)^2} \tag{4-2}$$

with

$$r = \frac{Cov_{sim,obs}}{\sigma_{sim} \cdot \sigma_{obs}} \tag{4-3}$$

$$\alpha = \frac{\sigma_{sim}}{\sigma_{obs}} \tag{4-4}$$

$$b = \frac{\mu_{sim}}{\mu_{obs}} \tag{4-5}$$

where $Cov_{sim,obs}$ is the covariance between the simulated and observed heads, σ_{sim} is the standard deviation of the simulated heads, σ_{obs} is the standard deviation of the observed heads, μ_{sim} is the arithmetic mean of the simulated heads, and μ_{obs} is the arithmetic mean of the observed heads.

Conceptual model and data

The lateral model extent of the UMA system comprises almost the whole Arabian Platform (Fig. 4-2). In the West and in the Southwest, it is bounded by the outcrops of its geological formations. This constitutes a no-flow boundary as the sealing bottom layer (Hith Aquitard) also almost reaches the surface (Fig. 4-2). In the Northwest, the model boundary follows a structural high (Hail Arch) close to the border to Jordan. And in the East, the UMA System is bounded by a virtual line through the deepest areas of the Arabian Gulf. The latter two boundaries constitute no-flow boundaries as well. In the Southeast, the model is bounded by a major fault west of the Oman Mountains, where a constant inflow into the Neogene aquifer from adjacent subbasins is assumed (GIZ/DCo, 2014). In the Northeast, it is limited by the Euphrates and Schatt Al-Arab, which are constant head boundaries (Fig. 4-3). Vertically, the top boundary for the model is the ground/seafloor surface, whereby the seafloor surface of the Gulf constitutes again a constant head boundary. Here, we used equivalent freshwater heads for the corresponding water column. The bottom boundary is the Hith Aquitard, which constitutes again a no-flow boundary.

The general groundwater flow of the UMA system takes place from the outcrop areas in the West and South to the natural discharge areas in the East (Euphrates and Gulf). It is driven on the one hand by its fossil gradient and on the other hand by its sink and source terms (Fig. 4-3). The major source of the system is the recharge from precipitation (Annex A 14). Moreover, it receives an additional inflow via leakage from underlying aquifers through wadis intersecting the outcrops of both systems. A very important sink besides the discharge into Euphrates and Gulf is the groundwater evaporation from salt pans (Schulz et al., 2015). Furthermore, natural discharge occurred via springs, which almost all ran dry during intensive groundwater exploitation starting in the 1950s. Conversely, extensive groundwater abstraction from the UMA system started in the 1950s (Annex A 15). Lacking of precise abstraction data in time and space for other countries, we only considered abstraction in Saudi Arabia within our model.

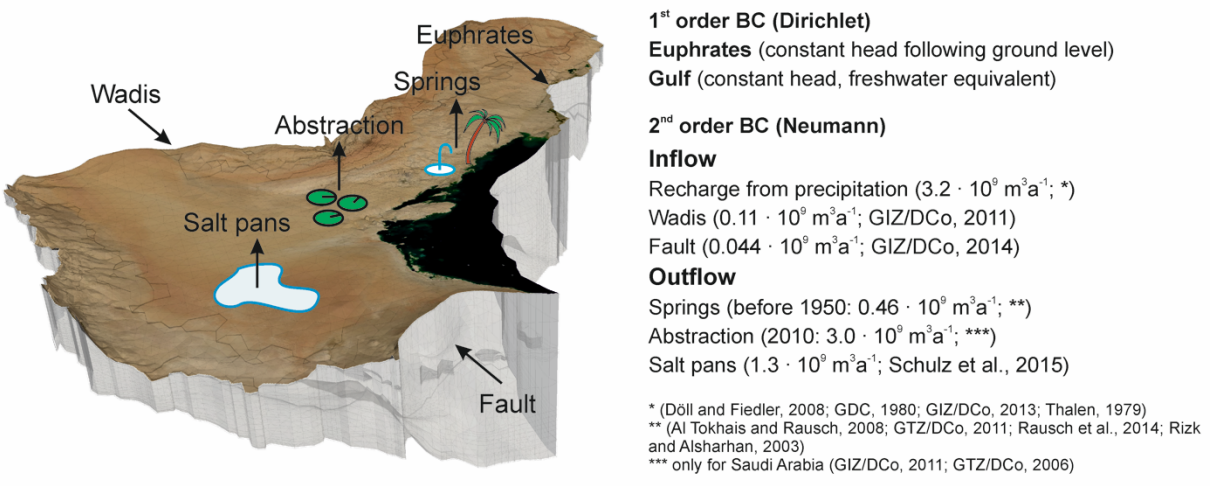

Fig. 4-3: Boundary conditions (BC) of the UMA system, vertical exaggeration of 100

We subdivided the system into ten hydrogeological units (as shown in Fig. 4-2, excluding the sealing bottom layer), whereby each is represented by two layers in the finite element mesh of the groundwater flow simulation model. The UMA system is a sedimentary basin which experienced different depositional environments over time. In general, its basin shaped geometry lead to deposition of coarser sediments at its margin and finer sediments in the centre, e.g. the Wasia aquifer (Fig. 4-4). Analysing these depositional environments of the basin, Ziegler (2001) mapped lithofacies distributions for the afore mentioned hydrogeological units. Based on this, we defined nine different hydrofacies types. Subsequently, we assigned the relevant hydrofacies types to the hydrogeological units, which is exemplarily shown in Fig. 4-4 for the Wasia aquifer. Hydrofacies zones (as we have implemented them in the numerical model) for the other hydrogeological units are presented in the Annex A 16.

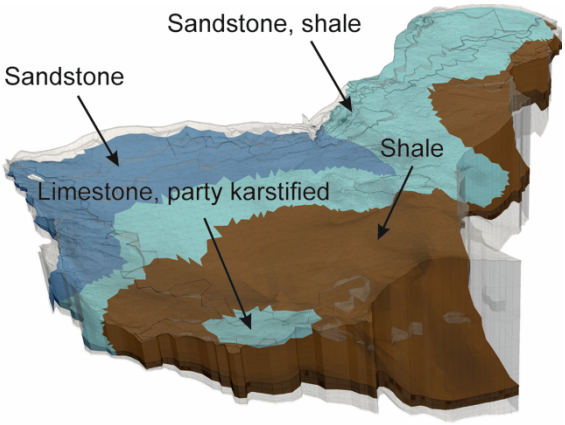

Fig. 4-4: Hydrofacies zones of the Wasia aquifer derived from the lithofacies zones of Ziegler (2001), vertical exaggeration of 100

Information about the parameterization of the hydrofacies zones are extracted from facies and pumping test analysis (GIZ/DCo, 2014, 2011; GTZ/DCo, 2006). These values are presented in the Annex A 17 and A 18 and are termed starting or initial parameters in the following.

Evidence for fossil gradients

The presence of fossil groundwater gradients in the UMA system, in particular for the Umm Er Radhuma aquifer, was already described by Bakiewicz et al. (1982). They justified their assumption of fossil gradients by pointing out analogies to other aquifer systems for which Bourdon (1977) and Lloyd and Farag (1978) postulated fossil gradients based on findings from resistance network modelling. Another indication for fossil gradients is given by an archaeological study from Larsen (1983). He dated settlements and irrigation systems on Bahrain and in Eastern Arabia and found a decreasing trend in their elevation over the last 5,000 a, which he traced back to a natural potentiometric head decline of artesian springs.

Within the present study, we provide two additional indications for the presence of fossil gradients. (i) We run a steady-state simulation with a numerical model of the pre-industrial UMA system, parameterized with the previously defined starting values. The resulting, simulated potentiometric heads are on average more than one hundred meters below the observed ones (see Annex A 19). This points towards the presence of paleo recharge mounds, i.e. fossil gradients. (ii) We applied an analytical method, proposed by Rousseau-Gueutin et al. (2013) to calculate the time to reach a new near steady-state condition after a so called large hydraulic perturbation for confined aquifer systems and mixed aquifer systems. In analogy to the Great Artesian Basin, which is the main study area of Rousseau-Gueutin et al. (2013), the large hydraulic perturbation is caused by a change in the boundary conditions of the system, i.e. a decrease of groundwater recharge after the last pluvial period during the Late Pleistocene to Early Holocene. Following their method, the calculated time to reach a new near steady-state for the UMA system is about 160,000 a and 120,000 a for a confined and a mixed (confined and unconfined parts) aquifer system, respectively. The details of this calculation are shown in the Annex A 20. As the last pluvial period is only about 8,000 a ago, it is very likely that the UMA system is still in a transient stage and shows fossil gradients. Petersen et al. (2014) proposed for the North-Western Sahara Aquifer System nine quite evenly distributed humid periods with groundwater recharge rates up to 60 mm a^{-1} during the last 775,000 a. Assuming comparable wet and dry cycles for the Arabian Peninsula would even lead to the conclusion that the UMA system is not in steady-state since several hundreds of thousands of years. Therefore, a time lag between two subsequent humid periods lower than the hydraulic equilibration time can explain persisting high hydraulic heads related to these substantial recharge periods.

Calibration approach

We already introduced potential calibration problems for groundwater systems with fossil gradients, i.e. equifinality, unknown initial heads, and unknown sink and source terms over the entire modelling period. In order to avoid these serious calibration problems, we introduce a novel calibration technique for the specific case of regional groundwater systems with fossil gradients.

The basic principle of that technique is to estimate the groundwater outflow (in our case the discharge into the Gulf and Euphrates, which are both constant head boundaries) originating from fossil recharge mounds. Subsequently, we balance out the system, which means that we create quasi steady-state conditions, by adding this additional outflow to the recharge. With the resulting steady state model, we are able to calibrate only the hydraulic conductivity (K). Finally, we calibrate a transient model of the last decades in order to fit the specific storage (S_S). In detail, this technique includes the following four processing steps.

First, we estimate the discharge amount into the Gulf and the Euphrates originating from fossil recharge mounds. For that purpose, we parameterized our model with starting parameter values (Annex A 17 and A 18). Sink and source fluxes are set to pre-industrial rates, i.e. no groundwater abstraction but spring discharge for 1950 (Fig. 4-3). Subsequently, we fill our model (setting the initial groundwater heads to ground surface) and run a transient simulation for 1×10^7 a in logarithmic time steps. For each time step, we evaluate the fit of the simulated to the observed pre-industrial heads at 40 randomly chosen observation points extracted from contour maps for each aquifer with the KGE criterion. Additionally, we obtain the total discharge to the Gulf and Euphrates. Then, we assume that the discharge at the simulation time of the best model fit is approximately the pre-industrial discharge. We, furthermore, assume steady-state discharge as soon the change in discharge from one time step to the next is smaller than $1 \cdot 10^6$ m^3a^{-1}. This somehow arbitrary threshold is justified as we are expecting fossil discharge rates to be about three orders of magnitude higher. Subtracting the steady-state discharge from the pre-industrial discharge previously identified yields an approximation for the discharge rate into Gulf (Q_{Gf}) and Euphrates (Q_{Ef}) originating from fossil recharge mounds. Further discussion on the significance of that artificial simulation is given below in section 3.1.

Second, we determine the origin of groundwater discharging into the Gulf and Euphrates within the model domain by backward particle tracking. This step is necessary to identify the location, where we have to add the additional outflow to the recharge in order to create the quasi steady-state conditions.

Third, we add the fossil outflow (Q_{Gf} and Q_{Ef}) to the recharge and run a steady state calibration in order to calibrate one value of K_v and K_h for each hydrofacies by fitting simulated to observed groundwater heads. We, hereby, distinguish between three different types of observed pre-industrial head data: (i) monitoring wells with a single measurement, (ii) monitoring wells with time series records and (iii)

head data extracted from contour maps (GIZ/DCo, 2014, 2011; GTZ/DCo, 2006). The latter have a questionable accuracy as they are derived from interpolated data; however, this data source has the crucial advantage that it covers the entire aquifer system. All water levels are given in equivalent fresh water heads. As we are expecting different levels of accuracy from the three different types of observed head data, we applied the specific weighting factors: 0.17, 0.5, and 1 for head data extracted from contour maps, monitoring wells with a single measurement, and monitoring wells with time series records, respectively.

Fourth, we run a transient simulation from 1950 to 2010 using the best fitting hydraulic conductivities from the previous step and varying the specific storage coefficient (S_S) to fit simulated groundwater drawdown to observed depression cones induced by pumping activities – an approach, which shows some analogies to a very large scale pumping test.

Sensitivity test and parameter refinement

In order to demonstrate the sensitivity of the presented calibration approach, we run the parameter fitting (steps three and four of our calibration approach) for four different cases, i.e. four different assumptions of fossil discharge rates into Gulf and Euphrates. Thus, we accounted for fossil discharge rates during

(i) mean best fitting time minus its standard deviation (highest fossil discharge)
(ii) mean best fitting time (assumed to represent the real case)
(iii) mean best fitting time plus its standard deviation
(iv) steady-state period (no fossil discharge).

Subsequently, we refined the parameter estimation of K and S_S. To this end, we updated the initial values for K and S_S by those resulting from the calibration of case (ii) and repeated the whole calibration procedure.

4.4 Results

Discharge into Gulf and Euphrates

During the first step of the calibration approach, we run a transient simulation parameterized with the starting values derived from pumping test analyses and initial heads set to ground surface. This yields different fits of simulated to observed present day heads for each time step. As the time of best model fit is not the same for each aquifer, we determined its arithmetic mean over time to be representative for the entire model (Fig. 4-5 A). At the mean best fitting time ($5.3 \cdot 10^4$ a), the groundwater discharge

originating from fossil recharge mounds to the constant head boundaries Gulf and Euphrates is 0.95 · 10^9 m^3a^{-1} and 0.25 · 10^9 m^3a^{-1}, respectively. Moreover, we calculated the fossil discharge rates for the mean time minus its standard deviation (1.23 · 10^9 m^3a^{-1} for Gulf and 0.67 · 10^9 m^3a^{-1} for Euphrates at 2.0 · 10^4 a) and plus standard its deviation (0.75 · 10^9 m^3a^{-1} for Gulf and 0.15 · 10^9 m^3a^{-1} for Euphrates at 8.5 · 10^4 a) in order to test the sensitivity and relevance of our approach (Fig. 4-5 B and C).

Although this transient simulation could give the impression to represent the temporal evolution of groundwater discharge into Gulf and Euphrates for the last couple of thousands of years, this is not the case. As we run this simulation with the pre-industrial (1950) sink and source terms, it is only valid for this time. It only provides an estimate for the discharge for 1950, which equals in good approximation the present-day discharge neglecting any man-made abstraction.

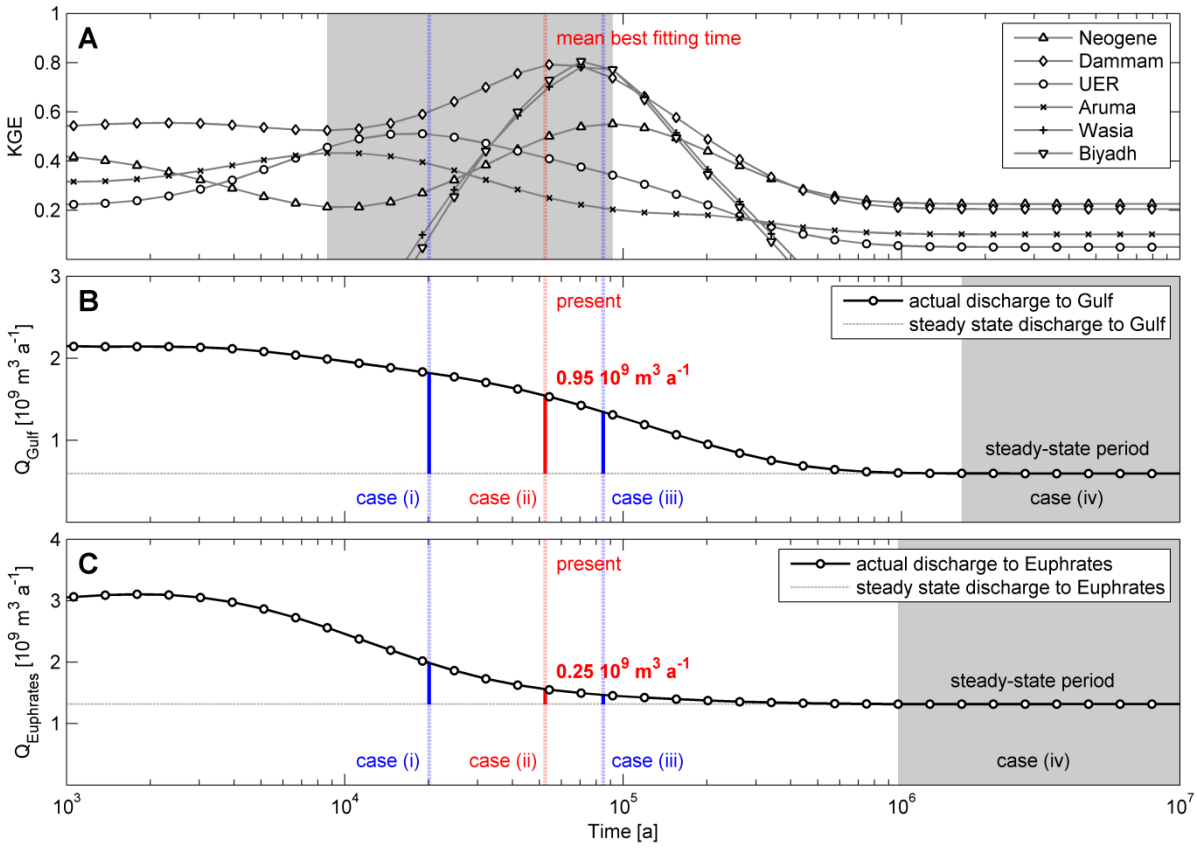

Fig. 4-5: (A) Goodness of fit (KGE) of simulated and pre-industrial heads of a draining transient model parameterized with starting values, the grey zone represents the range of the best fitting times for the six formations; (B) discharge into the Arabian Gulf; (C) discharge into the Euphrates basin

In phase two, backward particle tracking from the main pre-industrial discharge components (Gulf, Euphrates, and salt pans) illustrates the origin of the discharging groundwater. As expected, the groundwater catchment of the Euphrates within our model area is the entire northern part of the

model domain. However, in the middle and southern part, backward tracking demonstrates that the upper aquifers (Umm Er Radhuma, Dammam, and Neogene) predominantly discharge into the salt pans and only the lower aquifers (Biyadh and Wasia) predominantly discharge into the Gulf (Fig. 4-6). Based on this finding, we add the fossil discharge rates that reach the Euphrates to the entire northern part and those that enter the Gulf only to the outcrops of the Biyadh and Wasia aquifers in the middle and southern part. We, hereby, balanced out the system and hence created quasi steady-state condition for the further calibration of the hydraulic conductivity (K_h and K_v).

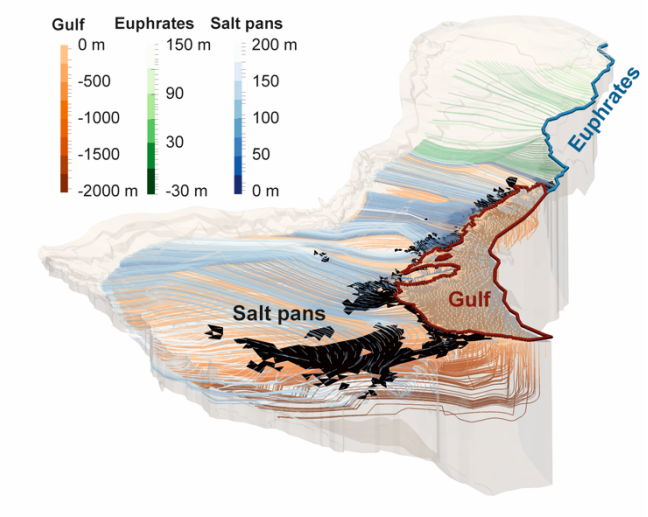

Fig. 4-6: Backward particle tracking from the main pre-industrial discharge components (Gulf, Euphrates and salt pans); vertical exaggeration of 100

Quasi steady-state model

In phase three, the steady-state model calibration, for which we only need to adjust the hydraulic conductivity, is performed for the previously mentioned four different cases. The goodness of fit of the calibrated model is evaluated with the root mean squared error (RMSE), KGE, and the bias. The evaluation criteria show comparable values for all cases with a mean RMSE of 22 m, a mean KGE of 0.87, and a mean absolute bias of 0.31 m. A scatter plot of simulated and observed heads for case (ii) and a table with calibrated hydraulic conductivities and the evaluation criteria (RMSE, KGE, and bias) for all cases is given in the Annex A 19 and A 17, respectively.

Fig. 4-7 shows the calibrated hydraulic conductivities for the previously mentioned model cases. Indicated by a parallel shift from the 1:1 line, it is notable that the orthotropy factor differs in a wide range from about 0.25 (evaporites) to almost 1000 (e.g. sandstone). Moreover, most hydrofacies show decreasing hydraulic conductivities from case (i) to case (iv) up to 2 orders of magnitude. Exceptions are limestone (karstified) and transition zone, and limestone (partly karstified), which are slightly

increasing in the horizontal hydraulic conductivity or vertical hydraulic conductivity, respectively. The general trend is also reflected by the geometric mean, which is commonly used as an approximation for block conductivity (Davis, 1987).

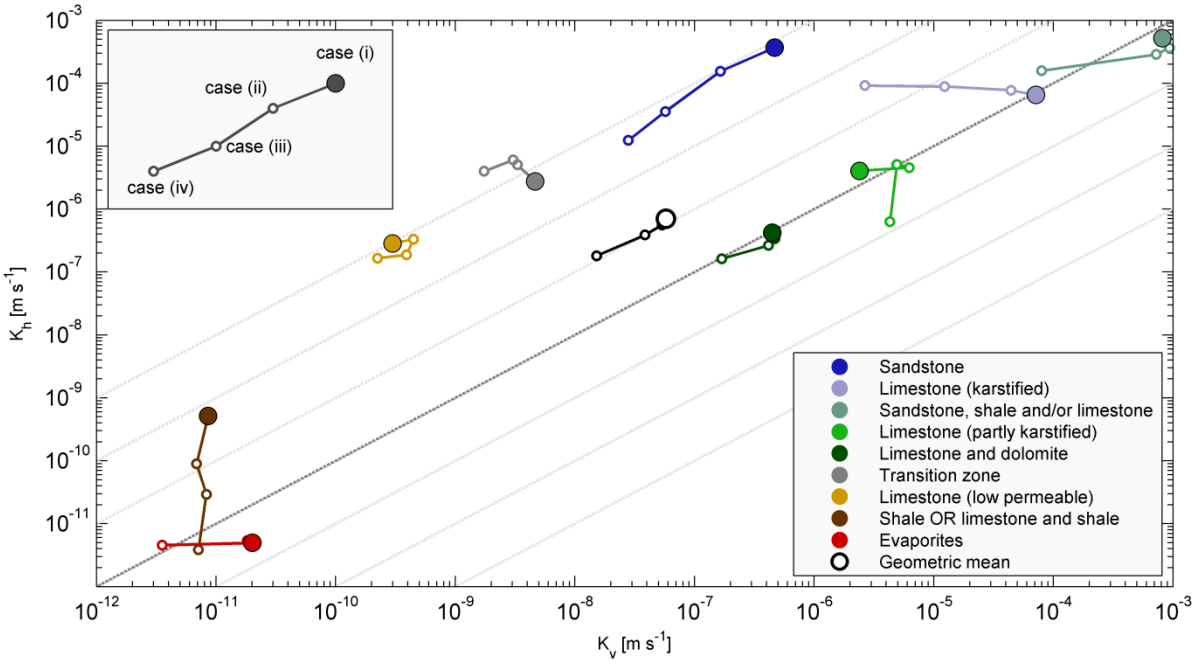

Fig. 4-7: Variability of horizontal and vertical hydraulic conductivity depending on the model response of cases (i) to (iv) for different hydrofacies zones

Transient Model

During the fourth and last step of the calibration approach, the transient model calibration is performed for the four previously mentioned cases for a simulation period from 1950 to 2010. The initial potentiometric head distribution for these transient simulations is extracted from the corresponding pre-industrial steady-state models. We kept the hydraulic conductivity fixed and only calibrate one specific storage (S_S) value for each hydrofacies zone where groundwater abstraction takes place (Annex A 18). Fig. 4-8 A shows the three major abstraction areas of the Wasia aquifer with their corresponding simulated cones of depression. The drawdown southeast of Riyadh is predominantly caused by agricultural abstraction around the city Kharj. For this area, we have no groundwater head observation data for the Wasia aquifer. The abstraction area northeast of Riyadh is the Wasia Well Field, which is an important water source for the domestic water supply of Riyadh. The largest continuous abstraction area in Fig. 4-8 A located in the eastern part of the Arabian Peninsula is mainly caused by groundwater abstraction for oil hauling around the Ghawar oil field – the largest oil

field of the world. Fig. 4-8 B to D exemplarily show simulated and observed heads over the simulation period.

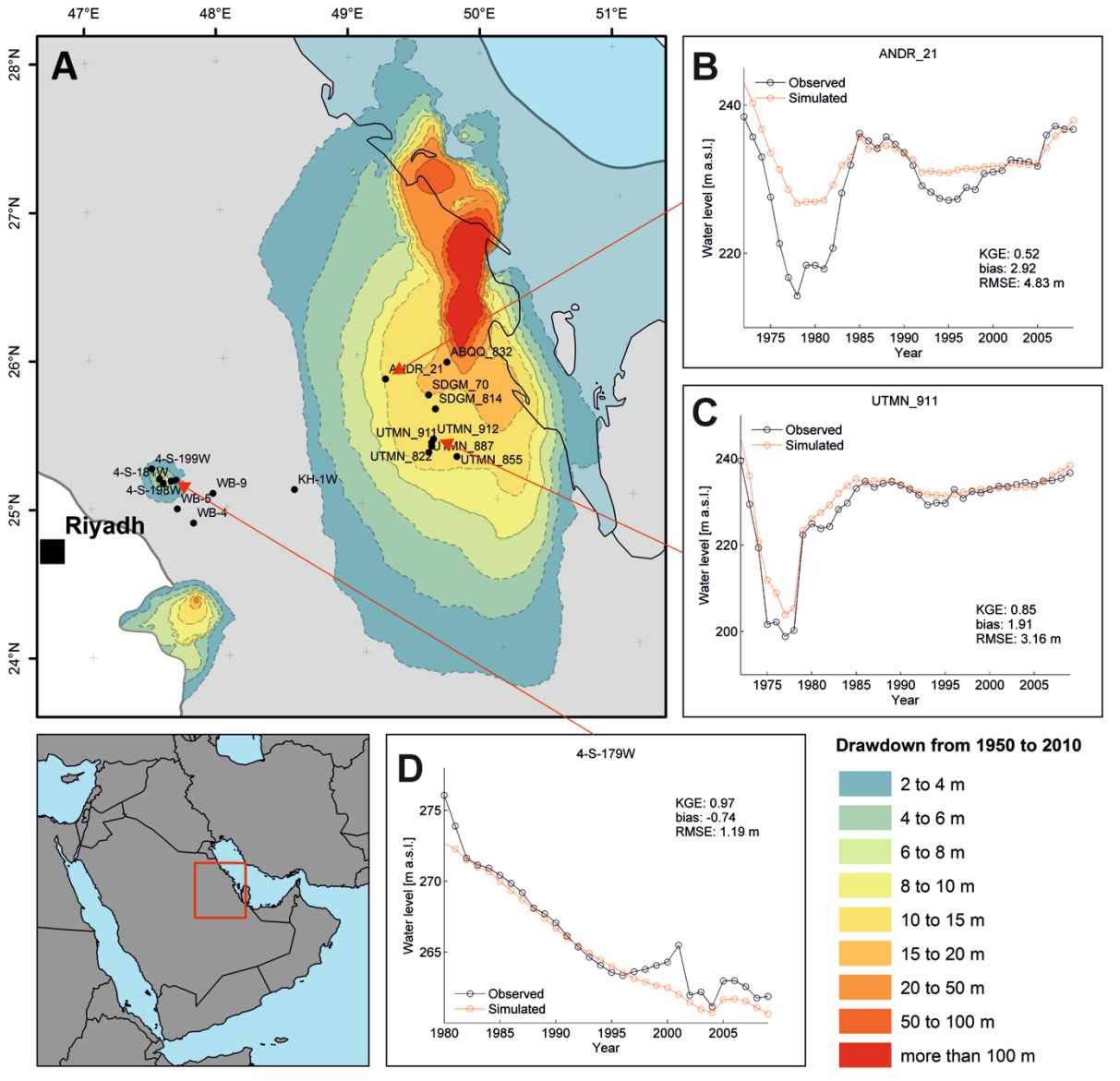

Fig. 4-8: (A) Simulated drawdown of the Wasia aquifer from 1950 to 2010 over space for case (ii), the grey, transparent area represents the extent the UMA system; (B to D) simulated (red) and observed (black) drawdown of the Wasia aquifer from 1950 to 2010 over time for case (ii)

In order to evaluate the goodness of fit for the transient simulation, we analyse the RMSE, KGE, and bias for each monitoring well individually as shown in Fig. 4-8 B to D. Averaging these values for all monitoring wells yields different model fits for different cases, whereby case (ii) shows the best fit (RMSE = 10 m, KGE = 0.61, bias = -0.06 m) and case (iv) shows the worst fit (RMSE = 13 m, KGE = -0.07, bias = -1.67 m). Neglecting the monitoring wells of the Wasia Well Field (e.g. Fig. 4-8 D) results in a

better fit, but the same trend is observed. A table with individual values for each case and the calibrated specific storage is given in the Annex A 18.

In analogy to the quasi steady-state model, Fig. 4-9 shows the calibrated storage coefficients for the model cases (i) to (iv). Three of five hydrofacies show an increasing specific storage from case (i) to case (iv). Sandstone shows no clear trend and Limestone (partly karstified) shows a decreasing trend. The general trend is indicated by the arithmetic mean, which is increasing from cases (i) to (iii) and case (iv). The mean of the specific storage for case (i) to case (iii) shows only a limited variability, however, more than doubles for case (iv).

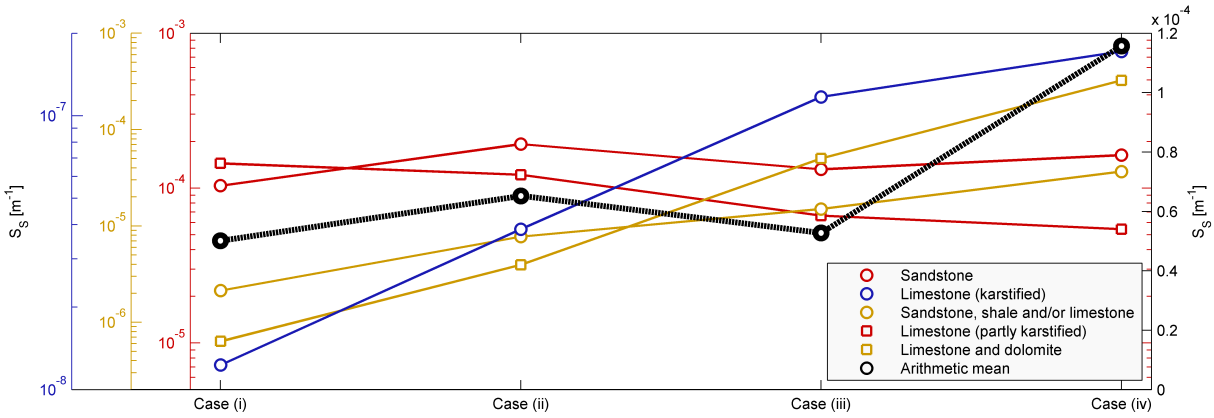

Fig. 4-9: Variability of specific storage depending on the model response of cases (i) to (iv) for different hydrofacies zones (the colour of the graphs correspond to the colour of the y-axes)

Refined results

The estimation of the fossil discharge amount (section 3.1) is influenced by model parameterization, i.e. starting values for the hydraulic conductivity and the specific storage. For some hydrofacies zones these starting values differ more than one order of magnitude from the calibrated values for K and S_S (Annex A 17 and A 18). In order to analyse the influence of the initial model parameterization on the calibrated values for K and S_S and likewise to refine its estimation, we repeated the whole calibration procedure starting with the fossil discharge estimation (section 3.1) using updated initial values. For this we replaced the original starting values (derived from pumping tests) by calibrated values of K and S_S of case (ii). The refined discharge estimation yields a fossil discharge component into the Gulf and Euphrates of $0.62 \cdot 10^9$ m^3a^{-1} and $0.12 \cdot 10^9$ m^3a^{-1}, respectively. The updated discharge estimation is presented in the Annex A 21. It is notable that the best fitting times for the aquifers plot in a significantly narrower range compared to the initial discharge estimation (Fig. 4-5).

Subsequently, we repeated calibration step three (quasi steady-state model calibration) and four (transient model calibration), which resulted in comparable model fits to case (i) to (iv). The refined

values for K and S_S (which we consider as final estimates) and their corresponding model fits are given in the Annex A 17 and A 18.

The final simulated potentiometric head distribution of the refined quasi steady-state model, i.e. pre-industrial state, and likewise the initial state for the transient simulation is shown in Fig. 4-10. Differences of simulated and observed heads (for monitoring wells and for head data extracted from contour maps) and likewise the model fit are presented in Annex A 22.

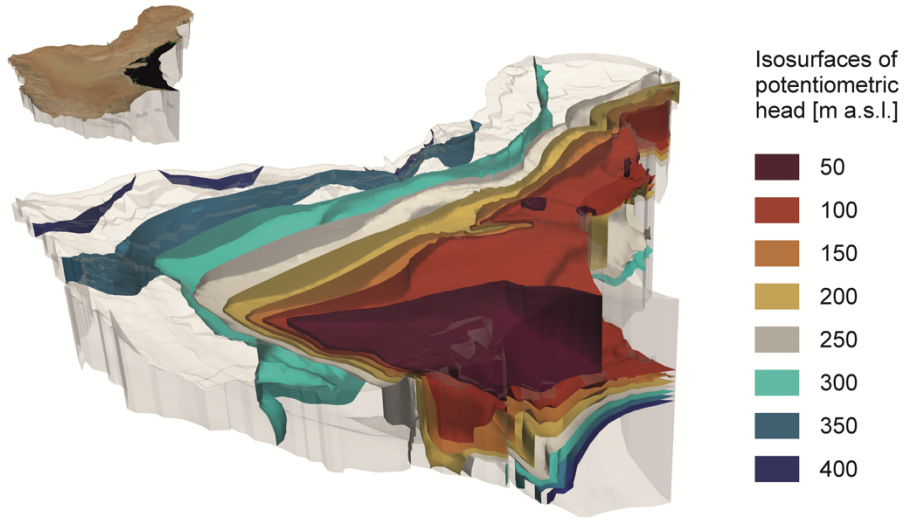

Fig. 4-10: Simulated pre-industrial head distribution of the refined quasi steady-state model (and initial state for the transient simulation); vertical exaggeration of 100

Summary of model results

A first transient simulation with an initial parameter configuration (based on pumping tests) yielded a first guess for the fossil discharge component into the Gulf and Euphrates of about $0.95 \cdot 10^9$ m^3a^{-1} and $0.25 \cdot 10^9$ m^3a^{-1}, respectively. Subsequently, backward particle tracking identified the main aquifers of origin of the fossil discharge. Based on this finding, the fossil discharge rates were added to the natural recharge areas of these aquifers in order to balance out the system and hence create quasi steady-state conditions. Now a "classic" steady-state calibration was possible, which resulted in the hydraulic conductivities (K) presented in Fig. 4-7. Afterwards, the hydraulic conductivities were kept constant and the specific storages (S_S) were calibrated by fitting the simulated to the observed potentiometric heads of the drawdown induced by pumping activities from 1950 to 2010. Results are presented in Fig. 4-9.

Finally, all previously described steps were repeated with an updated initial parameter configuration, i.e. calibrated values of K and S_S replaced the initial configuration based on the pumping tests. The

resulting refined aquifer parameters with the corresponding model fits are given in the Annex A 17 and A 18.

4.5 Discussion

In particular, the first step of the calibration approach might bear some uncertainties as the estimation of the amount of discharge and its fossil component relies on a model with a starting value (best guess) parameterization. Although the starting parameters are based on numerous pumping tests, this approach requires verification or at least a plausibility check. Unfortunately, not much is reported about groundwater discharge amounts into the Gulf and Euphrates and their temporal evolution. Only for direct discharge via springs, reliable measurements exist. Spring discharge into the Euphrates basins and into the Gulf via submarine springs amount to $19 \cdot 10^6$ m³ a^{-1} (Wagner, 2011) and $32 \cdot 10^6$ m³ a^{-1} (GDC, 1980), respectively. However, the greater part consists of diffuse discharge into the Euphrates and the adjacent Mesopotamian Marshes and diffuse submarine groundwater discharge into the Gulf from confined underlying aquifers. The latter was roughly estimated by Zektser et al. (2007) placing it at 0.2 l s^{-1} km^{-1}, or about $1.0 \cdot 10^9$ m³ a^{-1} in total. Although we have to be careful with those values, we can notice that the estimate of Zektser et al. (2007) points into the same direction as our estimate of $1.2 \cdot 10^9$ m³ a^{-1} (Annex A 21).

However, even more important than an absolute exact value for the total discharge and its fossil component is the approval of our hypothesis that there was more discharge in the past and that there is still a significant fossil component. A strong indication for that is given by an extensive study of Larsen (1983) about the evolution of human life on the Bahrain islands. Based on archaeological data, he estimated an ongoing pressure head decrease of 0.0048 m a^{-1} of artesian springs starting several thousands of years ago. Considering that these springs were fed by the upper aquifers (e.g. Umm Er Radhuma), it is very likely that deeper and hence slower aquifers of our system (e.g. Wasia) are even more far off steady-state.

During the third calibration step, we added the estimated fossil discharge amounts to the groundwater recharge in order to achieve pseudo steady-state conditions. This gave us the possibility to only calibrate the hydraulic conductivity and hence reduce the risk of equifinality and meaningless parameter configurations. We tested different assumptions for fossil discharge amounts in order to analyse the sensitivity and relevance of our approach. In general, we could observe a decreasing horizontal and vertical hydraulic conductivity from case (i) to case (iv).

During the previous quasi steady-state calibration we assigned a relatively high weighting factor to the initial head data of the monitoring wells, which are used during the transient calibration (calibration

step four). A reason for this is the attempt to reduce the model error at these locations by reducing the carryover of the model error from the previous calibration step. Alternatively, it would be possible to evaluate the drawdown or head gradients instead of absolute potentiometric heads in the objective function, which could help reduce the risk of a bias for S_S (White et al., 2014).

During the first application of the proposed calibration approach, we considered case (ii) as true and cases (i) and (iii) representing the error range due to uncertainties of the fossil discharge estimation (Fig. 4-5). In a second round, which we term refinement of results (section 3.4), we replaced the initial values of K and S_S (derived from pumping test) by those from case (ii) and repeated the whole calibration process. Comparing the final (refined) values for K and S_S – also in the context of the evolution of case (i) to case (iii) – with case (iv), i.e. neglecting fossil discharge, emphasizes the importance of considering this phenomenon (Fig. 4-11). Neglecting fossil discharge would first lead to a wrong description of the flow regime (underestimation of the hydraulic conductivity) and second to a substantial overestimation of the storage coefficient. In case of our example (the UMA system), neglecting it would result in an almost two times higher specific storage (Fig. 4-11).

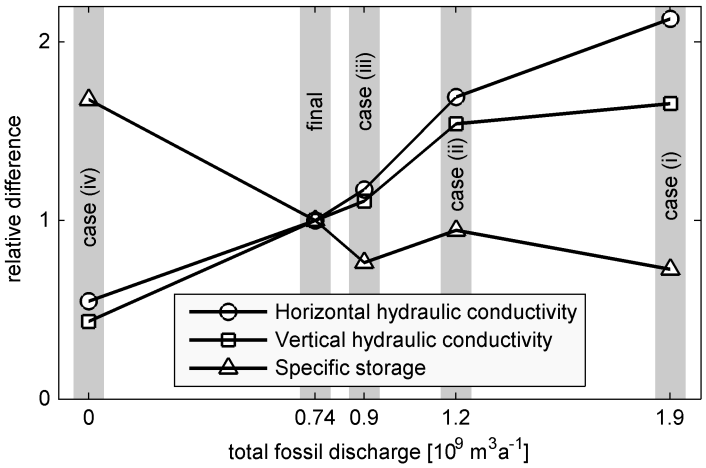

Fig. 4-11: Evolution of geometric mean of hydraulic conductivities (K) and arithmetic mean of the specific storage (S_S) for all cases normalized to the final (refined) values according to the fossil discharge rates

Besides, the orthotropy factor varies in a wide range. Particularly noteworthy are the hydrofacies zones Sandstone, Limestone (low permeable), and the Transition zone. These zones show up to three orders of magnitude lower vertical hydraulic conductivities compared to horizontal ones. In principle, this phenomenon could be an artefact of the inverse modelling. This means that other parameter configurations (potentially with less differences between vertical and horizontal hydraulic conductivities) could yield comparable matches with head observations. However, we believe the reason for that is the great thickness of the aquifer zones of up to a few hundred meters. During their

formation, these zones experienced different depositional environments, i.e. they are composed of various layers with different hydraulic properties (bedding planes). Here, layers with low hydraulic conductivities can be considered as bottlenecks for the water flow in vertical direction (Halvorsen, 1993).

Although our approach is not free from uncertainties, mainly due to the first guess parameterization, it has some crucial advantages compared to the previously presented methods dealing with fossil gradients. The major benefits are

(i) separation of calibration of hydraulic conductivity and storage capacity
(ii) no demand of information on historic initial heads,
(iii) no demand of recharge time series.

This leads to a number of advancements over the previous studies. First, our method reduces the danger of equifinality due to separation of K and S calibration. Particularly in areas with imperfect and scarce monitoring of groundwater heads and abstraction rates, a sufficient reconstruction of head drawdown induced by pumping activities is not possible. Second, we do not need assumptions about initial conditions and recharge rates several thousands of years ago. The majority of the previously presented studies assumed filled aquifers during wetter periods in the past (De Vries, 1984; Gossel et al., 2004; Heinl and Brinkmann, 1989; Houston and Hart, 2004; Lloyd and Farag, 1978; Thorweihe and Heinl, 2002; Wright et al., 1982). In fact, this assumption is quite unlikely for the Arabian Peninsula. As discussed above, during Late Pleistocene to Early Holocene the Arabian Peninsula experienced pluvial periods favouring higher recharge rates than today, however, far less compared to those which are typical for humid areas.

4.6 Conclusion

Understanding regional groundwater systems is an important, but very challenging task, due to limited availability of data. We need this understanding to apply good management schemes especially in areas, where groundwater is the predominant water source. A special case is fossil and hence finite groundwater resources. Here, sound strategies for water mining are needed in order to optimize volumes that can be extracted without risking quality deterioration. Furthermore, estimates on remaining amounts of groundwater resources allow appropriate water pricing as a controlling tool.

Within this study we set up a regional groundwater flow model of an important and intensively used aquifer system on the Arabian Peninsula – the Upper Mega Aquifer system. By this example we introduced a new calibration approach, which accounts for a groundwater flow dominated by fossil head gradients. Moreover, we analysed its relevance for the aquifer parameterization during the

calibration process and noted a significant overestimation of the aquifer storage capacity in case of neglecting fossil gradients. Although the method was illustrated using a rather specific example, we believe that this approach is transferable to other fossil groundwater reservoirs.

We further believe that our proposed method is a promising and valuable way to deal with fossil gradients and likewise improve large-scale groundwater models. Nevertheless, this approach is based on simplifications in the model setup, e.g. adding the fossil discharge to the recharge in order to achieve a quasi-steady-state status. Besides those potential structural model errors and as already mentioned in the previous section, we think that especially the estimation of discharge and its fossil component might cause errors in the proposed calibration approach (even though we refined our results by a second run of the calibration procedure with updated initial values). Therefore, an independent estimate of total discharge (or even better its fossil component) could significantly increase the reliability of the presented method. As an example, a very promising technique using helium isotopes as a tracer to better quantify diffuse and discrete cross formational fluxes is presented by Gardner et al. (2012) and Love et al. (2013), respectively. Moreover, the application of satellite gravimetry, e.g. from the "Gravity Recovery And Climate Experiment" (GRACE), could help to quantify the groundwater loss, i.e. fossil discharge, of a large-scale system such as presented within this study (Güntner et al., 2007; Strassberg et al., 2009).

4.7 Acknowledgements

We would like to thank the editor Graham Sander, the associated editor Adrian Werner, the reviewer Luk Peeters, and the other three anonymous reviewers for constructive and valuable comments that improved the manuscript. We also thank the Ministry of Water & Electricity of Saudi Arabia for providing several datasets. Furthermore, we acknowledge support from the BMBF funded project IWAS (grant code: 02WM1027).

4.8 References

Al-Rashed, M.F., Sherif, M.M., 2000. Water Resources in the GCC Countries: An Overview. Water Resour. Manag. 14, 59–75. doi:10.1023/A:1008127027743

Bakiewicz, W., Milne, D.M., Noori, M., 1982. Hydrogeology of the Umm Er Radhuma aquifer, Saudi Arabia, with reference to fossil gradients. Q. J. Eng. Geol. Hydrogeol. 15, 105–126. doi:10.1144/GSL.QJEG.1982.015.02.03

Bendel, D., 2009. Hydrologische Niederschlags-Abfluss Modellierung in ariden Gebieten unter Verwendung von Fernerkundungsdaten am Beispiel eines Einzugsgebietes im Königreich Saudi Arabien. Universität Stuttgart.

Beven, K., 2006. A manifesto for the equifinality thesis. J. Hydrol. 320, 18–36. doi:10.1016/j.jhydrol.2005.07.007

Bourdon, D.J., 1977. Flow of fossil groundwater. Q. J. Eng. Geol. Hydrogeol. 10, 97–124. doi:10.1144/GSL.QJEG.1977.010.02.02

Carrera, J., Neuman, S.P., 1986. Estimation of Aquifer Parameters Under Transient and Steady State Conditions: 2. Uniqueness, Stability, and Solution Algorithms. Water Resour. Res. 22, 211–227. doi:10.1029/WR022i002p00211

Cendón, D.I., Larsen, J.R., Jones, B.G., Nanson, G.C., Rickleman, D., Hankin, S.I., Pueyo, J.J., Maroulis, J., 2010. Freshwater recharge into a shallow saline groundwater system, Cooper Creek floodplain, Queensland, Australia. J. Hydrol. 392, 150–163. doi:10.1016/j.jhydrol.2010.08.003

Davis, A.D., 1987. Determination of mean transmissivity values in the modelling of groundwater flow, in: Solving Problems with Groundwater Models. National Water Well Association, Dublin, OH, pp. 1162–1173.

De Vries, J.J., 1984. Holocene depletion and active recharge of the Kalahari groundwaters — A review and an indicative model. J. Hydrol. 70, 221–232. doi:10.1016/0022-1694(84)90123-9

Doherty, J.E., Hunt, R.J., 2010. Approaches to highly parameterized inversion—A guide to using PEST for groundwater-model calibration. Reston, Virginia.

Engel, M., Brückner, H., Pint, A., Wellbrock, K., Ginau, A., Voss, P., Grottker, M., Klasen, N., Frenzel, P., 2012. The early Holocene humid period in NW Saudi Arabia – Sediments, microfossils and palaeo-hydrological modelling. Quat. Int. 266, 131–141. doi:10.1016/j.quaint.2011.04.028

Engelhardt, I., Rausch, R., Lang, U., Al-Saud, M., Schüth, C., 2013. Impact of Preboreal to Subatlantic shifts in climate on groundwater resources on the Arabian Peninsula. Environ. Earth Sci. 69, 557–570. doi:10.1007/s12665-013-2362-7

FAO, 2016. AQUASTAT Main Database [WWW Document]. URL www.fao.org/nr/aquastat/ (accessed 3.21.16).

FAO, 2009. Irrigation in the Middle East region in figures - AQUASTAT Survey - 2008, FAO Water Reports. Food and Agriculture Organization of the United Nations (FAO), Rome.

Fleitmann, D., Burns, S.J., Mudelsee, M., Neff, U., Kramers, J., Mangini, A., Matter, A., 2003. Holocene forcing of the Indian monsoon recorded in a stalagmite from southern Oman. Science 300, 1737–9. doi:10.1126/science.1083130

Foster, S., Loucks, D.P., 2006. Non-renewable groundwater resources - A guidebook on socially-sustainable management for water-policy makers. UNESCO, Paris.

Gardner, W.P., Harrington, G.A., Smerdon, B.D., 2012. Using excess 4He to quantify variability in aquitard leakage. J. Hydrol. 468–469, 63–75. doi:10.1016/j.jhydrol.2012.08.014

GDC, 1980. Bahrain Study - Volume 3: Hydrology. Cambridge.

GIZ/DCo, 2014. Detailed Groundwater Resources Studies in the Rub' Al Khali Desert. Riyadh.

GIZ/DCo, 2013. Detailed Groundwater Resources Studies of Khuff Jilh Minjur Dhruma and overlying Aquifers. Riyadh.

GIZ/DCo, 2011. Detailed Water Resources Studies of Wasia-Biyadh and Aruma Aquifers. Riyadh.

Gossel, W., Ebraheem, A.M., Wycisk, P., 2004. A very large scale GIS-based groundwater flow model for the Nubian sandstone aquifer in Eastern Sahara (Egypt, northern Sudan and eastern Libya). Hydrogeol. J. 12, 698–713. doi:10.1007/s10040-004-0379-4

Groucutt, H.S., Petraglia, M.D., 2012. The prehistory of the Arabian peninsula: Deserts, dispersals, and demography. Evol. Anthropol. Issues, News, Rev. 21, 113–125. doi:10.1002/evan.21308

GTZ/DCo, 2006. Investigations of Updating Groundwater Mathematical Model(s) for the Umm Er Radhuma and Overlying Aquifers. Riyadh.

Güntner, A., Stuck, J., Werth, S., Döll, P., Verzano, K., Merz, B., 2007. A global analysis of temporal and spatial variations in continental water storage. Water Resour. Res. 43, n/a-n/a. doi:10.1029/2006WR005247

Gupta, H. V., Kling, H., Yilmaz, K.K., Martinez, G.F., 2009. Decomposition of the mean squared error and NSE performance criteria: Implications for improving hydrological modelling. J. Hydrol. 377, 80–91. doi:10.1016/j.jhydrol.2009.08.003

Gutentag, E.D., Heimes, F.J., Krothe, N.C., Luckey, R.R., Weeks, J.B., 1984. Geohydrology of the High Plains Aquifer In Parts of Colorado, Kansas, Nebraska, New Mexico, Oklahoma, South Dakota, Texas, and Wyoming.

Halvorsen, C., 1993. Probe permeametry applied to a highly laminated sandstone reservoir. Mar. Pet. Geol. 10, 347–351. doi:10.1016/0264-8172(93)90079-8

Heinl, M., Brinkmann, P.J., 1989. A groundwater model of the Nubian aquifer system. Hydrol. Sci. J. 34, 425–447. doi:10.1080/02626668909491350

Houston, J., Hart, D., 2004. Theoretical head decay in closed basin aquifers: an insight into fossil groundwater and recharge events in the Andes of northern Chile. Q. J. Eng. Geol. Hydrogeol. 37, 131–139. doi:10.1144/1470-9236/04-007

Kalbus, E., Oswald, S., Wang, W., Kolditz, O., Engelhardt, I., Al-Saud, M.I., Rausch, R., 2011. Large-scale Modeling of the Groundwater Resources on the Arabian Platform. Int. J. Water Resour. Arid Environ. 1, 38–47.

Kolditz, O., Bauer, S., Bilke, L., Böttcher, N., Delfs, J.O., Fischer, T., Görke, U.J., Kalbacher, T., Kosakowski, G., McDermott, C.I., Park, C.H., Radu, F., Rink, K., Shao, H., Shao, H.B., Sun, F., Sun, Y.Y., Singh, A.K., Taron, J., Walther, M., Wang, W., Watanabe, N., Wu, Y., Xie, M., Xu, W., Zehner, B., 2012. OpenGeoSys: an open-source initiative for numerical simulation of thermo-hydro-mechanical/chemical (THM/C) processes in porous media. Environ. Earth Sci. 67, 589–599. doi:10.1007/s12665-012-1546-x

Larsen, C.E., 1983. Life and Land Use on the Bahrain Islands. The University of Chicago Press, Chicago.

Lloyd, J.W., Farag, M.H., 1978. Fossil Ground-Water Gradients in Arid Regional Sedimentary Basins. Groundwater 16, 388–392. doi:10.1111/j.1745-6584.1978.tb03251.x

Love, A.J., Shand, P., Karlstrom, K., Crossey, L., Rousseau-Gueutin, P., Priestley, S., Wholing, D., Fulton, S., Keppel, M., 2013. Geochemistry and Travertine Dating Provide New Insights into the Hydrogeology of the Great Artesian Basin, South Australia. Procedia Earth Planet. Sci. 7, 521–524. doi:10.1016/j.proeps.2013.03.065

Margat, J., Foster, S., Droubi, A., 2006. Concept and importance of non-renewable resources, in: Foster, S., Loucks, D.P. (Eds.), Non-Renewable Groundwater Resources - A Guidebook on Socially-Sustainable Management for Water-Policy Amakers. UNESCO, Paris, p. 97.

Margat, J., van der Gun, J., 2013. Groundwater around the World: A Geographic Synopsis. CRC Press/Taylor & Francis Group.

McGuire, V.L., 2009. Water-level changes in the High Plains aquifer, predevelopment to 2007, 2005–06, and 2006–07: U.S. Geological Survey Scientific Investigations Report 2009–5019.

Meredith, K.T., Hollins, S.E., Hughes, C.E., Cendón, D.I., Chisari, R., Griffiths, A., Crawford, J., 2015. Evaporation and concentration gradients created by episodic river recharge in a semi-arid zone aquifer: Insights from Cl−, δ18O, δ2H, and 3H. J. Hydrol. 529, 1070–1078. doi:10.1016/j.jhydrol.2015.09.025

Pauw, E. De, 2002. An Agroecological Exploration of the Arabian Peninsula. ICARDA - International Center for Agricultural Research in the Dry Areas, Dubai.

Petersen, J.O., Deschamps, P., Gonçalvès, J., Hamelin, B., Michelot, J.L., Guendouz, A., Zouari, K., 2014. Quantifying paleorecharge in the Continental Intercalaire (CI) aquifer by a Monte-Carlo inversion approach of 36 Cl/Cl data. Appl. Geochemistry 50, 209–221. doi:10.1016/j.apgeochem.2014.04.014

Reilly, T.E., Goodman, A.S., 1987. Analysis of saltwater upconing beneath a pumping well. J. Hydrol. 89, 169–204. doi:10.1016/0022-1694(87)90179-X

Rousseau-Gueutin, P., Love, A.J., Vasseur, G., Robinson, N.I., Simmons, C.T., de Marsily, G., 2013. Time to reach near-steady state in large aquifers. Water Resour. Res. 49, 6893–6908. doi:10.1002/wrcr.20534

Salem, O.M., 1992. The great manmade river project: A partial solution to Libya's future water supply. Int. J. Water Resour. Dev. 8, 270–278. doi:10.1080/07900629208722564

Sarnthein, M., 1978. Sand deserts during glacial maximum and climatic optimum. Nature. doi:10.1038/272043a0

Scanlon, B.R., Keese, K.E., Flint, A.L., Flint, L.E., Gaye, C.B., Edmunds, W.M., Simmers, I., 2006. Global synthesis of groundwater recharge in semiarid and arid regions. Hydrol. Process. 20, 3335–3370. doi:10.1002/hyp.6335

Schulz, S., de Rooij, G.H., Michelsen, N., Rausch, R., Siebert, C., Schüth, C., Al-Saud, M., Merz, R., 2016. Estimating groundwater recharge for an arid karst system using a combined approach of time-lapse camera

monitoring and water balance modelling. Hydrol. Process. 30, 771–782. doi:10.1002/hyp.10647

Schulz, S., Horovitz, M., Rausch, R., Michelsen, N., Mallast, U., Köhne, M., Siebert, C., Schüth, C., Al-Saud, M., Merz, R., 2015. Groundwater evaporation from salt pans: Examples from the eastern Arabian Peninsula. J. Hydrol. 531, 792–801. doi:10.1016/j.jhydrol.2015.10.048

Strassberg, G., Scanlon, B.R., Chambers, D., 2009. Evaluation of groundwater storage monitoring with the GRACE satellite: Case study of the High Plains aquifer, central United States. Water Resour. Res. 45, n/a-n/a. doi:10.1029/2008WR006892

Thorweihe, U., Heinl, M., 2002. Groundwater Resources of the Nubian Aquifer System NE-Africa. Berlin.

Tsur, Y., 1990. The stabilization role of groundwater when surface water supplies are uncertain: The implications for groundwater development. Water Resour. Res. 26, 811–818. doi:10.1029/WR026i005p00811

UN-ESCWA, BGR, 2013. Inventory of Shared Water Resources in Western Asia. United Nations Publication, Beirut.

Wada, Y., van Beek, L.P.H., van Kempen, C.M., Reckman, J.W.T.M., Vasak, S., Bierkens, M.F.P., 2010. Global depletion of groundwater resources. Geophys. Res. Lett. 37, n/a-n/a. doi:10.1029/2010GL044571

Wagner, W., 2011. Groundwater in the Arab Middle East. Springer Berlin Heidelberg, Berlin, Heidelberg. doi:10.1007/978-3-642-19351-4

White, J.T., Doherty, J.E., Hughes, J.D., 2014. Quantifying the predictive consequences of model error with linear subspace analysis. Water Resour. Res. 50, 1152–1173. doi:10.1002/2013WR014767

Wood, W.W., Imes, J.L., 1995. How wet is wet? Precipitation constraints on late quaternary climate in the southern Arabian Peninsula. J. Hydrol. 164, 263–268. doi:10.1016/0022-1694(94)02551-L

Wright, E.P., Benfield, A.C., Edmunds, W.M., Kitching, R., 1982. Hydrogeology of the Kufra and Sirte basins, eastern Libya. Q. J. Eng. Geol. Hydrogeol. 15, 83–103. doi:10.1144/GSL.QJEG.1982.015.02.02

Zektser, I.S., Dzhamalov, R.G., Everett, L.G., 2007. Submarine Groundwater. CRC Press/Taylor & Francis Group, Boca Raton.

Ziegler, M.A., 2001. Late Permian to Holocene Paleofacies Evolution of the Arabian Plate and its Hydrocarbon Occurrences. GeoArabia 6, 445–504.

5 Model results and conclusion

The present thesis cumulates three major studies, which are presented in the previous three chapters. Two of them deal with water balance components of the UMA system. First, a specific type of groundwater recharge is described and quantified: groundwater recharge in the karst outcrops of the Umm Er Radhuma aquifer (chapter 2; Schulz et al., 2016). Second, the groundwater evaporation from salt pans, which constitutes one of the major outflow components of the system, is thoroughly investigated (chapter 3; Schulz et al., 2015). The third major study deals with the numerical groundwater flow model. It describes the model set-up and its calibration by considering fossil head gradients; and furthermore, it quantifies the natural discharge into the Persian Gulf and into the Euphrates (chapter 4; Schulz et al., 2017). These studies fill a data gap and hence, help to improve the understanding of hydrological and hydrogeological processes of the UMA system. Likewise, they are the base for numerical groundwater flow simulations, which could support future decision making processes.

This final chapter deals with simulations performed with the previously built up groundwater flow model (chapter 4; Schulz et al., 2017). Using these simulations, the present state of the groundwater resources stored in the UMA system are described; and subsequently, three different development scenarios are performed and evaluated. It should be noted here that the modelled groundwater abstractions from the UMA system are limited to the major abstraction areas in Saudi Arabia. Due to non-accessibility of appropriate data series, abstractions from other countries sharing the UMA system are not considered in the present work.

Finally, this thesis closes with an outlook for future research possibilities to further improve the understanding of the UMA system and likewise other aquifer systems showing comparable settings.

5.1 Present state of groundwater resources

The transboundary UMA system is almost non-renewable and therefore, it has to be considered as a finite reservoir. Nevertheless, it is one of the major regional water sources on the Arabian Peninsula and it is intensively exploited in many areas. As a consequence, profound knowledge about the aquifer system and the present state of its groundwater resources is absolutely essential in order to find a good balance between economic growth and keeping water reserves for the future. In this regard, the calibrated numerical groundwater flow model (chapter 4; Schulz et al., 2017) serves as a base for the evaluation of the present state of groundwater resources (Fig. 5-1).

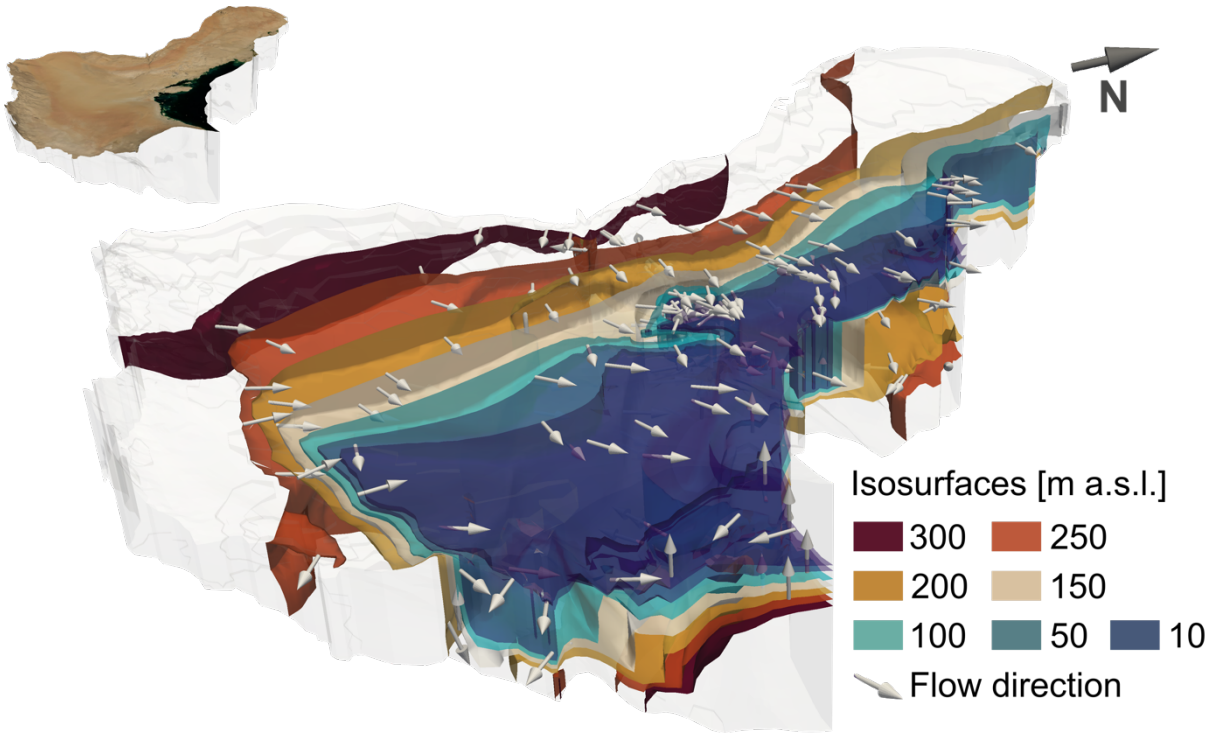

Fig. 5-1: Isosurfaces of potentiometric head distribution and arrows indicating the flow direction for 2010; in the upper left corner, an overview figure of the model geometry with a satellite image texture is shown; vertical exaggeration of 100

Impact of present day use

The groundwater reserves of the UMA system are used for (i) domestic supply in areas without access to desalinated seawater (Fig. 5-2 B), (ii) various industrial purposes, but predominantly the injection of water for oil hauling, and (iii) irrigation agriculture, which is by far the largest groundwater consumer (Fig. 5-1 A).

Fig. 5-2: (A) Groundwater abstraction for irrigation agriculture via center pivot; (B) Maintenance of a domestic supply well in Wadi Nisah; (C) Ayn Al-Harrah (Hofuf) with open water pool and free flowing springs in 1958 (Facey, 2000); (D) Ayn Al-Harrah (Hofuf) with open water pool and pumping wells in 2014

The domestic supply wells tapping the UMA system are predominantly spread over the western part of the UMA system (Fig. 5-3). The first reason for that is the groundwater salinity increase towards east (GIZ/DCo, 2014, 2011; GTZ/DCo, 2006) and the second one is the availability of desalinated seawater in coastal areas. Besides some industrial supply wells of minor significance, the oil production supply wells around the Ghawar oil field, tapping the Wasia and Biyadh aquifers, are the largest groundwater abstraction sites of the industrial sector. Agricultural areas are spread over the entire study area. 100% of these areas must be irrigated and 97% of the irrigation water supply is covered by groundwater (FAO, 2009). Consequently, all agricultural areas have to be considered as groundwater abstraction sites. Main agricultural areas tapping the Wasia and Biyadh aquifers are Sakaka, Kharj, and Aflaj, which are located in the western parts close to the aquifer outcrops. Agricultural areas, which are located more eastward (Ullya, Sharguia, Qatif, Hofuf, and Yabrin), tap the overlying aquifers Aruma, Umm Er Radhuma, Dammam, and Neogene (Fig. 5-3).

Before industrialization in the 1950s, springs were the major water source in the study area. A very prominent example are the springs in Hofuf (Fig. 5-2 C), which formed one of the largest oases of the world (Al Tokhais and Rausch, 2008).

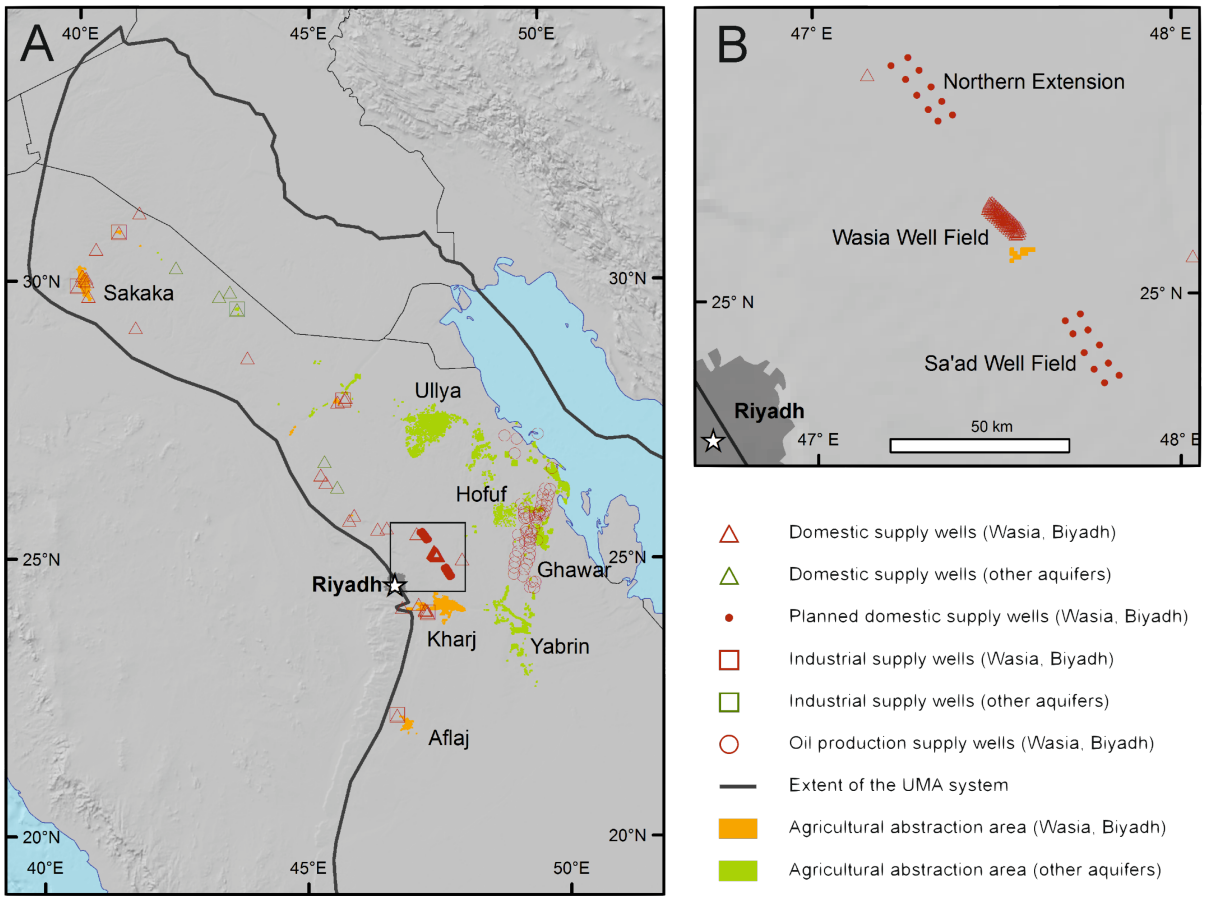

Fig. 5-3: Major abstraction areas in Saudi Arabia; other aquifers are Aruma, Umm Er Radhuma, Dammam, and Neogene (GIZ/DCo, 2011; GTZ/DCo, 2006)

Time series of the temporal evolution of groundwater abstraction, which are used in the simulations of this study, are extracted from the consulting reports GIZ/DCo (2011) and GTZ/DCo (2006). It is particularly noteworthy that the agricultural abstraction rates experienced a strong increase especially during the first two decades of available data (Fig. 5-4). The reason for that is the launch of an agricultural subsidy program in 1974 in Saudi Arabia to reduce the strong reliance on food imports. As a consequence of the rapid groundwater drawdown, caused by the increased agricultural abstractions, the Saudi Arabian government cut these subsidies again stepwise from 1993 to 1995 (WaterWatch, 2006). This policy change resulted in the strong reduction of the cultivation of cheap crops like wheat and led to decreasing agricultural abstraction rates for a couple of years after 1995. Moreover, two tipping points in the industrial abstraction rate time series are notable. The first one occurred after the first oil crisis in 1973. As a follow-up to that crisis, the oil prize strongly increased and Saudi Arabia enhanced its oil production rate and hence, the abstraction rate of injection water (Fig. 5-4). In the years after 1978 the groundwater abstraction in the industrial sector decreased again, which is not

explainable by a reduction of oil production, but by a replacement of groundwater by desalinated seawater for the injection activities.

In contrast to the domestic and industrial abstraction rates, those for the irrigation agriculture supply are usually not directly measured by e.g. water meters. Although estimates about these agricultural abstraction rates were obtained by extensive field surveys and satellite image analyses during the studies of GIZ/DCo (2011) and GTZ/DCo (2006), these values have to be considered as good guesses showing a certain error. Therefore, these values were checked against those from an independent study, which estimated historical abstraction rates of the agricultural sector in Saudi Arabia by satellite image analyses (WaterWatch, 2006). A comparison of these studies could show that both time series follow the same temporal patterns and that the abstraction rates are in the same order of magnitude (Fig. 5-4).

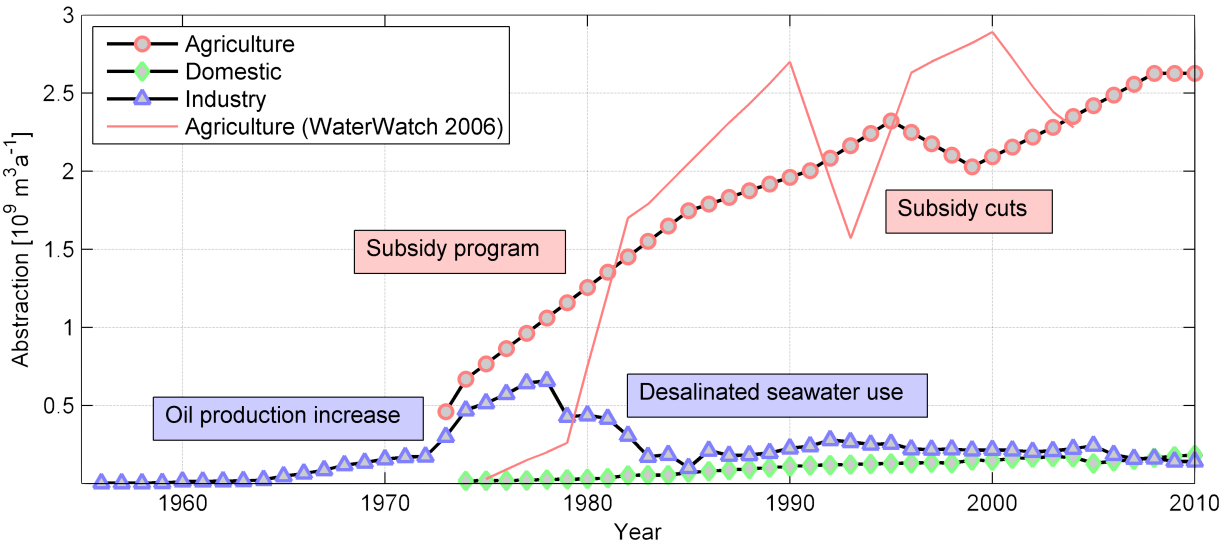

Fig. 5-4: Temporal evolution of groundwater abstraction in Saudi Arabia by sector (GIZ/DCo, 2011; GTZ/DCo, 2006) and abstraction rates of the agricultural sector estimated by an independent study (WaterWatch, 2006)

The aforementioned abstraction activities have a strong impact on the groundwater resources of the UMA system. In various areas, the hydraulic head declined for several tens of meters during the last decades from the pre-industrial stage (1950) to 2010 (Fig. 5-5). Some of these abstraction activities show a rather local impact like those of the Wasia Well Field or those which are even not visible in Fig. 5-5. Others, like the agricultural abstraction areas Kharj, Yabrin, and Hofuf and the industrial abstraction activities around the Ghawar oil field, have a more regional impact. Especially in urbanized areas like Kharj and Hofuf, the drawdown at regional scale due to the agricultural consumption has to be evaluated as critical, because here potential future drinking water reserves are depleted.

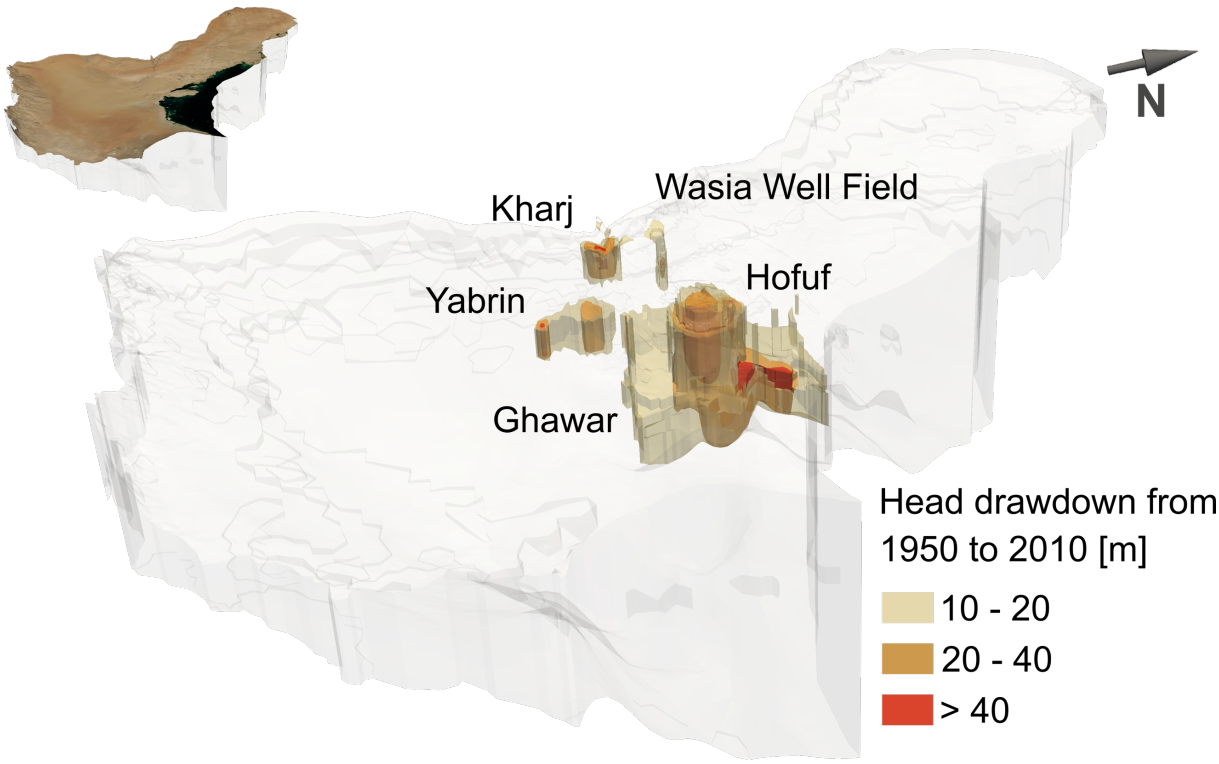

Fig. 5-5: Potentiometric head drawdown from 1950 to 2010 for the major abstraction areas in Saudi Arabia; in the upper left corner, an overview figure of the model geometry with a satellite image texture is shown; vertical exaggeration of 100

As already mentioned, it has to be noted that only abstraction areas in Saudi Arabia are considered for the simulations during this study. For the other countries, hosting part of the transboundary UMA system (Bahrain, Iraq, Kuwait, Oman, Qatar, UAE and Yemen), no continuous time series and exact abstraction locations are available for this study. However, UN-ESCWA and BGR (2013) provided at least for some years on a country-scale the abstraction rates from the principal aquifers of the UMA system (Tab. 5-1). Summing up all given abstraction rates from Tab. 5-1 results in a total net abstraction rate of $630 \cdot 10^6$ m^3 a^{-1}. It has to be noted that abstraction from the Western Gravel Aquifer and the share of irrigation return flow are not considered. Although the years of available data vary over four decades, this value indicates that the abstraction of all other countries, besides Saudi Arabia, is in the range of some tens of percent of those considered in the simulations of this study (Fig. 5-4). Thus, considering the additional abstraction rates would significantly affect the modelling results.

Tab. 5-1: Groundwater abstraction from the principal aquifers of the UMA system by neighbouring countries according to UN-ESCWA and BGR (2013); *with an irrigation return flow rate of 84%, **estimation bases on population size, ***no exact year is given, but cited from a study from 2001, ****actually not from the Neogene aquifer, but from an alluvial aquifer (Western Gravel Aquifer) overlying the Neogene aquifer, *****only negligible abstraction from single deep wells by nomads

Country	Neogene [10^6 m^3 a^{-1}]	Dammam [10^6 m^3 a^{-1}]	Umm Er Radhuma [10^6 m^3 a^{-1}]	Wasia, Biyadh, Aruma [10^6 m^3 a^{-1}]
Bahrain		97 (2010) 218 (1994)	54 (2010)	
Iraq	370 (1980s)*		4 (early 1990s)	60 (2000)**
Kuwait	92 (1988)	120 (1988)		
Oman		45 (before 2001)***		
Qatar			43 (1971) 91 (1983)	
UAE	443 (1985)****	8 (2011)		
Yemen				< 1 (2013)*****

Exploitable groundwater resources

Due to the low replenishment rate, the groundwater resources of the UMA system are considered as non-renewable and groundwater withdrawal must be understood as mining of a finite resource. Consequently, answering the question of "How much water is left?" is one the key challenges for the development of appropriate management schemes.

The transboundary UMA system covers large areas of the Arabian subcontinent, laterally extents over about $1.7 \cdot 10^6$ km^2 and reaches up to several thousands of meters of thickness. Thus, gigantic volumes of water are stored in this aquifer system. However, not all of this water is exploitable, due to economic and technical limitations. Based on the following three threshold values, GTZ/DCo (2010) estimated the exploitable groundwater volumes for the aquifers of the UMA system (Tab. 5-2).

- Drilling depth less than 2,000 m
- Maximum pumping height of 300 m
- Groundwater salinity (TDS) less than 2,000 mg/l

These threshold values limit the exploitable groundwater volume of the UMA system to only 0.06% of the total aquifer volume. Moreover, it has to be noted that large parts of exploitable resources are located in remote and sparsely populated areas like the Rub' Al-Khali desert.

Tab. 5-2: Aquifer volumes (calculated from the geometric model of this study) and exploitable groundwater volumes of the UMA system (GTZ/DCo, 2010)

Aquifer	Hydrofacies	Volume [10^9 m^3]	Exploitable water [10^9 m^3]
Neogene	Sandstone, shale and/or limestone	268,990	24
Dammam	Sandstone	522	100
	Limestone (partly karstified)	96,106	
Umm Er Radhuma	Sandstone	2,506	200
	Limestone (karstified)	368,576	
	Limestone (partly karstified)	70,589	
Aruma	Sandstone	22,308	150
	Sandstone, shale and/or limestone	38,640	
	Limestone (partly karstified)	348,895	
Wasia	Sandstone	68,082	390
	Sandstone, shale and/or limestone	160,561	
	Limestone (partly karstified)	12,934	
Biyadh	Sandstone	103,067	
	Sandstone, shale and/or limestone	73,855	
	Limestone and dolomite	106,162	
Total		1,464,926	864

5.2 Management scenarios

A major function of numerical groundwater flow models and likewise powerful decision making support systems are forecasting the response of an aquifer system depending on different management scenarios. In the following, three different possibilities of the future groundwater exploitation of the UMA system and its consequences are described. Due to the non-accessibility of recent data sets (2011 to 2016), all management scenarios start in the year 2011 and run until 2050. They only consider the previously described major abstraction areas in Saudi Arabia.

Development scenario 1: Status quo

This scenario assumes that the abstraction rates of 2010 stay constant over the whole forecasting period from 2011 to 2050.

Development scenario 2: Decreasing groundwater abstraction

The groundwater abstraction from the UMA system could be reduced by several initiatives. Agriculture is by far the largest groundwater consumer in the study area (Fig. 5-3) and thus, this sector bears the largest water saving potential. As a consequence, the Saudi Arabian governance introduced stepwise subsidy cuts for the agricultural sector from 1993 to 1995, which resulted in decrease of wheat production in the following years (WaterWatch, 2006). Following the intention of this action, a linear decrease of wheat production starting from 2011 until a total stop in 2020 and no production from 2020 to 2050 is assumed during this development scenario. The groundwater saving potential of this

initiative is 683 · 10^6 m^3 a^{-1} or 26% of the total agricultural groundwater consumption 2625 · 10^6 m^3 a^{-1} in 2008 (Tab. 5-3).

Tab. 5-3: Agricultural groundwater demand for 2008 (GIZ/DCo, 2011)

Location	Cultivated area of wheat [%]	Groundwater consumption of wheat [%]	Total groundwater consumption [10^6 m^3 a^{-1}]
Sakaka	49	34	18
Ullya	94	86	434
Sharguia	36	20	188
Qatif	0	0	169
Hofuf	1	1	713
Kharj	34	21	273
Yabrin	43	24	816
Aflaj	61	40	14
Total		26	2625

A further possibility for groundwater saving is its replacement by water from unconventional sources like treated waste water. The World Bank (2005) reported that 98 · 10^6 m^3 of treated waste water was used in Saudi Arabia in the year 2000. However, only 41% of treated waste water was used and only 23% of waste water was treated. Assuming all waste water would be treated and afterwards used, the waste water reuse potential is 1,039 · 10^6 m^3 a^{-1}. For this development scenario, it is presumed that one third of the total waste water reuse potential of Saudi Arabia (346 · 10^6 m^3 a^{-1}) is used to reduce the groundwater withdrawal from the UMA system. This initiative starts in the year 2021 with a linear decrease of groundwater abstraction until 2030 and subsequently remains constant until 2050 (Fig. 5-6).

Both initiatives for the agricultural sector result in a strong decrease of the groundwater withdrawal, which goes along with the ambition of the National Transformation Program 2020 (objective 4 for the Ministry of Environment, Water and Agriculture) to halve the amount of water used in the agricultural sector until 2030 (KSA, 2016).

Moreover, it is assumed that groundwater abstraction for oil production within 100 km from the coast is replaced by seawater desalinisation with a linear transition phase from 2011 to 2030 (Fig. 5-6). Other industrial and domestic abstractions remain constant, because increased demand due to economic and population growth is balanced out by increased water use efficiency, e.g. decreased water loss due to a better pipeline network and increased people's awareness of water shortage.

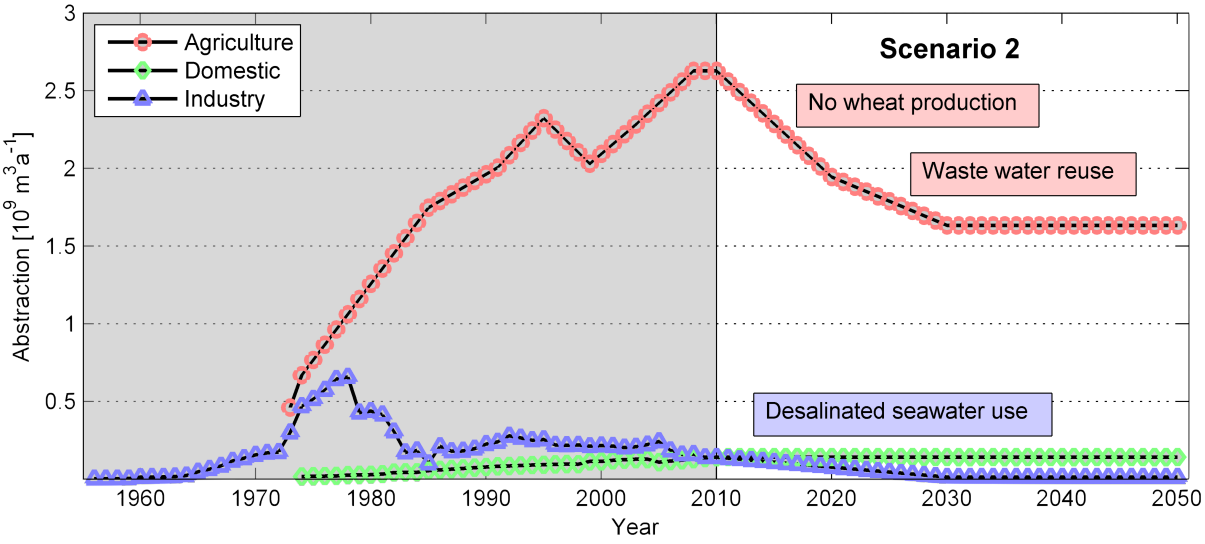

Fig. 5-6: Estimated groundwater abstraction from 1950 to 2010 (GIZ/DCo, 2011) and prognostic groundwater abstraction from 2011 to 2050 according to development scenario 2 for the major abstraction areas in Saudi Arabia for the UMA system

Development scenario 3: Increasing groundwater abstraction

The groundwater withdrawal from the UMA system for agriculture increased on average by $50 \cdot 10^6$ m^3 a^{-1} from 1973 to 2010. The same rate of increase is assumed for the forecasting period from 2011 to 2050 for the development scenario 3 (Fig. 5-7). Note that, even during this scenario, still a lot of virtual water import via agricultural products would be needed (Mekonnen and Hoekstra, 2011).

Due to a population and likewise a domestic water demand increase of the city Riyadh, the Saudi Arabian authorities together with the National Water Company (NWC) are planning an extension of the Wasia Well Field. They are planning two additional well fields: one located in the northwest with a total production rate of $100 \cdot 10^6$ m^3 a^{-1} and another one in the southeast (Sa'ad Well Field) with a total production rate of $127 \cdot 10^6$ m^3 a^{-1} (Fig. 5-7, GIZ/DCo, 2011). For this scenario, both well fields will start operating in 2020 with a constant abstraction rate until 2050. Other abstraction rates for domestic supply followed the prognostic population rise of Saudi Arabia with a linear increase of 64% from 2010 to 2050 (UN, 2015).

Following a prognosis of GIZ/DCo (2011), the groundwater demand for oil production (injection activities mainly around Ghawar Oil Fields) linearly increases to $500 \cdot 10^6$ m^3 a^{-1} from 2011 to 2020 and subsequently stays constant until 2050. Furthermore, it is assumed that other industrial groundwater consumptions double over the period from 2010 to 2020. The reason for this are industrial development and diversification initiatives until 2020 (UNIDO, 2006). After 2020 these abstraction rates stay constant as well.

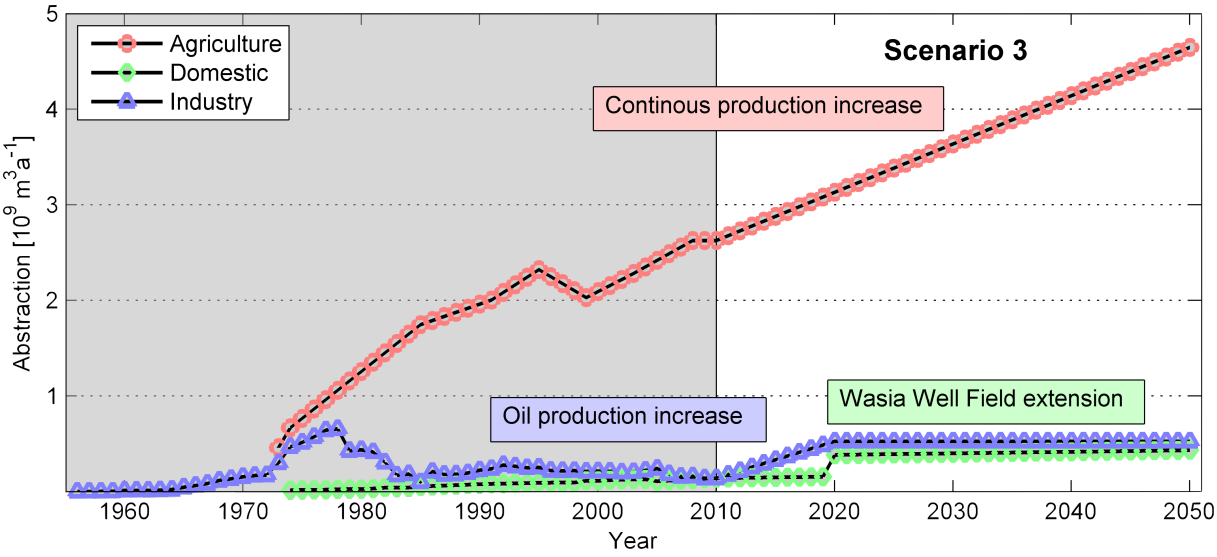

Fig. 5-7: Estimated groundwater abstraction from 1950 to 2010 (GIZ/DCo, 2011) and prognostic groundwater abstraction from 2011 to 2050 according to development scenario 3 for the major abstraction areas in Saudi Arabia for the UMA system

Comparison of scenario simulation results

The previously described groundwater abstraction scenarios were simulated with the numerical groundwater flow model of the UMA system. One of the simulation results is the spatial distribution of the potentiometric head drawdown, i.e. the difference in groundwater head between 1950 and 2010 or 2050, respectively (Fig. 5-8). The comparison of the drawdown between the different development scenarios yields the following key findings.

First, the drawdown caused by agricultural abstraction expands for all three development scenarios compared to 2010. Even in case of scenario 2 (significantly reduced agricultural abstraction rates), the groundwater reserves are not recovered (Fig. 5-8). This observation results from the low replenishment rate of the aquifer system. Hence, it clearly shows that groundwater withdrawal of some cubic kilometres per year from the UMA system has to be seen as mining of a finite resource.

Second, the extension of the Wasia Well Field (doubling its abstraction rate during development scenario 3) still has only a local impact (Fig. 5-8). This is probably caused by the high yield of the Wasia/Biyadh system in that part of the aquifer system. Consequently, the extension of the Wasia Well Field seems to be in an acceptable range.

Third, in contrast to the agricultural abstraction areas, the drawdown in the Wasia and Biyadh aquifers around the Ghawar oil field significantly recovers during scenario 2 (Fig. 5-8). At the first glance, this is somehow surprising as the Wasia and Biyadh aquifers in that part of the aquifer system are sealed from the overlying aquifers by the Upper Wasia / Lower Aruma shales. Moreover, they are far away from their outcrop (recharge) areas. As a consequence of both, a low replenishment rate is expected.

A possible explanation for the recovery of the drawdown would be that the strong drawdown is caused by a low aquifer yield in that area; and after the stop of pumping, the drawdown is recovered by the inflow from surrounding fossil groundwater reserves.

In more humid areas, where management schemes usually follow the principles of a sustainable groundwater production, the recovery of an aquifer depends on its replenishment rate mainly resulting from the infiltration of precipitation. In contrast, the recovery during scenario 2 shows that the recovery rate of the drawdown in the Wasia-Biyadh system seems to depend on the potentiometric head and amount of groundwater stored in its vicinity. Generally expressed, the drawdown recovery rate of a non-renewable aquifer decreases as soon as the number of abstraction areas or rates in its vicinity increases. This relationship in turn suggests that considering the previously mentioned additional abstraction rates from the UMA system (Fig. 5-1) probably affects the aquifer response due to abstraction and recovery.

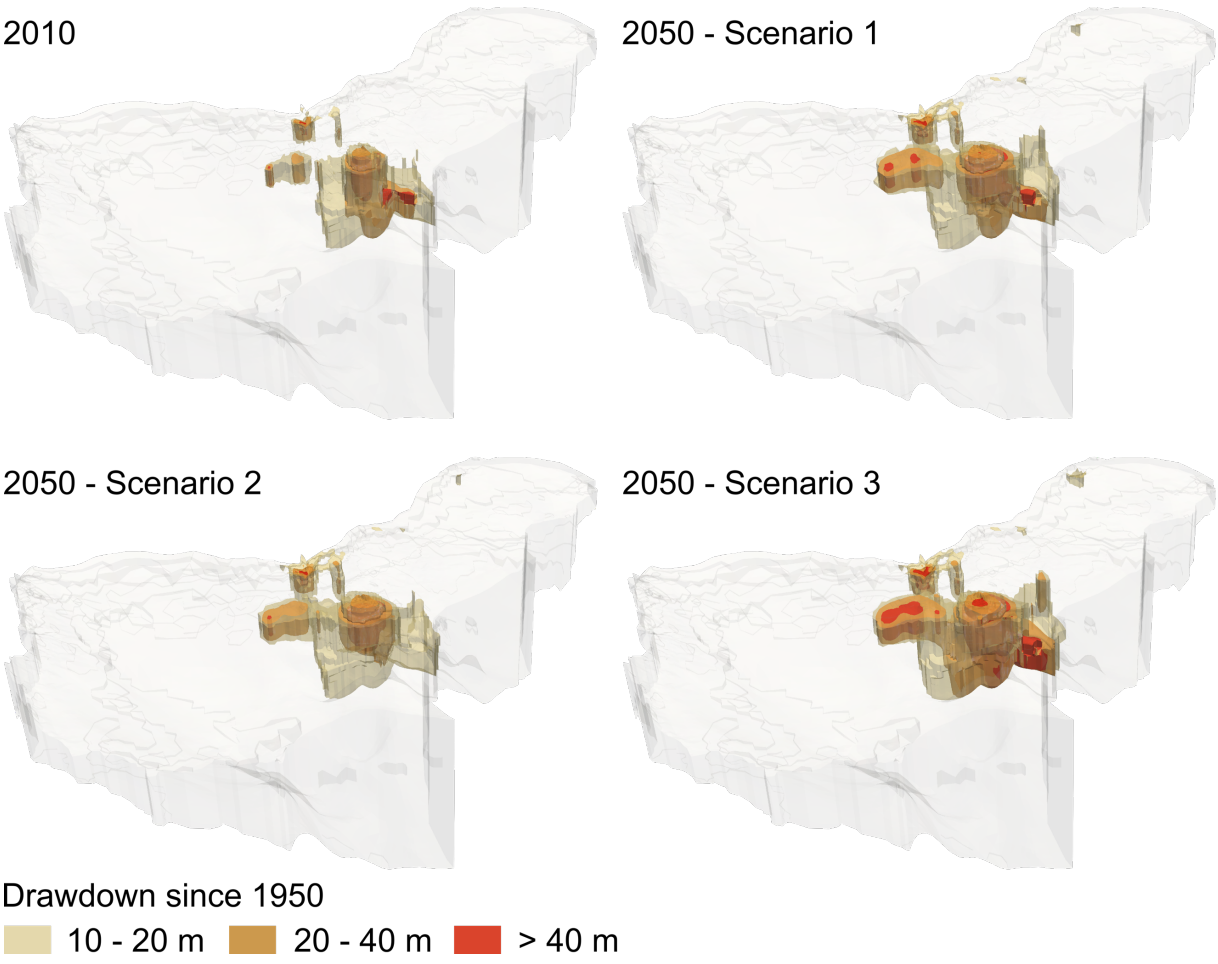

Fig. 5-8: Potentiometric head drawdown since 1950 until 2010 and until 2050 for three different development scenarios (vertical exaggeration of 100)

The water balances of the UMA system for the pre-industrial state, for the period from 1950 to 2010, and for the three development scenarios (2010 to 2050) are presented in Tab. 5-4. Due to the fossil gradients and the resulting fossil discharge component into the Persian Gulf and into the Euphrates (chapter 4; Schulz et al., 2017), already the pre-industrial state shows a negative water balance with a groundwater storage change of about $-1 \cdot 10^9$ m^3a^{-1}. Based on the exploitation of enormous quantities of crude oil beginning in the 1950s, Saudi Arabia experienced a rapid economic growth accompanied with a strong increase of groundwater withdrawal from the UMA system. Although the artificial groundwater abstraction leads to a slight decrease of discharge into the Persian Gulf, the groundwater withdrawal from 1950 to 2010 caused a significant raise of groundwater storage change for this period to about $-2.6 \cdot 10^9$ m^3a^{-1} on average. Simulation results of scenario 1 (abstraction rates of 2010 stay constant) suggest an average groundwater storage change of about $-3.3 \cdot 10^9$ m^3a^{-1}. This value reflects in good approximation the state of the year 2010. Interesting to note are the simulation results of scenario 2 (decreasing groundwater abstraction), which suggest an average groundwater storage change of about $-2.4 \cdot 10^9$ m^3a^{-1}. This value is only slightly less than the one for the period from 1950 to 2010, which shows that even extensive water saving initiatives will not stop the depletion of groundwater reserves. The most negative impact on the remaining groundwater resources arise out of increased groundwater abstraction, simulated in scenario 3. In this case, a groundwater storage change of about $-4.8 \cdot 10^9$ m^3a^{-1} is suggested.

Considering only the main abstraction rates from Saudi Arabia, the estimated exploitable groundwater resources will last about 260, 350, and 180 years according to the estimation of the total exploitable groundwater resources of the UMA system of $864 \cdot 10^9$ m^3 (Tab. 5-2) and the simulated average storage change of scenario 1, 2, and 3, respectively. Here, it has to be noted that these calculations base on average values for a period up to 2050 and further development extending the scenario period are not considered. Moreover, it has to be noted that (i) a part of these resources is located in remote and sparsely populated areas (e.g. Rub' Al-Khali desert) and therefore not readily available for purposes like the domestic supply of larger cities; and (ii) that only groundwater abstraction in Saudi Arabia is considered.

Tab. 5-4: Simulated groundwater balance components [10^6 m^3a^{-1}] for the UMA system

	Groundwater balance component	Pre-industrial state	1950 to 2010	Scenario 1 (2010 to 2050)	Scenario 2 (2010 to 2050)	Scenario 3 (2010 to 2050)
Inflow	Groundwater recharge	2867	2867	2867	2867	2867
	Wadi inflow	114	114	114	114	114
	Oman fault	44	44	44	44	44
Outflow	Mean Gulf discharge	-1597	-1484	-1398	-1399	-1381
	Mean Euphrates discharge	-663	-669	-682	-682	-682
	Salt pans	-1351	-1351	-1351	-1351	-1351
	Springs	-434	-3	-3	-3	-3
	Mean agricultural abstraction	0	-1845	-2625	-1841	-3634
	Mean industrial abstraction	0	-209	-141	-46	-475
	Mean domestic abstraction	0	-79	-142	-142	-346
Net	Mean groundwater storage change	-1020	-2615	-3317	-2439	-4847

5.3 Outlook

The present thesis comprises several studies of the Upper Mega Aquifer system on the Arabian Peninsula and – hopefully – contributes to the overall scientific discussion of hydrological and hydrogeological processes in arid environments. Although some steps towards a better understanding of the UMA system are made, there is still an enormous research potential left and many more PhD-theses could be written. Very relevant studies, to mention just a few, would comprise:

(i) further analysis of groundwater recharge processes, like direct recharge in sand dunes and indirect recharge in wadis;

(ii) interpretation of satellite gravimetry (e.g. GRACE) for the validation of the overall water balance;

(iii) combining numerical modelling with isotope studies, like the incorporation of groundwater ages (e.g. ^{14}C-dating) into the calibration of a numerical groundwater flow model;

(iv) further investigations of the climate evolution during the Holocene and its incorporation into a transient groundwater model to better understand how the UMA system was filled;

(v) further improvement of visualization and data management systems for a better dissemination and accessibility of model results and likewise raising people's awareness.

Another crucial – maybe the most relevant project would be the integration of scientific findings into a holistic management concept for the finite water resources of the UMA system. For such a concept,

researchers and stakeholders from various disciplines and sectors must develop smart mining schemes to find a good balance between satisfying today's demand (for e.g. economic growth and food security) and preserving enough freshwater reserves for future generations.

5.4 References

Al Tokhais, A.S., Rausch, R., 2008. The Hydrogeology of Al Hassa Springs, in: The 3rd International Conference on Water Resources and Arid Environments. Riyadh.

Facey, W., 2000. The Story of the Eastern Province of Saudi Arabia. Stacey International, London.

FAO, 2009. Irrigation in the Middle East region in figures - AQUASTAT Survey - 2008, FAO Water Reports. Food and Agriculture Organization of the United Nations (FAO), Rome.

GIZ/DCo, 2014. Detailed Groundwater Resources Studies in the Rub' Al Khali Desert. Riyadh.

GIZ/DCo, 2011. Detailed Water Resources Studies of Wasia-Biyadh and Aruma Aquifers. Riyadh.

GTZ/DCo, 2010. Kingdom of Saudi Arabia - Assessment and Strategic Plan of the Water Sector. Riyadh.

GTZ/DCo, 2006. Investigations of Updating Groundwater Mathematical Model(s) for the Umm Er Radhuma and Overlying Aquifers. Riyadh.

KSA, 2016. Vision 2030 - National Transformation Program 2020. Riyadh, Saudi Arabia.

Mekonnen, M.M., Hoekstra, A.Y., 2011. National water footprint accounts: the green, blue and grey water footprint of production and consumption. Delft.

Schulz, S., de Rooij, G.H., Michelsen, N., Rausch, R., Siebert, C., Schüth, C., Al-Saud, M., Merz, R., 2016. Estimating groundwater recharge for an arid karst system using a combined approach of time-lapse camera monitoring and water balance modelling. Hydrol. Process. 30, 771–782. doi:10.1002/hyp.10647

Schulz, S., Horovitz, M., Rausch, R., Michelsen, N., Mallast, U., Köhne, M., Siebert, C., Schüth, C., Al-Saud, M., Merz, R., 2015. Groundwater evaporation from salt pans: Examples from the eastern Arabian Peninsula. J. Hydrol. 531, 792–801. doi:10.1016/j.jhydrol.2015.10.048

Schulz, S., Walther, M., Michelsen, N., Rausch, R., Dirks, H., Al-Saud, M., Merz, R., Kolditz, O., Schüth, C., 2017. Improving large-scale groundwater models by considering fossil gradients. Adv. Water Resour. accepted.

UN, 2015. World Population Prospects 2015.

UN-ESCWA, BGR, 2013. Inventory of Shared Water Resources in Western Asia. United Nations Publication, Beirut.

UNIDO, 2006. Industry 2020 - Industrial Strategies to Enhance Diversification and Competitiveness in the Kingdom of Saudi Arabia. Vienna.

WaterWatch, 2006. Historic Groundwater Abstractions at National Scale in the Kingdom of Saudi Arabia - An independent remote sensing investigation. Wageningen.

World Bank, 2005. A Water Sector Assessment Report on the Countries of the Cooperation Council of the Arab States of the Gulf.

6 Annex

6.1 Annex – Chapter 1

A 1 – Thickness and equivalent freshwater head of the Neogene Aquifer (GIZ/DCo, 2014, 2011; GTZ/DCo, 2006):

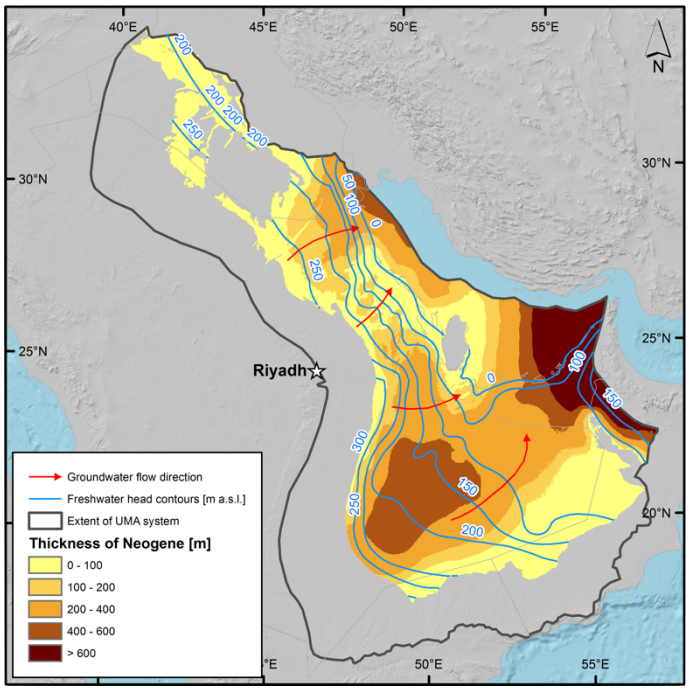

A 2 – Thickness and equivalent freshwater head of the Dammam Aquifer (GIZ/DCo, 2014, 2011; GTZ/DCo, 2006):

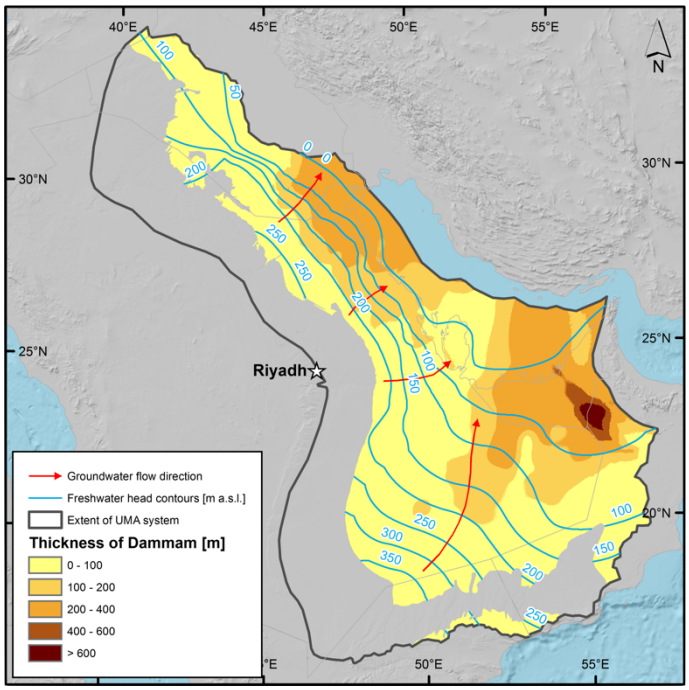

A 3 – Thickness and equivalent freshwater head of the Umm Er Radhuma Aquifer (GIZ/DCo, 2014, 2011; GTZ/DCo, 2006):

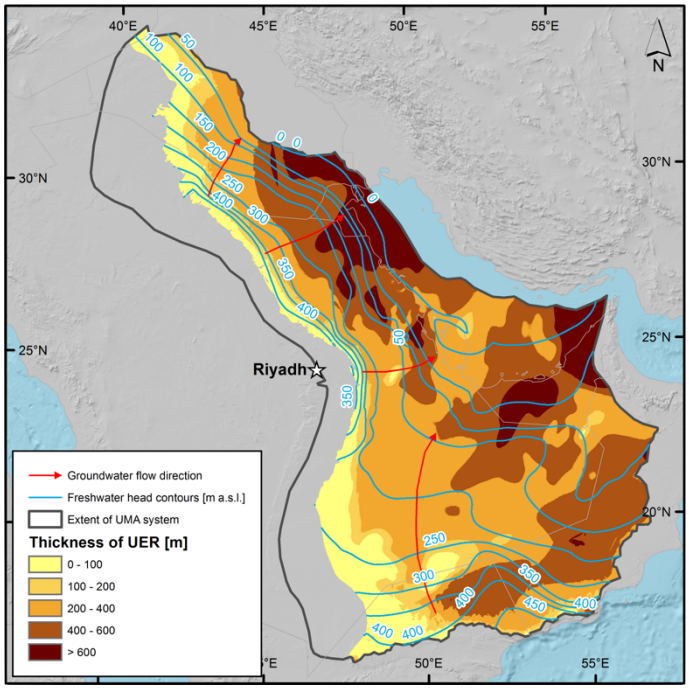

A 4 – Thickness and equivalent freshwater head of the Aruma Aquifer (GIZ/DCo, 2014, 2011; GTZ/DCo, 2006):

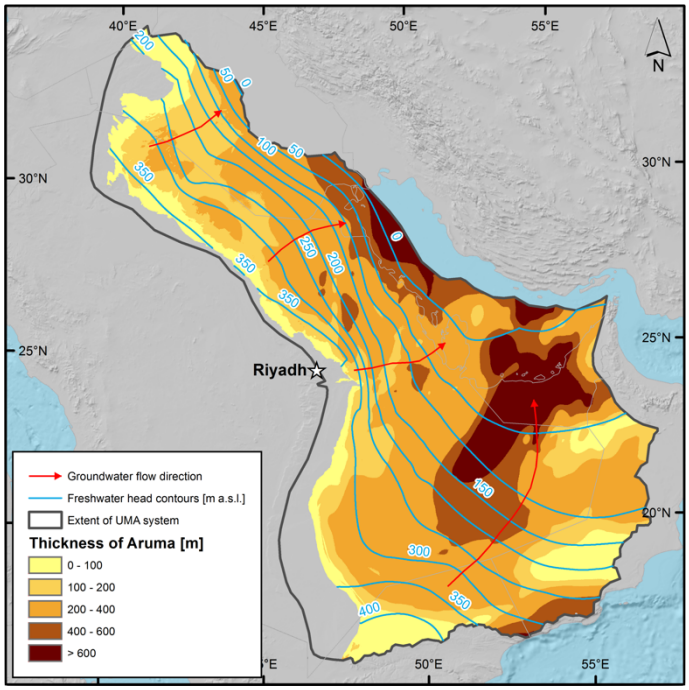

A 5 – Thickness and equivalent freshwater head of the Wasia Aquifer (GIZ/DCo, 2014, 2011; GTZ/DCo, 2006):

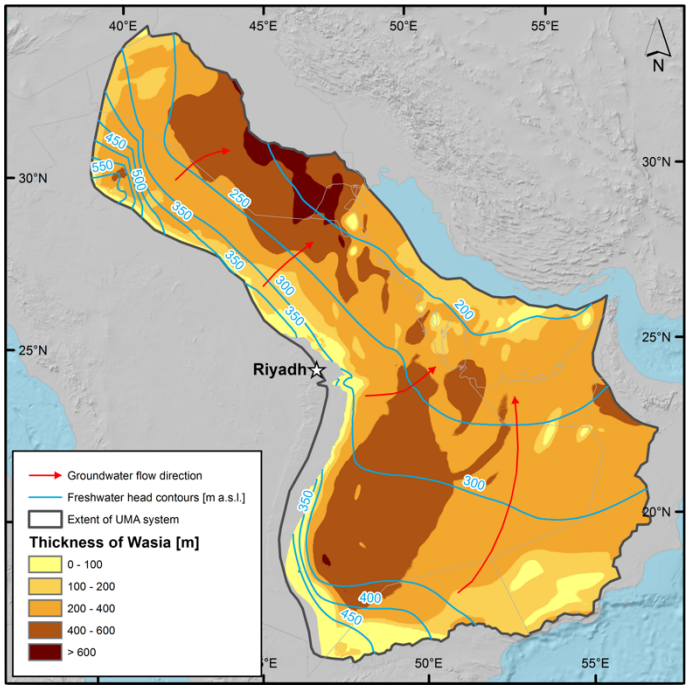

A 6 – Thickness and equivalent freshwater head of the Biyadh Aquifer (GIZ/DCo, 2014, 2011; GTZ/DCo, 2006):

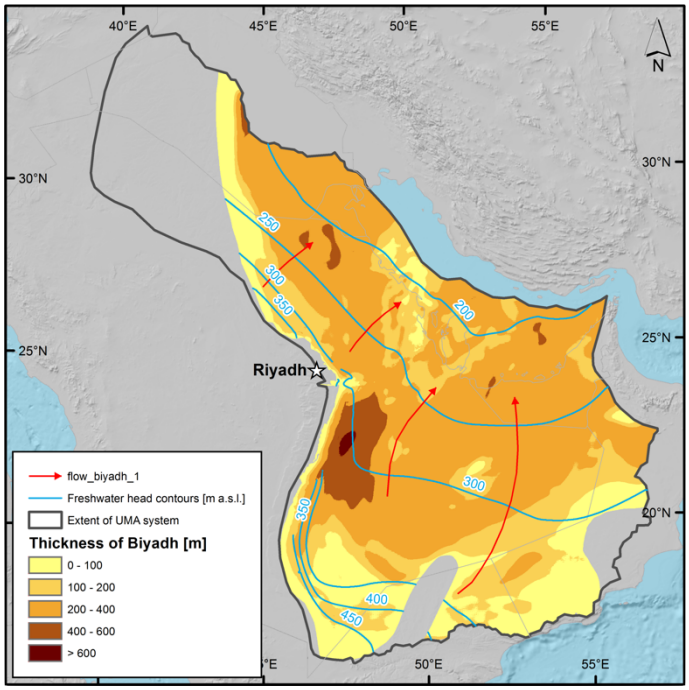

A 7 – Selected groundwater recharge estimations on the Arabian Peninsula:

Id	Country	Recharge rate [mm a^{-1}]	Precipitation rate [mm a^{-1}]	Recharge-precipitation-ratio	Method	Remarks	Source
1	Saudi Arabia	5.1	61	0.08	Water balance model	Karst outrcrops (As Sulb plateau)	(Schulz et al., 2016)
2	Saudi Arabia	3	79.5	0.04	Water balance model	Wasia outcrop	(Caro and Eagleson, 1981)
3	Saudi Arabia	15	129.8	0.12	Water balance model	Minjur outcrop	(Caro and Eagleson, 1981)
4	Saudi Arabia	1.9	62	0.03	Water balance model	UMA system (only Saudi Arabia)	(GIZ/DCo, 2013), (Kummerow et al., 1998)
5	Saudi Arabia	4	47.7	0.08	Water balance model	Wasia	(Subyani and Sen, 1991)
6	Saudi Arabia	19	177	0.11	CMB	Wadi Yalamlam (shield)	(Subyani and Şen, 2006)
7	Saudi Arabia	7	108	0.06	Water balance model	Six wadis close to Kharj	(Bendel, 2009)
8	Saudi Arabia	20	80	0.25	Tritium	Ad Dahna sand dunes; infiltration not real recharge	(Dincer et al., 1974)
9	Saudi Arabia	4.4	130	0.03	CMB	Several wadis in western KSA (without outliers)	(Bazuhair and Wood, 1996)
10	Saudi Arabia	6	60	0.1	Not specified	Aquifer outcrops in the eastern province	(Wagner, 2011)
11	Saudi Arabia	2.0	67	0.029	Not specified	Whole country	(Khater, 2002)
12	Saudi Arabia	0.9	62	0.015	Global scale water balance model	Whole country	(Döll and Fiedler, 2008), (Kummerow et al., 1998)
13	Saudi Arabia	1.0	62	0.016	Not specified	Whole country	(FAO, 2016), (Kummerow et al., 1998)
14	Saudi Arabia	0.45	114	0.004	Not specified	Whole country	(Chowdhury and Al-Zahrani, 2015)
15	Saudi Arabia	0.48	50	0.01	Not specified	Whole country	(Mohorjy, 1988)
16	Saudi Arabia	0.58	62	0.009	Not specified	Whole country	(Farooq and Al-Layla, 1985), (Kummerow et al., 1998)
17	Saudi Arabia	1.8	62	0.029	Not specified	Whole country	(World Bank, 2005), (Kummerow et al., 1998)
18	Saudi Arabia	1.1	62	0.018	Not specified	Whole country	(Alsharhan et al., 2001), (Kummerow et al., 1998)
19	Qatar	6.9	81	0.085	Not specified	Whole country	(Wagner, 2011), (Kummerow et al., 1998)
20	Qatar	5.1	81	0.063	Not specified	Whole country	(Amer, 2008), (Kummerow et al., 1998)
21	Qatar	8	107	0.075	Not specified	Whole country	(Khater, 2002), (Kummerow et al., 1998)
22	Qatar	9	75	0.12		Northern zone	(Eccleston and Harhash, 1982)
23	Qatar	4.5	75	0.06	Not specified	Southern zone; rainfall rate reported to be slightly less than 75 mm a^{-1}	(Eccleston and Harhash, 1982)

24	Qatar	1.3	107	0.012	Global scale water balance model	Whole country	(Döll and Fiedler, 2008), (Kummerow et al., 1998)
25	Qatar	4.5	107	0.042	Not specified	Whole country	(FAO, 2016), (Kummerow et al., 1998)
26	Qatar	8	80	0.1	Not specified	Northern half of the country	(Pike, 1983)
27	Qatar	2.0	107	0.019	Not specified	Whole country	(Lloyd, 1994), (Kummerow et al., 1998)
28	Qatar	4.3	107	0.04	Not specified	Whole country	(World Bank, 2005), (Kummerow et al., 1998)
29	Iraq	29.8	170	0.175	Not specified	Whole country	(Khater, 2002), (Kummerow et al., 1998)
30	Iraq	17.9	170	0.105	Global scale water balance model	Whole country	(Döll and Fiedler, 2008), (Kummerow et al., 1998)
31	Iraq	1.8	174	0.01	CMB	Northeastern Missan Governorate	(Atiaa et al., 2004)
32	Iraq	110	700	0.157	Not specified	Northern part of the Foothill Aquifer system	(Krásný et al., 2006)
33	Iraq	20	550	0.036	Not specified	Erbil Plain	(Krásný et al., 2006)
34	Iraq	2.7	170	0.016	Not specified	Whole country	(FAO, 2016), (Kummerow et al., 1998)
35	Kuwait	9.5	130	0.073	Not specified	Whole country	(Khater, 2002), (Kummerow et al., 1998)
36	Kuwait	1.2	130	0.009	Global scale water balance model	Whole country	(Döll and Fiedler, 2008), (Kummerow et al., 1998)
37	Kuwait	12.4	226	0.055	Water balance model	Raudatain catchment	(Al-Dousari et al., 2010)
38	Kuwait	7.6	211	0.036	Water balance model	Umm Al Aish catchment	(Al-Dousari et al., 2010)
39	Kuwait	9.0	130	0.069	Not specified	Whole country	(World Bank, 2005), (Kummerow et al., 1998)
40	Bahrain	12.75	78	0.16	Water table fluctuations	Alat aquifer (member of Dammam aquifer)	(Al-Noaimi, 2004)
41	Bahrain	2.2	80	0.028	Not specified	Dammam aquifer, outcrop area of 228 km² (USGS and ARAMCO, 1963)	(Zubari, 1999)
42	UAE	8.8	130	0.07	Water balance model	Al Ain area	(Osterkamp and Lane, 2003)
43	UAE	1.29	52	0.025		Whole country	(Rizk and Alsharhan, 2003), (Kummerow et al., 1998)
44	UAE	1.8	52	0.035	Not specified	Whole country	(Khater, 2002), (Kummerow et al., 1998)
45	UAE	3.0	52	0.058	Global scale water balance model	Whole country	(Döll and Fiedler, 2008), (Kummerow et al., 1998)

46	UAE	1.4	52	0.027	Not specified	Whole country	(FAO, 2016), (Kummerow et al., 1998)
47	UAE	2.3	52	0.044	Not specified	Whole country	(World Bank, 2005), (Kummerow et al., 1998)
48	Oman	4	70	0.057	Groundwater flow model	Interior of Dhofar	(Müller, 2012)
49	Oman	3.1	43	0.073	Not specified	Whole country	(Khater, 2002), (Kummerow et al., 1998)
50	Oman	2.6	43	0.06	Global scale water balance model	Whole country	(Döll and Fiedler, 2008), (Kummerow et al., 1998)
51	Oman	3.1	43	0.072	Not specified	Whole country	(FAO, 2016), (Kummerow et al., 1998)
52	Oman	8.8	130	0.068	Water balance model	Oman Mountains	(Osterkamp et al., 1995)
53	Oman	4.2	43	0.098	Not specified	Whole country	(World Bank, 2005), (Kummerow et al., 1998)
54	Oman	1.8	43	0.042	Not specified	Whole country	(Shahin, 2007), (Kummerow et al., 1998)
55	Oman	2.8	43	0.065	Not specified	Whole country	(Alsharhan et al., 2001), (Kummerow et al., 1998)
56	Yemen	3.5	126	0.028	Not specified	Whole country	(Khater, 2002), (Kummerow et al., 1998)
57	Yemen	2.6	126	0.021	Global scale water balance model	Whole country	(Döll and Fiedler, 2008), (Kummerow et al., 1998)
58	Yemen	2.8	126	0.022	Not specified	Whole country	(FAO, 2016), (Kummerow et al., 1998)
59	Yemen	3.3	126	0.026	Not specified	Whole country	(Alsharhan et al., 2001), (Kummerow et al., 1998)
60	Yemen	30	330	0.091	Water balance	Sana'a basin	(Charalambous, 1982)
61	Yemen	12	195	0.062	Water balance model	Sana'a basin	(Alderwish, 1995)
62	Yemen	14.1	235	0.06	Not specified	Sana'a basin	(Foppen et al., 2005)

References:

Al-Dousari, A., Milewski, A., Din, S.U., Ahmed, M., 2010. Remote Sensing Inputs to SWAT Model for Groundwater Recharge Estimates in Kuwait. Adv. Nat. Appl. Sci. 4, 71–77.

Al-Noaimi, M.A., 2004. Development of water resources in Bahrain: A combined approach of supply - demand analysis. University of Plymouth.

Alderwish, A.M.A., 1995. Estimation of Groundwater Recharge to Aquifers of Sana'a Basin, Yemen. University of London.

Alsharhan, A.S., Rizk, Z.A., Nairn, A.E.M., Bakhit, D.W., Alhajari, S.A., 2001. Hydrogeology of an Arid Region: The Arabian Gulf and Adjoining Areas. Elsevier, Amsterdam.

Amer, K.M., 2008. Groundwater resources sustainability in Qatar: Problems and perspectives, in: Bhattacharya, P., Ramanathan, A., Mukherjee, A.B., Bundschuh, J., Chandrasekharam, D., Keshari, A.K. (Eds.), Groundwater for Sustainable Development: Problems, Perspectives and Challenges. CRC Press/Taylor & Francis Group, Boca Raton, pp. 25–37.

Atiaa, A.M., Al-Shamma'a, M.A., Aljabbari, M.H., 2004. Estimation of Groundwater Recharge for the Main Aquifer in the Northeastern Missan Governorate, South of Iraq Using Chloride Mass Balance Technique. Iraqi J. Sci. 55, 463–470.

Bazuhair, A.S., Wood, W.W., 1996. Chloride mass-balance method for estimating ground water recharge in arid areas: Examples from western Saudi Arabia. J. Hydrol. 186, 153–159. doi:10.1016/S0022-1694(96)03028-4

Bendel, D., 2009. Hydrologische Niederschlags-Abfluss Modellierung in ariden Gebieten unter Verwendung von Fernerkundungsdaten am Beispiel eines Einzugsgebietes im Königreich Saudi Arabien. Universität Stuttgart.

Caro, R., Eagleson, P.S., 1981. Estimating aquifer recharge due to rainfall. J. Hydrol. 53, 185–211.

Charalambous, A.N., 1982. Problems of groundwater development in the Sana'a basin, Yemen Arab Republic, in: Improvements of Methods of Long Term Prediction of Variations in Groundwater Resources and Regimes Due to Human Activity: Proceedings of the Exeter Symposium. International Association of Hydrological Sciences Publication, Wallingford, Oxfordshire, pp. 265–274.

Chowdhury, S., Al-Zahrani, M., 2015. Characterizing water resources and trends of sector wise water consumptions in Saudi Arabia. J. King Saud Univ. - Eng. Sci. 27, 68–82. doi:10.1016/j.jksues.2013.02.002

Dincer, T., Al-Mugrin, A., Zimmermann, U., 1974. Study of the infiltration and recharge through the sand dunes in arid zones with special reference to the stable isotopes and thermonuclear tritium. J. Hydrol. 23, 79–109. doi:10.1016/0022-1694(74)90025-0

Döll, P., Fiedler, K., 2008. Global-scale modeling of groundwater recharge. Hydrol. Earth Syst. Sci. 12, 863–885. doi:10.5194/hess-12-863-2008

Eccleston, B.L., Harhash, I.E., 1982. The Hydro-Geology of Qatar: Water Resources and Agricultural Development Project Phase III.

FAO, 2016. AQUASTAT Main Database [WWW Document]. URL www.fao.org/nr/aquastat/ (accessed 3.21.16).

Farooq, S., Al-Layla, R.I., 1985. Potential of Water Development in Saudi Arabia. Water Int. 10, 151–155. doi:10.1080/02508068508686343

Foppen, J.W.A., Naaman, M., Schijven, J.F., 2005. Managing water under stress in Sana'a, Yemen. Arab. J. Sci. Eng. 30, 69–83.

GIZ/DCo, 2014. Detailed Groundwater Resources Studies in the Rub' Al Khali Desert. Riyadh.

GIZ/DCo, 2013. Detailed Groundwater Resources Studies of Khuff Jilh Minjur Dhruma and overlying Aquifers. Riyadh.

GIZ/DCo, 2011. Detailed Water Resources Studies of Wasia-Biyadh and Aruma Aquifers. Riyadh.

GTZ/DCo, 2006. Investigations of Updating Groundwater Mathematical Model(s) for the Umm Er Radhuma and Overlying Aquifers. Riyadh.

Khater, A.R., 2002. Intensive groundwater use in the Middle East and North Africa, in: Llamas, M.R., Custodio, E. (Eds.), Intensive Use of Groundwater: Challenges and Opportunities. CRC Press/Taylor & Francis Group, Boca Raton, pp. 355–386.

Krásný, J., Alsam, S., Jassim, S.Z., 2006. Hydrogeology, in: Jassim, S.Z., Goff, J.C. (Eds.), Geology of Iraq. Dolin, Prague, pp. 251–287.

Kummerow, C., Barnes, W., Kozu, T., Shiue, J., Simpson, J., 1998. The Tropical Rainfall Measuring Mission (TRMM) Sensor Package. J. Atmos. Ocean. Technol. 15, 809–817. doi:10.1175/1520-0426(1998)015<0809:TTRMMT>2.0.CO;2

Lloyd, J.W., 1994. Groundwater-Management Problems In The Developing World. Hydrogeol. J. 2, 35–48. doi:10.1007/s100400050042

Mohorjy, A., 1988. Water Resources Management in Saudi Arabia and Water Reuse. Water Int. 13, 161–171. doi:10.1080/02508068808687065

Müller, T., 2012. Recharge and residence times in an arid area aquifer. Technische Universität Dresden.

Osterkamp, W., Lane, L.J., 2003. Ground-water recharge estimates in arid areas using channel morphology and a simulation model. Dev. Water Sci. 50, 281–286. doi:10.1016/S0167-5648(03)80024-2

Osterkamp, W.R., Lane, L.J., Menges, C.M., 1995. Techniques of ground-water recharge estimates in arid/semi-arid areas, with examples from Abu Dhabi. J. Arid Environ. 31, 349–369. doi:10.1016/S0140-1963(05)80038-2

Pike, J.G., 1983. Groundwater resources development and the environment in the central region of the Arabian Gulf. Int. J. Water Resour. Dev. 1, 115–132. doi:10.1080/07900628308722280

Rizk, Z.S., Alsharhan, A.S., 2003. Water resources in the United Arab Emirates. pp. 245–264. doi:10.1016/S0167-5648(03)80022-9

Schulz, S., de Rooij, G.H., Michelsen, N., Rausch, R., Siebert, C., Schüth, C., Al-Saud, M., Merz, R., 2016. Estimating groundwater recharge for an arid karst system using a combined approach of time-lapse camera monitoring and water balance modelling. Hydrol. Process. 30, 771–782. doi:10.1002/hyp.10647

Shahin, M., 2007. Water Resources and Hydrometeorology of the Arab Region, Water Science and Technology Library. Springer Netherlands, Dordrecht. doi:10.1007/1-4020-5414-9

Subyani, A., Sen, Z., 1991. Study of Recharge Outcrop Relation of the Wasia Aquifer in Central Saudi Arabia. J. King Abdulaziz Univ. Earth Sci. 4, 137–147.

Subyani, A., Şen, Z., 2006. Refined chloride mass-balance method and its application in Saudi Arabia. Hydrol. Process. 20, 4373–4380. doi:10.1002/hyp.6172

USGS, ARAMCO, 1963. Geologic map of the Arabian Peninsula - U.S. Geological Survey Misc. Inv. Map I-270 A, scale 1:2,000,000.

Wagner, W., 2011. Groundwater in the Arab Middle East. Springer Berlin Heidelberg, Berlin, Heidelberg. doi:10.1007/978-3-642-19351-4

World Bank, 2005. A Water Sector Assessment Report on the Countries of the Cooperation Council of the Arab States of the Gulf.

Zubari, W.K., 1999. The Dammam aquifer in Bahrain - Hydrochemical characterization and alternatives for management of groundwater quality. Hydrogeol. J. 7, 197–208. doi:10.1007/s100400050192

6.2 Annex – Chapter 3

A 8 – Literature data about the depth to the water table in salt pans:

Name	Coordinates		Watertable	Distance to Gulf	Altitude	Source
	Latitude	Longitude	[m b.g.l.]	[km]	[m]	
As Sarrar	27.029977	48.420507	0.3	83	77	Al Saafin (1996)
As Sarrar	27.012054	48.416344	0.75	84	77	Al Saafin (1996)
Jeb Awiyad	26.281026	49.896708	0.65	15.6	1	Al Saafin (1996)
Half Moon K	26.098816	49.94989	0.75	3.2	2	Al Saafin (1996)
Azizia Z	26.222835	50.20834	0.8	0.8	1	Al Saafin (1996)
Ar Riyyas	26.812147	49.85638	0.8	5	3	Al Saafin (1996)
As Summ	26.94114	49.666033	0.78	3.2	1	Al Saafin (1996)
Al Budu Edge	23.228103	49.261269	1.8	239	104	Al Saafin (1996)
Al Budu Central	23.22822	49.310123	0.9	234	106	Al Saafin (1996)
Sabkha Nr.2	27.169311	49.313463	0.8	6.2	-1	Barth (1998)
Sabkha Nr.3	27.0875	49.405556	0.5	3.3	3	Barth (1998)
Sabkha Nr. 5	27.077643	49.184695	0.4	22.7	9	Barth (1998)
Sabkha Nr.4	27.080589	49.209928	0.4	20.2	4	Barth (1998)
Sabkha Nr. 6	26.975573	49.433303	0.5	17.4	7	Barth (1998)
E021	22.183729	54.316875	1.86	215	70	Smith (1981)
E020	22.211788	54.322817	1.72	212	70	Smith (1981)
E016	22.182079	54.353121	1.04	216	71	Smith (1981)
B-10	28.629272	48.356033	1	2.7	1	Robinson and Gunatilaka (1991)
C-1	28.618048	48.343591	0.4	4.2	2	Robinson and Gunatilaka (1991)
B-8	28.616228	48.368993	0.4	1.9	1	Robinson and Gunatilaka (1991)
Zone A	21.619928	55.91597	0.5	292	55	Heathcote and King (1998)
Zone B	21.532588	55.797131	1.25	308	55	Heathcote and King (1998)
Zone C	21.822922	55.935137	1.6	273	59	Heathcote and King (1998)

A 9 - Hydrochemistry and isotope data from the salt pan study:

Sabkha = S ; Gulf Water = G ; Well = W ; Sabkha with free water surface = L

S 20 = Yabrin; S 22 = Matti; S 25 = RAK

									H_2O Isotopes			SO_4 - Isotopes	
ID	Sample Date	Coordinates		Watertable	Distance to Gulf	Altitude	pH	EC	O-18	H-2	Excess	S-34	O-18
		Latitude	Longitude	[m b.g.l.]	[km]	[m]	[-]	[mS/cm]	[‰-VSMOW]	[‰-VSMOW]	[-]	[‰-CDT]	[‰-VSMOW]
S 1	06-05-13	27.157199	49.386181	0.75	0.5	0	7.01	204	6.9	25.3	-30.2	19.12	9.8
S 2	06-05-13	27.112085	49.382963	0.85	1.4	1	7.45	149	4.1	15.7	-17.4	19.44	8.4
S 3	05-05-13	26.84271	49.814879	0.76	4	2	6.92	221	4.5	12.9	-23.2	18.96	10.9
S 4	05-05-13	26.773453	49.862696	0.56	9	2	6.5	221	3.9	4.9	-26.0	19.59	12.5
S 5	05-05-13	26.65464	49.85185	0.86	14	3	6.5	204	4.7	7.2	-30.5	11.37	8.4
S 6	05-05-13	26.503974	49.941405	0.73	9	2	6.72	213	7.0	15.4	-40.9	7.44	10.8
S 7	05-05-13	26.319716	49.897448	0.69	19	8	7.01	145	3.2	3.0	-22.3	11.34	10.6
S 8	05-05-13	26.239807	49.567865	0.7	45	33	6.43	209	8.4	22.2	-45.0	9.59	6.7
S 9	15-02-14	26.19826	50.12092	0.7	5	2		224	7.5	17.1	-43.2	9	10.5
S 10	15-02-14	26.09911	49.985154	0.72	0.8	3		207	7.0	29.6	-26.2	19.9	8
S 11	15-02-14	25.944975	50.003063	0.73	4	1		201	4.7	16.0	-21.2	12.2	16.8
S 12	14-02-14	25.412768	49.860391	0.7	43	107		197.4	5.8	11.6	-35.1	10.8	12
S 13	27-11-12	24.286581	51.313657	1.2	0.9	5	7.57	106.6	6.4	28.6	-22.8	20.14	10.1
S 14	27-11-12	24.269185	51.278685	1.03	4	5	7.16	175.5	8.8	25.9	-44.9	16.32	11.6
S 15	22-02-14	24.156521	54.299247	0.58	10	2		195.3	5.6	12.7	-31.7	16	10.3
S 16	27-11-12	24.14598	51.537921	1.3	12	9	6.74	244	5.1	19.3	-21.3	16.23	9
S 18	27-11-12	24.099631	51.146333	0.79	27	10	6.94	226	10.4	24.6	-58.9	14.01	7.8
S 19	22-02-14	24.067489	53.309587	0.69	3	6		209	2.6	7.6	-13.3	15.6	10.2
S 20	13-11-12	23.151666	48.971205	0.76	260	175	7.27	46.4	-2.4	-23.0	-3.7	12.78	12.7
S 21	06-05-13	23.151666	48.971205	0.71	260	175	7.16	44	-3.2	-26.4	-0.6	11.49	13.6
S 22	26-11-12	23.196191	51.737051	1.06	89	44	7.23	216	11.0	23.5	-64.3	13.85	9.9
S 23	13-11-12	23.236855	49.299454	0.57	230	105	7.95	33.4	-1.8	-19.8	-5.5	16.85	12.7
S 24	06-05-13	23.236855	49.299454	0.52	230	105	6.64	36	-2.2	-22.3	-4.5	16.39	11.8
S 25	26-11-12	22.595449	53.752901	1.74	188	83	7.26	115.5	8.8	15.8	-54.7	15.66	13.1
L 1	06-05-13	27.052527	49.459953	-	7	12	7.2	45	8.2	42.4	-23.6	20.03	15.3
L 2	06-05-13	26.820982	49.581891	-	19	12	7.73	12	2.3	3.1	-15.4	10.2	14.1
W 1	06-05-13	26.891549	49.471644	-	-	-	7.57	2.7	-3.4	-22.5	5.0	8.25	12.5
W 2	06-05-13	26.117292	49.384226	-	-	-	7.7	3.4	-5.1	-37.1	3.9	12.8	12.9
W 3	28-11-12	23.30562	48.968634	-	-	-	7.78	1.34	-4.3	-29.2	5.0	14.26	12.2
W 4	28-11-12	23.124935	48.968386	-	-	-	7.545	1.351	-4.4	-26.9	8.1	13.42	12.9
G 1	06-05-13	27.007537	49.668874	-	-	-	7.8	64	4.2	24.9	-8.7	20.46	8.5
G 2	06-05-13	27.1561	49.40046	-	-	-	7.8	64	2.5	14.4	-5.4	20.25	7.8
G 3	27-11-12	24.293932	51.31603	-	-	-	8.13	70.2	3.8	24.0	-6.1	20.76	8.9

	Hydrochemistry																			
ID	Chlorid	Sulfat	Bromid	Phosphat	Nitrat	HCO3	B	Ba	Ca	Fe	K	Li	Na	Mg	Si	Sr	As (ICP-MS)	Cs (ICP-MS)	Mn (ICP-MS)	Rb (ICP-MS)	U (ICP-MS)
	[mg/l]	[mg/l]	[mg/l]	[mg/l]	[mg/l]	[mg/l]	[mg/l]	[mg/l]	[mg/l]	[mg/l]	[mg/l]	[mg/l]	[mg/l]	[mg/l]	[mg/l]	[mg/l]	[ng/l]	[ng/l]	[ng/l]	[ng/l]	[ng/l]
S 1	130655	8010	275	<0.1	<46	-	5.26	0.05	1490	<0.003	2220	1.13	66010	6910	2.17	32.8	11.4	0.99	108	660	0.4
S 2	74950	5936	138	<0.1	<46	-	5.28	0.085	1590	<0.003	1290	0.731	36830	3670	5.12	30.9	19	1.4	3.3	400	3
S 3	150763	3488	249	<0.1	<46	-	2.14	0.0102	2590	<0.003	2610	1.14	81630	6420	1.34	44.1	3.7	2.7	230	670	4.5
S 4	151176	2517	321	<0.1	<46	-	4.35	0.042	3410	<0.003	3060	1.84	75010	7730	5.94	59.7	3	3.2	370	860	1.7
S 5	171148	1501	182	<0.1	103	-	0.507	0.24	5500	<0.003	2840	2.7	75730	12820	2.25	98.7	1	30	85	1030	6.1
S 6	177497	5102	48.1	<0.1	129	-	1.36	0.038	1550	0.005	4150	9.38	84880	7550	2.13	25.5	1.5	6.1	810	1430	1.7
S 7	81553	3469	<0.5	<0.1	101	-	3.16	0.102	3370	0.005	1620	2.71	39220	4400	4.35	76.5	2.1	2.9	160	390	2.9
S 8	190084	5725	75.1	<0.1	253	-	<0.5	0.081	1310	0.004	5370	5.77	100580	5530	1.44	27.2	1.4	10.2	27	1380	<0.16
S 9	176749	2199	550	-	-	-	2.5	0.072	3460	0.78	6420	2.83	78440	16030	1.1	101	0.5	3.7	110	1700	2.1
S 10	123961	9333	357	-	-	-	6.93	0.035	979	0.4	2350	1	67370	6270	1.41	29.1	0.94	1.2	6.8	700	0.69
S 11	115131	12595	37.9	-	-	-	1.63	0.0045	917	0.36	2770	3.35	65540	6240	1.4	21.2	0.4	1	9.6	1200	<0.075
S 12	123928	14786	79.2	-	-	-	6.08	0.042	817	0.37	3000	3.81	63650	10330	1.64	17.4	2.3	1.8	14	810	17
S 13	49783	5260	90.3	0.17	0.07	116.247884	7.45	<0.3	1090	<0.3	1030	<0.7	27230	2930	2.55	21.2	4.8	0.99	39	330	33
S 14	101309	10288	34.7	0.1	39.82	95.6223972	24.1	<0.3	1220	<0.3	2090	4.61	55820	5280	2.66	24.1	<1.8	1.23	67	530	0.51
S 15	114889	3289	4.4	-	-	-	0.525	0.045	3980	0.84	2580	1.62	61450	3590	1.65	88.1	0.38	0.39	12	380	0.3
S 16	203746	1483	<6.5	<0.07	5220	1.22993855	1.04	<0.3	2520	<0.3	5230	2.19	113960	2600	1.7	47.5	<1.8	1.43	190	830	0.58
S 18	175100	1327	<6.5	<0.07	1	4.85881236	14.3	<0.3	4700	<0.3	2610	7.88	90370	6210	1.71	81.8	<1.8	1.9	7.9	760	0.19
S 19	117723	12885	6.12	-	-	-	3.26	0.0055	965	0.38	1850	1.5	76860	861	1.81	27.1	1.2	0.58	17	270	2.1
S 20	17610	3423	<6.5	0.33	0.08	250.921513	1.99	<0.3	1380	<0.3	363	<0.7	9420	1170	27.7	28.3	3.2	0.27	147	148	11.3
S 21	16389	3827	<0.5	<0.1	<23	-	1.39	0.065	1320	0.003	296	<0.7	7430	967	20.1	24.2	4	0.28	52	100	3.1
S 22	146273	5318	13.8	<0.07	1	2.3927629	9.44	<0.3	1670	1.84	1590	1.88	85560	3210	2.41	29.1	2.5	0.6	24	260	0.66
S 23	10705	4455	<6.5	<0.07	0.13	48.5876947	1.61	<0.3	822	<0.3	441	<0.7	8210	307	13.1	17.2	<1.8	0.13	11.6	82	0.06
S 24	10705	4851	<0.5	<0.1	<23	-	1.66	0.019	942	0.015	454	<0.7	6440	274	14.1	18	2.5	0.091	6.2	75	<0.16
S 25	56514	3810	<6.5	0.36	5320	21.1222479	5.94	<0.3	2230	1.51	475	0.789	30470	2030	7.8	39.3	2.7	1.7	18	155	5.1
L 1	15217	4281	19.2	<0.1	<23	-	6.63	0.096	1340	0.006	376	<0.7	7810	820	2.28	25.9	14	<0.057	140	150	1.27
L 2	2758	1990	<0.5	<0.1	<23	-	1.27	0.045	701	0.008	88	<0.7	1500	302	18.8	16.4	4.9	0.102	23	27	53
W 1	447	498	<0.1	<0.1	13	-	<0.5	0.03	200	0.003	13.3	<0.7	257	68.2	6.65	3.79	0.57	0.072	3	8.8	7.4
W 2	692	450	<0.1	<0.1	<4.6	-	<0.5	0.027	179	0.022	30.3	<0.7	404	71.5	11	6.28	0.47	0.16	4.1	19	1.01
W 3	233	192	<0.13	<0.07	6.18	177.763358	<0.5	<0.3	74.4	<0.3	4.96	<0.7	92.6	32.7	6.38	1.81	<1.8	0.058	3.5	4.3	2.9
W 4	226	202	<0.13	<0.07	44.21	175.944381	<0.5	<0.3	95.2	<0.3	11.3	<0.7	170	41.6	7.58	2.45	<1.8	0.061	7.4	3.9	3.1
G 1	32882	4169	93.8	<0.1	<23	-	6.32	0.02	649	0.005	626	<0.7	16330	2120	<0.6	11	2.4	1.16	1.6	190	4.7
G 2	25331	3127	71.8	<0.1	<23	-	5.01	0.0131	515	0.003	487	<0.7	12660	1640	<0.6	9.24	5.8	0.72	1.09	150	3.5
G 3	29006	3290	49.7	0.14	21.16	144.325639	5.72	<0.3	592	<0.3	561	<0.7	15760	1960	<0.6	10	2	0.43	8.5	170	4.7

A 10 - Grainsize distribution of the salt pan soil columns:

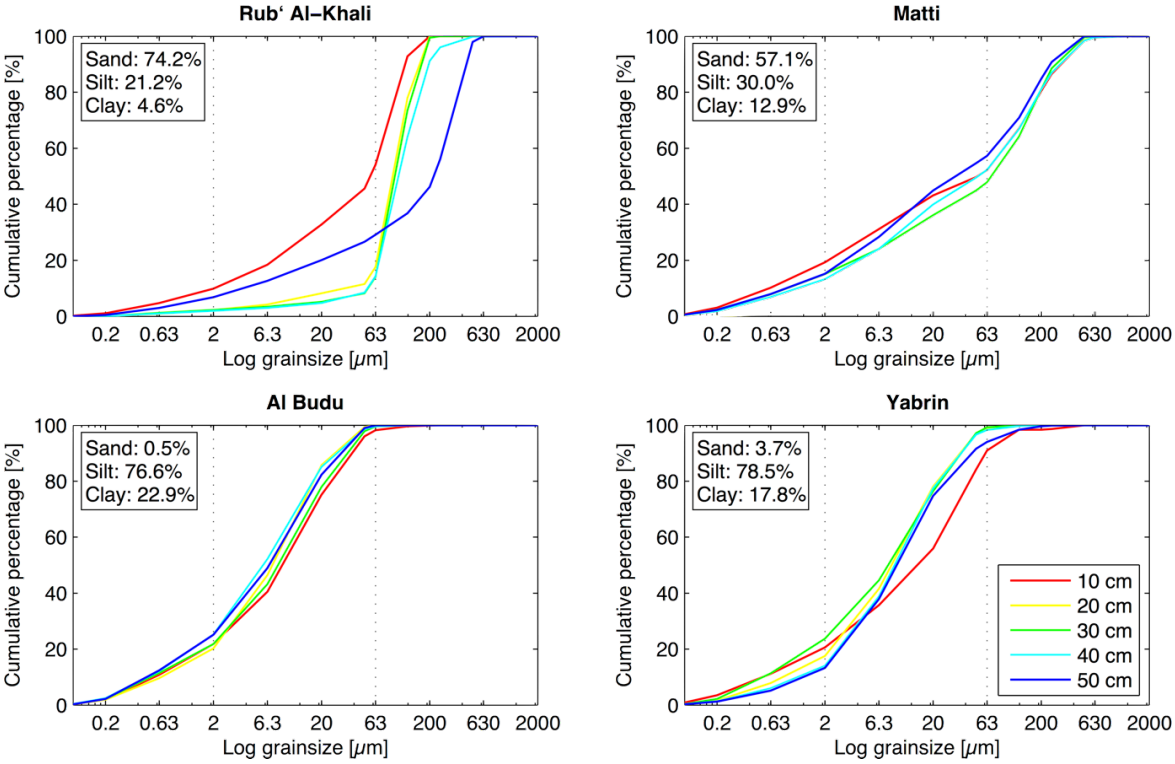

A 11 – Technical drawing of the soil core sampler:

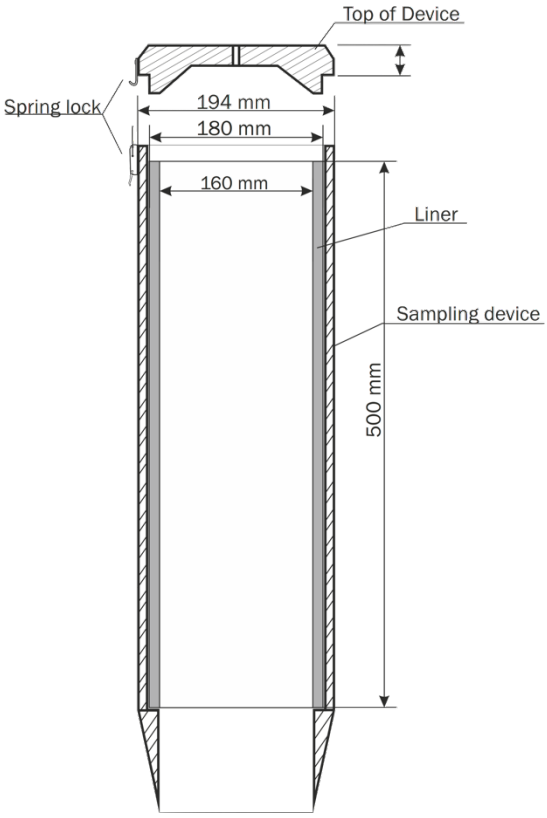

A 12 – Soil core sampler in operation:

6.3 Annex – Chapter 4

A 13 – Rock art site "Graffiti Rock" about 100 km west of Riyadh:

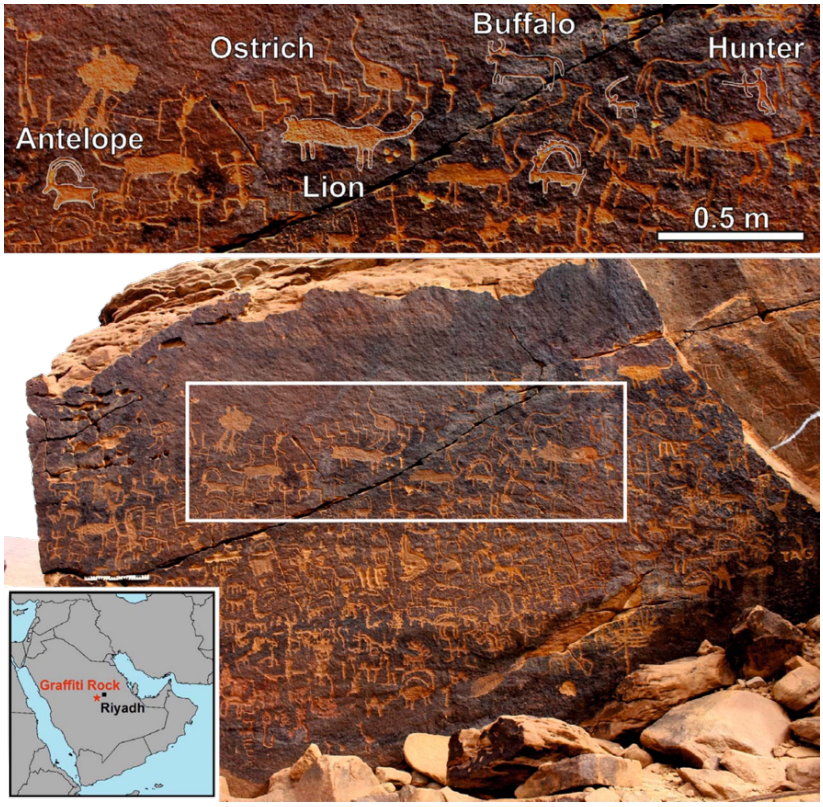

A 14 – Rock art site "Graffiti Rock" about 100 km west of Riyadh:

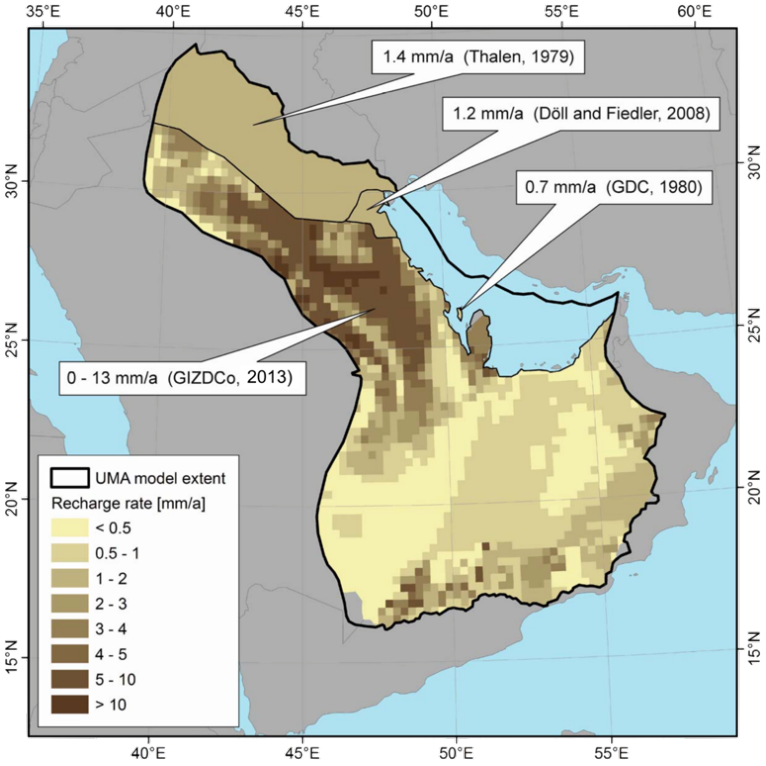

References:

Döll, P., Fiedler, K., 2008. Global-scale modeling of groundwater recharge. Hydrol. Earth Syst. Sci. 12, 863–885. doi:10.5194/hess-12-863-2008

GDC, 1980. Bahrain Study - Volume 3: Hydrology. Cambridge.

GIZ/DCo, 2013. Detailed Groundwater Resources Studies of Khuff Jilh Minjur Dhruma and overlying Aquifers. Riyadh.

Thalen, D. C.P., 1979. Ecology and Utilization of Desert Shrub Rangelands in Iraq. Springer Netherlands, Dordrecht. doi:10.1007/978-94-009-9622-9

A 15 – Groundwater abstraction in Saudi Arabia from the UMA system:

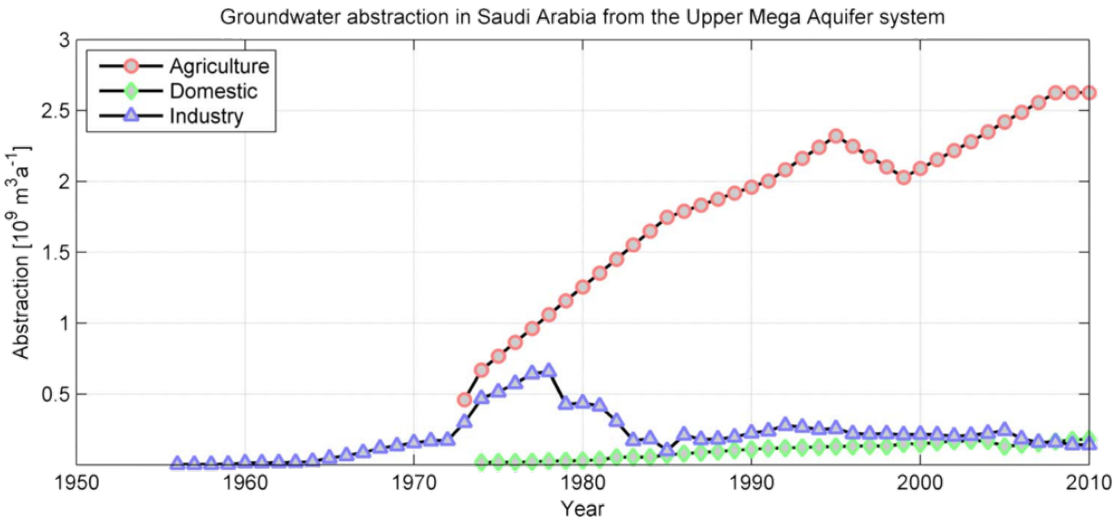

A 16 – Hydrofacies zones for the hydrostratigraphic units of the UMA system:

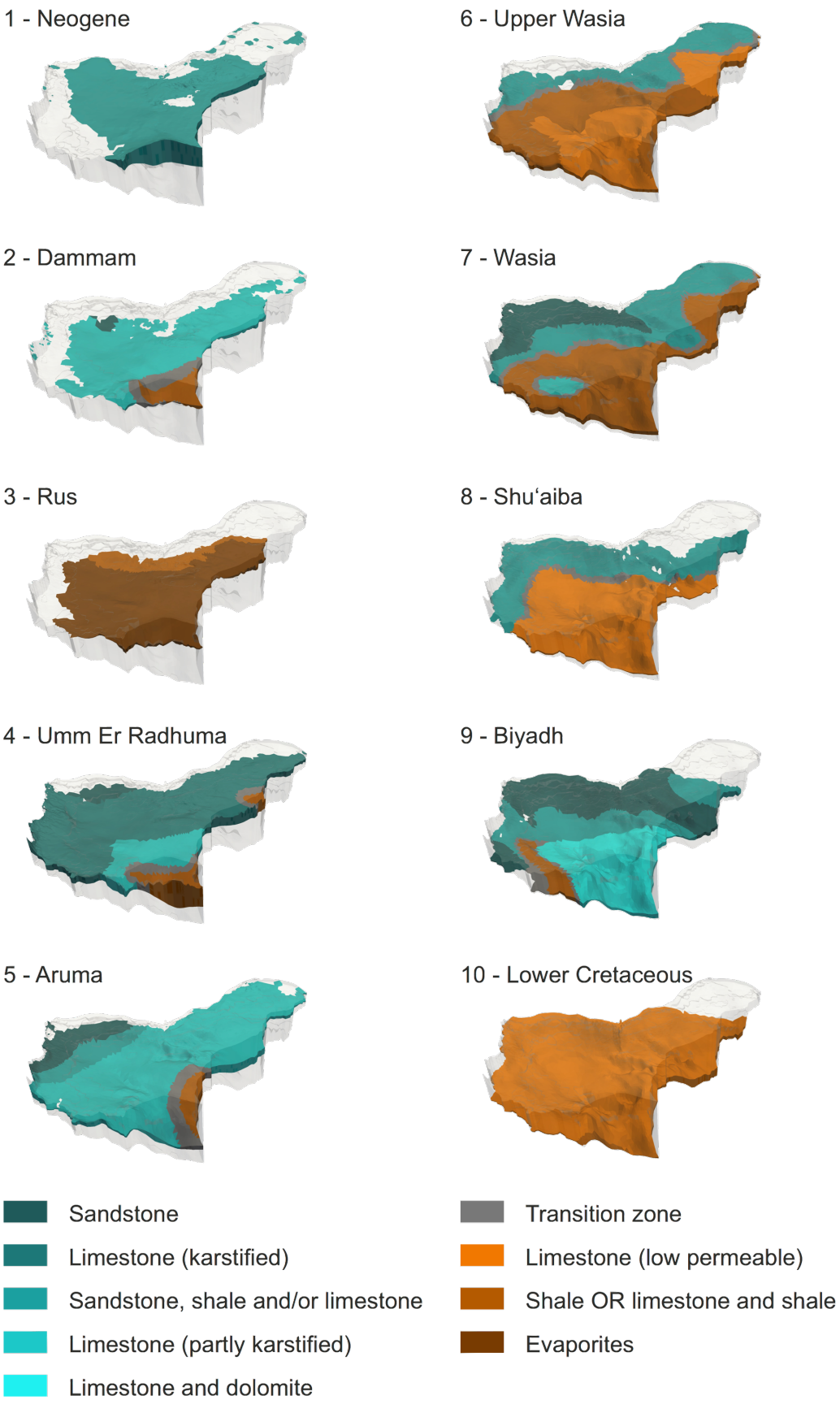

A 17 – Hydraulic conductivity for the hydrofacies zones:

Id	Hydrofacies	Starting values		Case (i)		Case (ii)		Case (iii)		Case (iv)		Final values	
		Kh	Kv	Kh	Kv	Kh	Kv	Kh	Kv	Kh	Kv	Kh	Kv
1	Sandstone	3.0E-04	1.5E-04	3.7E-04	4.7E-07	1.6E-04	1.6E-07	3.6E-05	5.7E-08	1.2E-05	2.8E-08	3.0E-05	5.0E-08
2	Limestone (karstified)	2.0E-04	2.0E-04	6.5E-05	7.1E-05	7.7E-05	4.4E-05	8.9E-05	1.2E-05	9.2E-05	2.6E-06	8.0E-05	8.5E-06
3	Sandstone, shale and/or limestone	2.0E-04	2.0E-04	5.2E-04	8.1E-04	3.7E-04	9.3E-04	2.9E-04	7.3E-04	1.6E-04	8.0E-05	2.7E-04	5.8E-04
4	Limestone (partly karstified)	2.0E-05	2.0E-05	4.0E-06	2.4E-06	4.6E-06	6.2E-06	5.1E-06	4.9E-06	6.3E-07	4.3E-06	5.0E-06	4.3E-06
5	Limestone and dolomite	2.0E-05	2.0E-05	4.2E-07	4.5E-07	3.4E-07	4.7E-07	2.6E-07	4.2E-07	1.6E-07	1.7E-07	1.8E-07	3.9E-07
6	Transition zone	2.5E-07	1.9E-07	2.8E-06	4.6E-09	5.1E-06	3.3E-09	6.0E-06	3.0E-09	4.0E-06	1.7E-09	5.4E-06	2.9E-09
7	Limestone (low permeable)	3.0E-09	1.5E-09	2.8E-07	3.0E-10	3.3E-07	4.5E-10	1.9E-07	3.9E-10	1.7E-07	2.2E-10	2.1E-07	4.1E-10
8	Shale OR limestone and shale	3.0E-10	6.0E-11	5.2E-10	8.6E-12	8.9E-11	6.9E-12	2.9E-11	8.3E-12	3.9E-12	7.1E-12	1.5E-11	7.9E-12
9	Evaporites	3.0E-11	3.0E-12	5.0E-12	2.0E-11	5.4E-12	1.8E-11	4.9E-12	1.9E-11	4.6E-12	3.5E-12	4.7E-12	2.0E-11
	Geometric mean	6.8E-07	3.7E-07	7.1E-07	5.8E-08	5.6E-07	5.4E-08	3.9E-07	3.9E-08	1.8E-07	1.5E-08	3.3E-07	3.5E-08
	KGE	-		0.89		0.88		0.86		0.83		0.88	
	R^2	-		0.88		0.89		0.89		0.81		0.88	
	RMSE	-		21.34 m		20.26 m		20.34 m		26.71 m		21.15 m	
	bias	-		0.51 m		0.39 m		0.2 m		0.15 m		-0.91 m	

all values for the hydraulic conductivity (K) are given in m s^{-1}

A 18 – Specific storage for the hydrofacies zones:

Id	Hydrofacies	Starting values	Case (i)	Case (ii)	Case (iii)	Case (iv)	Final values
		S_S	S_S	S_S	S_S	S_S	S_S
1	Sandstone	2.0E-03	1.0E-04	1.9E-04	1.3E-04	1.6E-04	1.6E-04
2	Limestone (karstified)	7.0E-04	1.2E-08	3.9E-08	1.2E-07	1.7E-07	1.3E-07
3	Sandstone, shale and/or limestone	5.0E-04	2.1E-06	7.7E-06	1.5E-05	3.7E-05	1.6E-05
4	Limestone (partly karstified)	7.0E-04	1.4E-04	1.2E-04	6.6E-05	5.4E-05	1.2E-04
5	Limestone and dolomite	5.0E-04	6.3E-07	4.0E-06	5.0E-05	3.2E-04	5.2E-05
6	Transition zone *	4.0E-06	4.0E-06	4.0E-06	4.0E-06	4.0E-06	4.0E-06
7	Limestone (low permeable) *	3.0E-08	3.0E-08	3.0E-08	3.0E-08	3.0E-08	3.0E-08
8	Shale OR limestone and shale *	3.0E-09	3.0E-09	3.0E-09	3.0E-09	3.0E-09	3.0E-09
9	Evaporites *	3.0E-11	3.0E-11	3.0E-11	3.0E-11	3.0E-11	3.0E-11
	Aritmetic mean **	8.8E-04	5.0E-05	6.5E-05	5.3E-05	1.2E-04	6.9E-05
	KGE		0.59	0.61	0.40	-0.07	0.46
	RMSE		12.43	9.97	10.64	12.52	10.35
	bias		1.54	-0.06	1.93	1.67	-0.92
	KGE ***		0.67	0.68	0.62	0.52	0.66
	RMSE ***		13.81	11.63	12.43	13.78	11.73
	bias ***		4.77	1.49	1.86	2.56	0.66

* not calibrated due to no groundwater abstraction in these hydrofacies zones

** only for hydrofacies zones 1 to 5

*** without Wasia Well Field

all values for the specific storage (S_S) are given in m^{-1}

A 19 – Steady state model performance for starting values:

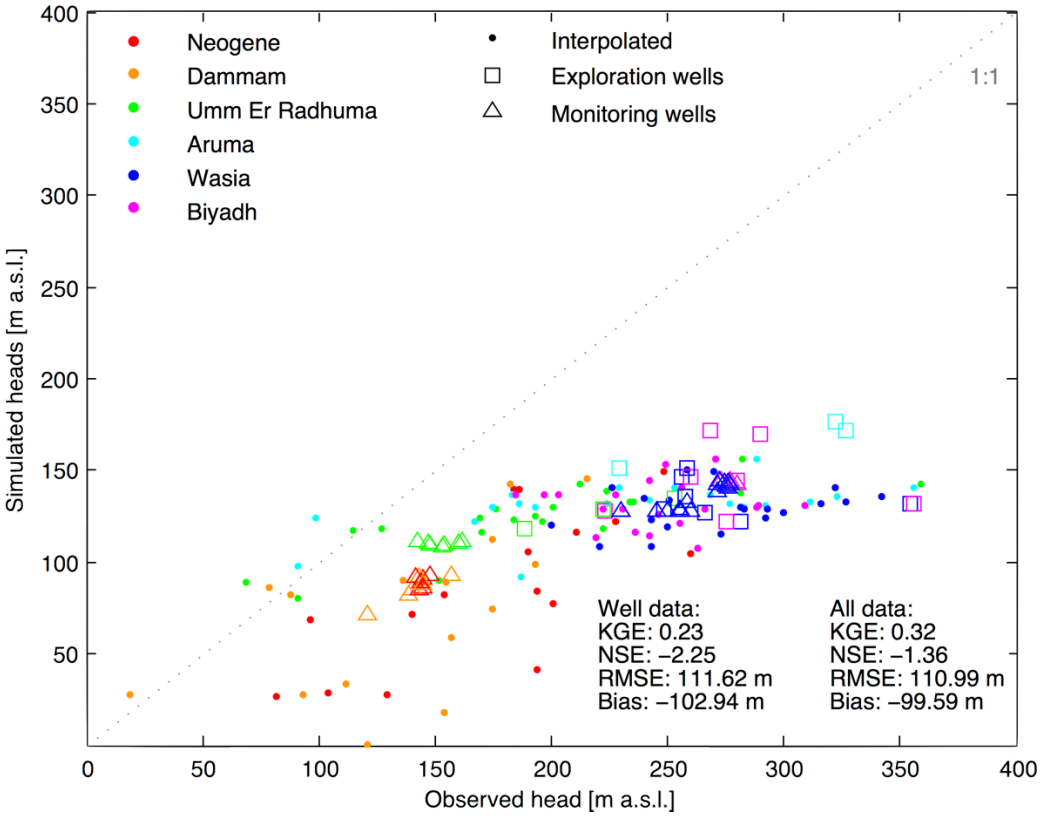

A 20 – Analytical model to calculate the time to near steady-state:

Time to near steady-state (t_{NE}) after a large hydraulic perturbation according to (Rousseau-Gueutin et al. (2013) for

(i) confined aquifer systems:

$$t_{NE} = 3 \cdot \frac{4L^2}{D\pi^2}$$

where L is the aquifer length, and D is the hydraulic diffusivity defined by $D = K/S_S$. We calculated the hydraulic diffusivity for each hydrofacies from the starting values for K and S_S given in the Supplementary Material E and F, respectively. Subsequently, we assumed that the geometric mean of the hydraulic diffusivity is representative for the whole aquifer system. This yields D = 0.14 m^2s^{-1}. For the aquifer length (L), we used a minimum (400 km) and maximum (1,000 km) value. Finally, we calculated the time to near steady-state t_{NE} = 44,000 a (for L = 400 km) and t_{NE} = 275,000 a (for L = 1,000 km). Its arithmetic mean is t_{NE} = 160.000 a.

(ii) mixed (confined and unconfined parts) aquifer systems:

$$t_{NE} \approx \frac{3S_U L_U}{T}\left(L_C + \frac{L_U}{2}\right)$$

where S_U is the specific yield for the unsaturated part, L_U is the aquifer length of the unsaturated part, T is the transmissivity defined by $T = K \cdot d$ (where d is the saturated thickness of the aquifer), and L_C is the aquifer length of the saturated part. We calculated the Transmissivity (T = 0.0014 m^2s^{-1}) from the geometric mean of the starting values of K (Supplementary Material E) and an average aquifer system thickness (d) of about 2,000 m. We assumed for the specific yield of the unsaturated part (S_U) a value of 3%. The main part (approximately 90%) of the Upper Mega Aquifer system is confined (GIZ/DCo, 2014, 2011; GTZ/DCo, 2006). This yields L_U = 40 km and L_C = 360 km (for L = 400 km) and L_U = 100 km and L_C = 900 km (for L = 1,000 km). The resulting times to near steady-state (t_{NE}) are 32,000 and 203,000 a. Its arithmetic mean is t_{NE} = 118.000 a.

A 21 – Refined discharge estimation:

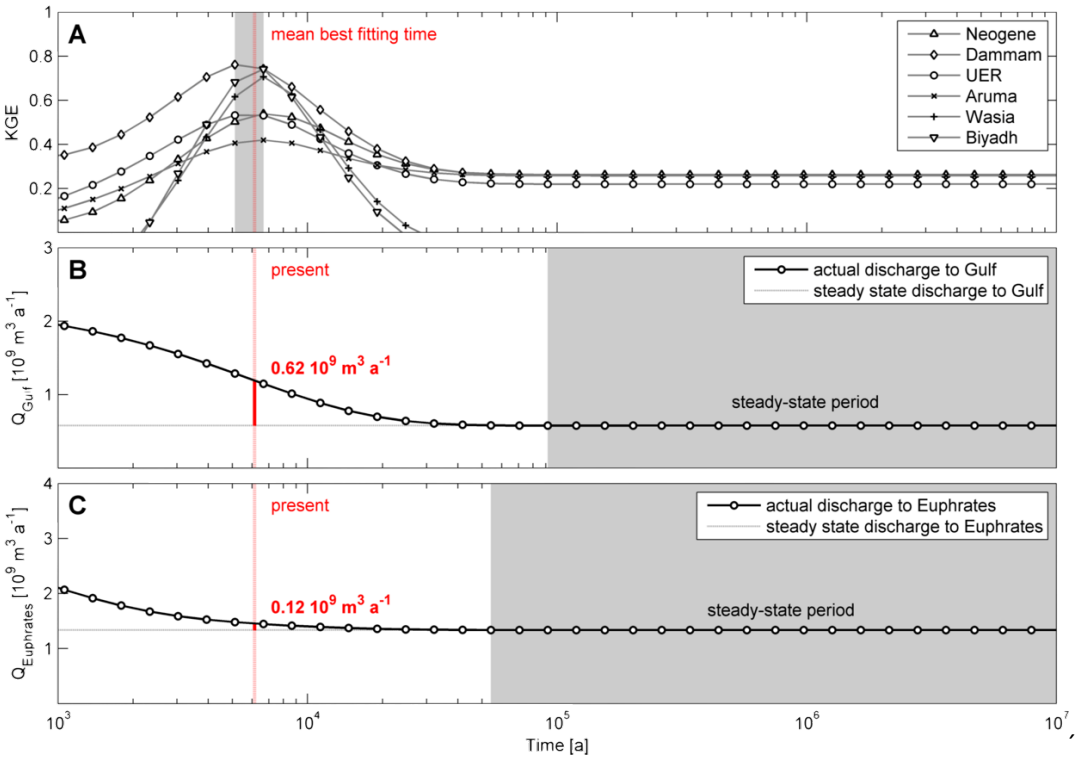

A 22 - Steady state model performance for final values: